12-2011

Development of a Scale Model Wind Turbine for Testing of Offshore Floating Wind Turbine Systems

Heather Rae Martin

DEVELOPMENT OF A SCALE MODEL WIND TURBINE FOR TESTING OF OFFSHORE FLOATING WIND TURBINE SYSTEMS

by

Heather Rae Martin

B.S. Civil and Environmental Engineering, 2009

A THESIS

Submitted in Partial Fulfillment of the

Requirements for the Degree of

Master of Science

(in Civil Engineering)

The Graduate School

The University of Maine

December, 2011

Advisory Committee:

Andrew J. Goupee, Research Assistant Professor of Mechanical Engineering, Advisor

Richard W. Kimball, Professor of Engineering, Maine Maritime Academy

William G. Davids, John C. Bridge Professor of Civil and Environmental Engineering

THESIS ACCEPTANCE STATEMENT

On behalf of the Graduate Committee for Heather Martin I affirm that this manuscript is the final and accepted thesis. Signatures of all committee members are on file with the Graduate School at the University of Maine, 42 Stodder Hall, Orono, Maine.

_____

Chair's Name, & Title   Date

LIBRARY RIGHTS STATEMENT

In presenting this thesis in partial fulfillment of the requirements for an advanced degree at The University of Maine, I agree that the Library shall make it freely available for inspection. I further agree that permission for "fair use" copying of this thesis for scholarly purposes may be granted by the Librarian. It is understood that any copying or publication of this thesis for financial gain shall not be allowed without my written permission.

Signature:

Date:

DEVELOPMENT OF A SCALE MODEL WIND TURBINE FOR TESTING OF

OFFSHORE FLOATING WIND TURBINE SYSTEMS

By Heather Rae Martin

Thesis Advisor: Dr. Andrew Goupee

This thesis presents the development of a 1/50th scale 5 MW wind turbine

intended for wind and wave basin model testing of commercially viable floating wind

turbine structures. The design is based on a popular 5 MW wind turbine designed by the

National Renewable Energy Laboratory (NREL) commonly utilized in numerical

modeling efforts. The model wind turbine is to accompany generic floating model

platforms for basin model testing. The ultimate goal of the model development testing

program is to collect data for validating various floating wind turbine simulation codes

such as those developed by NREL.

This thesis will present an overview of the model testing program and detailed

information on the scaling methodology, design and physical characterization of the final

wind turbine model. The discussion of scaling methodology will include a presentation

of scaling relationships used to ensure loads and forces controlling global motions and

internal reactions are properly scaled during basin model testing. Particular attention is

paid to Reynolds number effects that control the aerodynamic performance of a wind

turbine model. Design methods, final designs and all instrumentation and components of

the 1/50th scale model are disclosed with additional discussion concerning special

fabrication techniques and component testing where applicable. Finally, physical characterization and wind turbine performance results from analytical analyses and basin model test data are provided and compared to determine the overall effectiveness of the created model wind turbine for basin model testing.

iv

TABLE OF CONTENTS

LIST OF TABLES

LIST OF FIGURES

LIST OF NOMENCLATURE

a	=	axial induction factor	k	=	stiffness coefficient
A	=	area	kg	=	kilograms
d	=	water depth	L	=	length
c/D	=	chord length to rotor diameter ratio	m	=	meter
			M	=	mass
c	=	chord length	M_G	=	gyroscopic moment
C	=	wave celerity	N	=	Newton
C_D	=	drag coefficient	N_{crit}	=	laminar to turbulent transition effect log factor
C_L	=	lift coefficient			
C_P	=	power coefficient	Pa	=	Pascal
C_T	=	thrust coefficient	Q	=	wave celerity to wind speed ratio
df/dx	=	meanline slope			
D	=	diameter	R	=	radius
E	=	elastic modulus	r/R	=	local radius/rotor radius
f	=	wave frequency	Re	=	Reynolds number
f_n	=	natural bending frequency	t	=	time unit
$f(x)$	=	meanline distribution	t/c	=	thickness to chord ratio
F_D	=	drag force	$t(x)$	=	thickness distribution
F_L	=	lift force	T	=	wave period
F_Q	=	torque force	u	=	deflection
Fr	=	Froude number	$u_a{}^*$	=	axial induced velocity
F_T	=	thrust force	$u_t{}^*$	=	tangential induced velocity
g	=	acceleration due to gravity			
G	=	shear modulus	U	=	wind speed
H_o	=	angular momentum of rotor	v	=	fluid velocity
Hz	=	hertz	V^*	=	resultant inflow velocity
I	=	area moment of inertia			
J	=	mass moment of inertia	V	=	volt
J_T	=	polar moment of inertia	W	=	watts

x/c	=	point location/chord
x_p/c	=	pitch axis location/chord
y	=	neutral axis location
α	=	angle of attack
β_i	=	resultant inflow angle
β_n	=	boundary condition factor
λ	=	scale factor
μ	=	dynamic viscosity of a fluid
μm	=	micrometer
Ω	=	angular velocity of rotor
ω	=	structural frequency
ψ	=	angular velocity
ρ	=	density
σ	=	stress
θ_p	=	blade pitch angle

Subscripts

m	=	denotes scale model
p	=	denotes full-scale prototype

Unit Prefixes

μ	=	micro ($\times 10^{-6}$)
m	=	milli ($\times 10^{-3}$)
c	=	centi ($\times 10^{-1}$)
k	=	kilo ($\times 10^{3}$)
M	=	mega ($\times 10^{6}$)
G	=	giga ($\times 10^{9}$)

LIST OF ABBREVIATIONS AND ACRONYMS

2D	two dimensional
CG	center of gravity
DU	Delft University
DAQ	CompacDAQ Data Acquisition System
DOE	Department of Energy
EMI	electromagnetic interference
FA	fore to aft
FAST	An aeroelastic design code for horizontal axis wind turbines.
GUI	graphical user interface
HAWT	horizontal axis wind turbine
HDPE	high-density polyethylene
ILS	interlaminar shear strength
LAC	Linear actuator control
MA3	Miniature Absolute Analogue
MIT	Massachusetts Institute of Technology
NI	National Instruments
NREL	National Renewable Energy Lab
NWTC	National Wind Technology Center
OC3	Offshore Code Comparison Collaboration
PSD	power spectral density
RMP	rotations per minute

SS   side to side

SWL   still water line

TLP   Tension Leg Platform

TSR   tip speed ratio

UC Davis   University of California Davis

VI   Virtual Instrument

CHAPTER 1. INTRODUCTION

Modern civilization in the United States has come to function and depend on energy over the last century. Transportation, food production and agriculture, households, businesses, industry and many other key societal functions are reliant on energy to perform every-day tasks.   However, over 75% of the United States' (US) primary energy production is from non-renewable, finite fossil fuels such as coal, oil, gas, and natural gas (EIA, 2010). A major challenge facing future generations in the US and around the world is to meet future energy demands by investing in new energy production technologies especially those in the renewable energy sector (DOE, 2008). An energy resource assessment made by the National Renewable Energy Lab (NREL) has shown the US offshore wind resource has the potential to be a major renewable energy contributor, yet technology to capture the vast majority of offshore wind, located in waters over 60m deep, is currently in an early development stage (Schwartz, et al., 2010). This thesis work is a primary component of an initial research effort consisting of scale model testing for floating wind turbine technologies aimed at advancing technology that efficiently captures offshore wind in deep-water environments. This introduction will present the motivation and background for pursuing floating wind turbine technology and the objective of the model testing research program.

1.1.   MOTIVATION

The United States has a great opportunity to harness an indigenous abundant renewable energy resource, offshore wind. In 2010, NREL estimated there to be over 4,000 GW of potential offshore wind energy found within 50 nautical miles of US

coastlines. The US Energy Information Association (EIA) reported the total annual US electric energy generation in 2010 was 4.12 quadrillion kilowatt-hours or 940 GW (EIA, 2010), less than a quarter of the potential offshore wind resource. In addition, offshore wind is the dominant ocean energy resource available in the US comprising 70% of the total assessed ocean energy resource as compared to tidal and geothermal resources (Musial, 2008). Through these assessments it is clear offshore wind could be a major contributor to the US energy resource.

In particular, the Gulf of Maine is home to a significant portion of the US offshore wind resource. Within the 50 nautical mile band extending from Maine's coast resides an estimated installed wind energy capacity of 156 GW of electricity (Schwartz, et al., 2010). For comparison, Maine's highest annual electric demand is 4.3 GW during the summer months (EIA, 2011). Capturing 3.2% of Maine's offshore wind total estimated capacity, or 5 GW, would cover Maine's peak energy demand and leave surplus energy for potential distribution to surrounding political entities.

Many benefits to the US economy and environment would result if floating wind turbine technology is commercialized. One benefit is that electric power from offshore wind turbines could help increase US energy independence. In Maine, nearly 90% of the energy used for home heating, electricity generation and transportation is derived from fossil fuels leaving Maine citizens, like many US citizens, at the mercy of fluctuating and inflating fossil fuel prices (Ocean Energy Task Force, 2009). Energy from offshore wind has the potential to help control energy cost instability by providing clean electrons at a predictable, reliable cost. Additionally, Maine's billions of energy dollars exported annually could be spent in a domestic market, helping to sustain local economies. Wind

power also has environmental benefits such as reduction of green house gas emissions due to energy production that contribute to global warming (Serchuk, 2000). These are only a few of the economic and environmental benefits that justify active pursuit of onshore and offshore wind energy in the US.

The caveat to capturing offshore wind in the Gulf of Maine and much of the US coast is deep water. Figure 1.1 illustrates that nearly 60% or 2,450 GW of the estimated US offshore wind resource is located in water depths of 60m or more, (Musial, et al., 2006). At water depths over 60m building fixed offshore wind turbine foundations, such as those found in Europe, is likely economically unfeasible (Musial & Ram, 2010). Therefore floating wind turbine technology is seen as the next best option to provide a vessel for extraction of the majority of offshore wind energy in the US.

Region	GW by Depth (m)		
	0 - 30	30 - 60	> 60
New England	100.2	136.2	250.4
Mid Atlantic	298.1	179.1	92.5
S. Atlantic Bight	134.1	48.8	7.7
California	4.4	10.5	573.0
Pacific Northwest	15.1	21.3	305.3
Great Lakes	176.7	106.4	459.4
Gulf of Mexico	340.3	120.1	133.3
Hawaii	2.3	5.5	629.6
Total	1,071.2	628.0	2,451.1
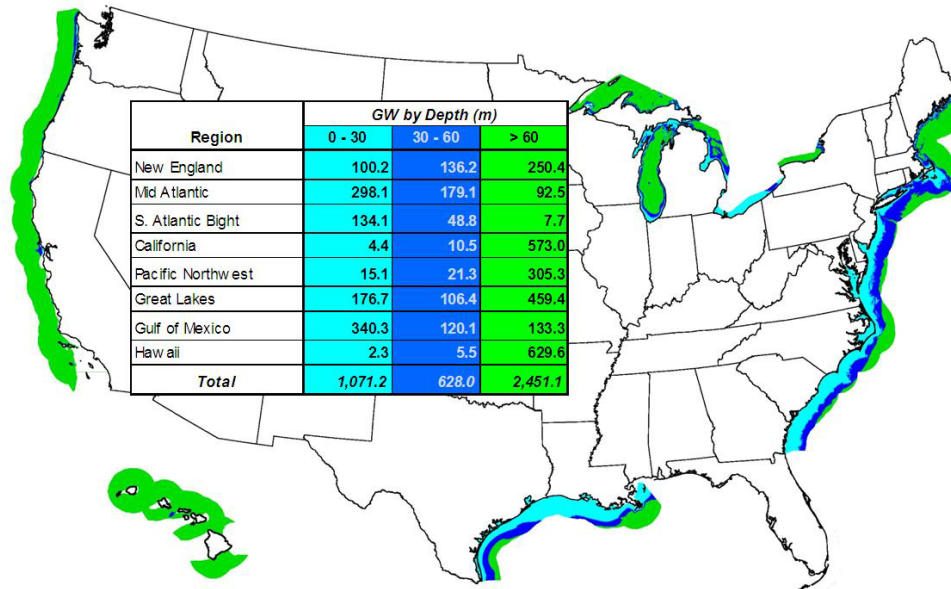
Figure 1.1. US offshore wind resource by region and depth for annual average wind speeds above 7.0m/s, (Musial & Ram, 2010). *Reprinted with permission.*

As of 2009 the US was a leading producer of wind energy in the world with over 35,000 MW of onshore wind energy production (DOE, 2010). Even so, there is still a

need to continue growth of wind energy production in the US in order to meet future energy demand. As reported by the DOE, future wind energy growth should continue onshore but also expand into offshore developments (2008). The DeepCwind Consortium, lead by the University of Maine and supported by the DOE, NREL, and several other private and public entities, is leading the US in deepwater floating wind turbine development. Basin model testing of floating wind turbine platforms is an essential part of the first phase of DeepCwind's Maine Offshore Wind Plan established to promote the development of 5 GW of offshore wind capacity in the Gulf of Maine by 2030 (University of Maine & James W. Sewall Company, 2011). Development of the fully functional 1/50th scale 5 MW wind turbine, detailed in this thesis, was critical for the completion of basin model testing and the progression of the Maine Offshore Wind Plan. Furthermore, basin model testing provided real data to aid in improving and validating fully-coupled simulation tools, discussed in subsequent sections, vital for commercial design and development of floating wind turbine platforms.

1.2. BACKGROUND

In order to pursue commercial development of floating wind turbine technology a validated aero-hydro-servo-elastic numerical model, or fully-coupled simulator, is needed to accurately predict the dynamic system behavior to efficiently optimize floating platform designs. Currently, there is only one prominent publicly available fully-coupled simulator used to model the performance of floating wind turbines developed by NREL (Jonkman & Buhl, 2007). NREL's fully-coupled simulator was developed by interfacing two wind industry-accepted simulation modules, FAST for servo-elastic simulation and AeroDyn for aerodynamic simulation, and one oil and gas industry-accepted

4

hydrodynamic simulation code, WAMIT. However this tool has yet to be validated against real data, and other coupled simulators such as Hydro Oil & Energy's SIMO/RIFLEX/HAWC (Neilsen, et al., 2006), Principal Power's FastFloat (Cermelli, et al., 2010), a rotor-floater-mooring coupled simulator developed at Texas A&M (Bae et al., 2010), and MARIN's aNySIM, (Gueydon & Xu, 2011) have limited information currently published.

As of the writing of this thesis, there exists two commercial scale floating wind turbines in the world, the Hywind spar-buoy by Statoil Hydro (2010) and the WindFloat semi-submersible by Principle Power (2011). The Hywind spar-buoy floating platform supports a 2.3 MW Siemens horizontal axis wind turbine (HAWT) and is heavily instrumented to collect data of importance. However, the collected information is not publicly available, and therefore, is of little use for parties interested in validating and calibrating numerical analysis codes for floating wind turbines. Similarly, data collected from WindFloat which supports a 2 MW HAWT wind turbine is also not currently available. Other limited sources of data do exist for these two platforms, however, they are derived from wave basin scale model testing.

Basin model testing is a refined science and is commonly used to test designs of large scale offshore vessels and structures by the oil and gas industry, military, and marine industries (Chakrabarti, 1994). A basin model test is ideal as it requires less time, resources and risk than a full scale test while providing real and accurate data for model validation. Additionally, wave basin testing is valuable as the environment can be controlled. However even though wave basin testing is well refined in certain offshore

industries protocol for properly modeling the coupled wind and wave loads on a floating wind turbine in a wave basin test environment has not been established.

Figure 1.2 illustrates the difficulty of quantifying all the complicated dynamics of floating wind turbines. The significant loads on a floating wind turbine are characterized by turbulent wind profiles, irregular wave loads, underwater currents and many other complex factors. These varied environmental loads combined with fluid-structure interaction, turbine performance and flexible member structural dynamics phenomena make execution of an accurate scale model test a hearty challenge.
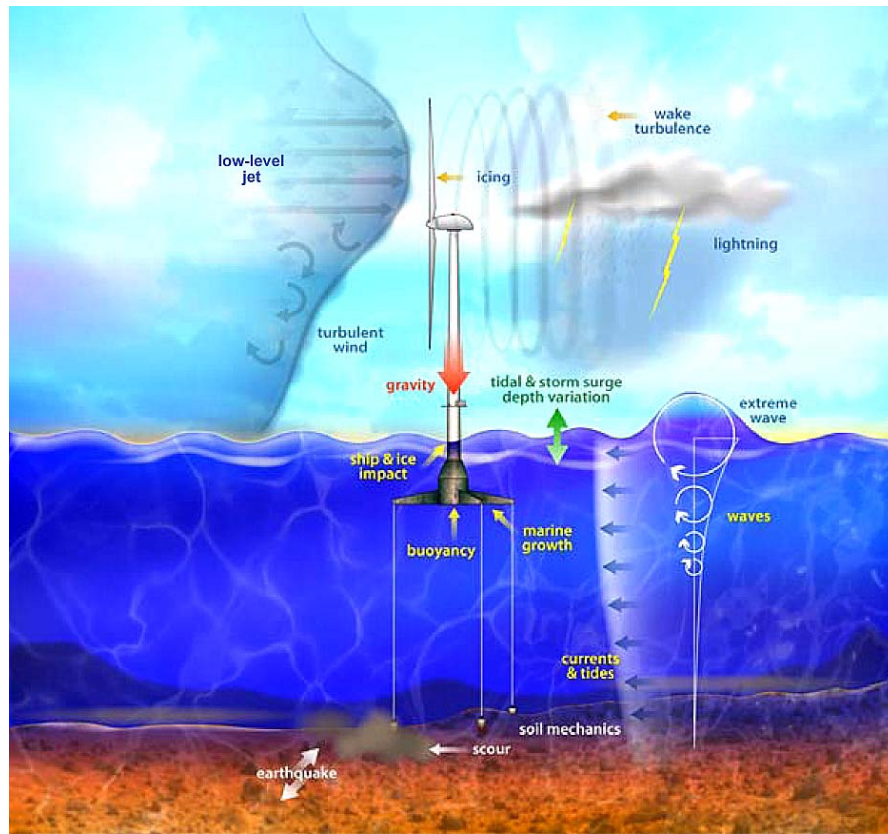
Figure 1.2.   Illustration of significant loads effecting floating wind turbine performance, (Robinson & Musial, 2006). *Reprinted with permission.*

Despite the challenge, a few select floating wind turbine basin model tests have been performed to the author's knowledge. Principal Power Inc. tested a 1/67th scale

6

semi-submersible wind turbine platform, WindFloat (Cermelli, et al., 2010). Test results were used to aid development of the first full scale WindFloat deployed in November, 2011 (Principle Power Inc., 2011). Also, test results were used as part of a proprietary numerical model validation effort and proof of platform design performance. In 2006, Hydro Oil & Energy conducted a 1/47th scale model test of a 5 MW spar-buoy floating wind turbine at Marintek's Ocean Basin Laboratory in Trondheim, Norway (Neilsen, et al., 2006). Another basin test by WindSea of Norway was performed under Froude scaled wind and waves at Force Technology on a 1/64.24th scale tri-wind turbine semi-submersible platform (WindSea, 2011). These model tests provided valuable information to respective stake holders and advanced knowledge of floating wind turbine dynamics. However, methodologies and techniques used during these model tests have not been thoroughly presented in the public domain. In addition, no test to date has made the effort to create the high-quality wind environment required for simulating proper wind turbine performance in a combined wind/wave test. Key differences between this basin model test and those previously mentioned are that this model test program was performed with fully-characterized Froude scaled wind loads, a fully functional model wind turbine and findings of the test will be disseminated in the public domain.

1.3. OBJECTIVE

The primary goal of the basin model test program was to properly scale and accurately capture real data of the rigid body motions and loads of different floating wind turbine platform technologies and then compare data with numerical model results from NREL's aero-hydro-servo-elastic floating wind turbine simulator, or fully-coupled simulator, for calibration and validation. Once the fully-coupled simulator is validated

against real data it could then be used with a much greater degree of confidence in design processes for commercial development of floating offshore wind turbines.

To gain an array of test data for simulator comparison, three generic floating platforms were tested during basin model testing: a semi-submersible, the OC3 Hywind spar-buoy (Jonkman, 2010), and a tension leg platform (TLP) shown in Figure 1.3. The models were tested under Froude scaled wind and wave loads, discussed further in Chapter 2. The model platforms were built by MARIN and model testing was performed at MARIN's Offshore Basin in Wageningen, The Netherlands (2010). The three generic platform designs are intended to cover the spectrum of currently investigated concepts, each based on viable floating offshore structure technology. The designs, as well as their accompanying performance data, will be made publicly available in proceeding

Figure 1.3. 1/50th scale floating platforms tested at MARIN. Clockwise from left: OC3 Hywind spar-buoy (left), TLP (top right), and semi-submersible (bottom right).
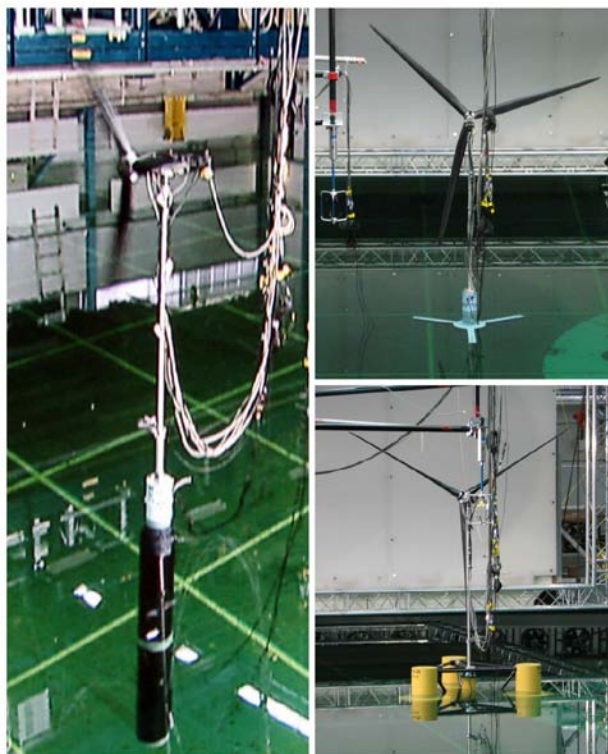
Figure 1.4. Images of basin model testing of the spar (left), TLP (top right), and semi-submersible (bottom right).

publications. Figure 1.4 provides images of the final $1/50^{th}$ scale model wind turbine fixed upon each of the floating platforms during basin model testing.

This thesis focuses on a single, but important aspect of this model test program. Specifically, the goal of the thesis work was to develop a fully functional scale model wind turbine with the ability to generate thrust and torque from wind loads, control rotor speed, pitch blades remotely and acquire necessary sensor data for the model test program. It is important to note that generation of the proper thrust forces was considered critical as it directly affected the response and global motions of the floating model. The generation of power was not considered critical as long as the proper gyroscopic moments were induced by the rotor speed. Additionally, it was decided to pursue a model equipped with a real rotor that included blades and pitching capability

9

over an actuator disk sized to achieve proper thrust forces under basin wind loads and a rotating mass to emulate gyroscopic moments for a couple of reasons. First, data collected from the real rotor allowed this research project to address unanswered questions on wind turbine performance in a wave basin environment. Second, the pitch capability of the model wind turbine will allow for future work to integrate active pitch capability on the model and simulate irregular or extreme condition simulations such as pitch mechanical failure where one blade is pitched while the other two are feathered. A sized disk and simulated mass would not allow for collection of performance data as well as provide a foundation for future basin model testing which could focus on blade pitching options. Another important point is that the goal of the wind turbine model design was to closely represent a full scale wind turbine. Numerical input files for the fully coupled simulator of the final wind turbine model will be created in future research efforts based on the characterization results presented in Chapter 4. In other words, a full scale numerical model of the physical model at full scale will be used for fully-coupled simulations. This thesis details the process and methods used to create the scale model wind turbine used for basin model testing and provides results from wind turbine characterization and performance testing.

From this scope of work, this thesis provides the following research contributions to the scientific community:

1. Defining scaling methods and modeling techniques needed to perform accurate wind/wave basin model tests of floating wind turbines.

2. Disclosing design details and characterization results of a 1/50th scale model of the NREL 5 MW wind turbine for others to use for future model tests.

3. Providing clarification of Reynolds number effects on model wind turbine performance under Froude scaled winds and provide methods that could be employed to correct for undesired effects.

In short, this work provides a basis for future scale model wind turbines for basin model testing of commercially viable floating wind turbine platforms.

The remaining structure of this thesis consists of four chapters. Chapter 2 presents the utilized scaling methodology and established scaling laws with a discussion of Reynolds number effects under Froude scaled conditions. Also presented in Chapter 2 are the target $1/50^{th}$ scale physical and mechanical parameters of the NREL 5 MW wind turbine used to guide model design. Chapter 3 details the design and fabrication of the model wind turbine. This chapter starts with the model nacelle design which includes instrumentation selection, housing design, hub design and the blade pitch control method. Following nacelle design is a description of the data acquisition and control system. Model blade design and composite fabrication is then presented and the chapter is concluded with the model tower design. Chapter 4 presents the characterization and performance data of the model wind turbine during fix-based wind only basin model testing as well as model blade structural testing results. In addition, this chapter provides suggestions for future designs of wind turbines utilized in a Froude scaled wind environment. Finally, Chapter 5 provides a conclusive overview of the methodology, design, and characterization of the final $1/50^{th}$ scale model test with suggestions for future floating wind turbine basin model tests.

CHAPTER 2. SCALING METHODOLOGY AND APPLICATION

Proper scaling of a model and environmental conditions for scale model testing is essential to complete a valid and reliable test. For floating wind turbine wind/wave testing, proper scaling and modeling techniques have yet to be established. This chapter will present and discuss the scaling relationships, scale factors, and modeling techniques used to design and build the 1/50th scale wind turbine and platforms and establish environmental conditions in the wave basin. In addition, target design values derived from scaling methodology for the scale model wind turbine is also presented.

2.1. METHODOLOGY

In order to properly model the dynamic behavior of a floating wind turbine system subjected to aerodynamic and hydrodynamic loading, an appropriate scaling methodology must be used. A major challenge is overcoming the inability to simultaneously maintain Froude and Reynolds numbers for a scaled floating wind turbine experiment. In wind tunnel testing Reynolds number scaling is commonly used to establish model parameters in order to properly represent the relationship of viscous and inertial forces for a fluid flow, (Çengel and Cimbala, 2006). In wave basin testing Froude number similitude is typically employed to properly scale the gravitational and inertial properties of wave forces, the dominant external forces for a floating vessel or structure, (Chakrabarti, 1994). In floating wind turbine testing maintaining Froude number was preferred as all wave forcing and inertial effects were properly scaled. However, special attention was paid to Reynolds-dependent phenomena in order to properly model the ratio of wind to wave forces during basin model testing. In the following section, the Froude

scaling relationships used to design the 1/50th scale wind turbine model are presented

with further elaboration on parameters particular to floating wind turbine modeling.

Subsequently, a more detailed discussion of the consequences of Reynolds number

dissimilitude, particularly for wind turbine performance, is included.

2.1.1. Scaling Relationships and Parameters

In order to establish scale relationships, certain scaling laws must be followed. The

scaling relationships employed for modeling of floating offshore wind turbines are as

follows:

1. *Froude number similitude is employed from prototype to scale model.* Offshore

   platform wave basin tests are typically scaled using Froude number and geometric

   similarity. Although a Froude model does not scale all parameters properly the

   dominant factor in the wave mechanics problem, inertia, is properly scaled

   (Chakrabarti, 1994). For a floating wind turbine, this covers most properties of

   interest which influence the global dynamic response of the system, excepting the

   aerodynamic wind forces. Employing a Reynolds number scaling scheme,

   common for model aerodynamic experiments, is impractical for a floating body

   subjected to wave forcing. Therefore, Froude scaling is best suited for model

   testing of floating wind turbines. The Froude number for a free surface wave is

$$Fr_{wave} = \frac{C}{\sqrt{gL}}, \tag{2.1}$$

   where C is the wave celerity, or propagation speed, g is the local acceleration due

   to gravity and L is a characteristic length. The scaling relationship maintained

   from model scale to the full scale prototype is given as

$$Fr_p = Fr_m, \tag{2.2}$$

where *p* and *m* stand for prototype and model, respectively. Forces reliant on Reynolds number, such as airfoil lift and drag are discussed in section 2.1.3.

2. *Froude scaled wind is employed during basin model testing.* If aerodynamic turbine features are insensitive to Reynolds number, then the wind force to wave force ratio from prototype to model scale is maintained by utilizing Froude scaled wind and can be shown as

$$Fr_{wind} = \frac{U}{\sqrt{gL}}. \tag{2.3}$$

An alternative, yet consistent, way to represent Froude scaled wind is by maintaining the ratio of wind speed to wave celerity from model to full scale. This ratio is identified by the variable *Q* and defined as

$$Q = \frac{U}{C}, \tag{2.4}$$

where *U* is the wind inflow velocity and *C* is the wave celerity.

3. *The wind turbine tip speed ratio, TSR, is to be maintained from prototype to scale model. TSR is computed as*

$$TSR = \frac{\Omega R}{U}, \tag{2.5}$$

where Ω is the rotor rotational speed, *R* is the blade tip radius and *U* is the wind inflow velocity. Maintaining *TSR* ensures that the turbine rotational speed as well as any system excitation frequencies resulting from rotor imbalance or aerodynamic interaction with the tower will scale properly. In addition, maintaining *TSR* will yield properly scaled turbine thrust forces and rotor torque

in conjunction with a Froude scaled wind environment, assuming a low

dependence on Reynolds number for the wind turbine airfoil section lift and drag

coefficients. Maintaining *TSR* between the prototype and model is given as

$$TSR_p = TSR_m .$$ (2.6)

By following these scaling relationships, the scale factors shown in Table 2.1

were obtained to characterize a scaled floating wind turbine. Additional parameters can

be found in Chakrabarti (1994).

Table 2.1.   Established scaling factors for floating wind turbine model testing.

Parameter	Unit(s)	Scale Factor
Length (e.g. displacement, wave height and length)	L	λ
Area	L^2	λ^2
Volume	L^3	λ^3
Density	M/L^3	1
Mass	M	λ^3
Time (e.g. wave period)	T	$\lambda^{0.5}$
Frequency (e.g. rotor rotational speed, structural)	T^{-1}	$\lambda^{-0.5}$
Velocity (e.g. wind speed, wave celerity)	LT^{-1}	$\lambda^{0.5}$
Acceleration	LT^{-2}	1
Force (e.g. wind, wave, structural)	MLT^{-2}	λ^3
Moment (e.g. structural, rotor torque)	ML^2T^{-2}	λ^4
Power	ML^2T^{-3}	$\lambda^{3.5}$
Stress	$ML^{-1}T^{-2}$	λ
Mass moment of inertia	ML^2	λ^5
Area moment of inertia	L^4	λ^4

2.1.2. Discussion of Parameters Particular to Floating Wind Turbines

By employing the scaling relationships shown previously, the following additional

parameters, not related to Reynolds number, yet relevant to a floating wind turbine

response were found to scale correctly from prototype to model.

The relationships shown in Table 2.1 are valid for both deep and shallow waves. Wave celerity is dependent on the relative depth which is the ratio of water depth, d, to wave length, L. The expression for wave celerity according to Main (1999) is

$$C = \sqrt{\frac{gL}{2\pi} \tanh(2\pi \frac{d}{L})} \, , \qquad (2.7)$$

and applies for all water depths. In shallow water where the relative depth, d/L approaches 0, tanh$(2\pi d/L)$ approaches $2\pi d/L$. For deep water where the relative depth is greater than 0.5, tanh$(2\pi d/L)$ approaches 1 simplifying the equation to the often recognized deep water expression,

$$C = \sqrt{\frac{gL}{2\pi}} \, . \qquad (2.8)$$

For a proper Froude scaled experiment, both L and d are each scaled by λ maintaining the depth ratio and hyperbolic tangent term in Equation 2.7 from prototype to model scale. Therefore, it is evident that wave celerity in deep to shallow water waves is scaled the same. The scale factor for wave celerity is determined with Equation 2.8, where wave length, L, is scaled by λ resulting in a celerity scale factor of $\lambda^{0.5}$ which is consistent with the scale factor for velocity given in Table 2.1.

In order to attain proper scaling of system dynamics, the ratio of the rotor rotation speed to wave frequency must scale in the same manner. By using the scale factor for frequency given in Table 2.1, the model wave frequency, f_m, is found by

$$f_m = \sqrt{\lambda} f_p \, . \qquad (2.9)$$

The turbine rotor rotational frequency scale factor is found by combining equations 2.5 and 2.6 and implementing scale factors for velocity and length from Table 2.1 to form

$$\frac{\Omega_p R_p}{U_p} = \frac{\Omega_m \frac{1}{\lambda} R_p}{\frac{1}{\sqrt{\lambda}} U_p},$$

(2.10)

which yields

$$\Omega_m = \sqrt{\lambda} \Omega_p.$$

(2.11)

Therefore, rotor rotational frequency scales in the same fashion as other frequencies such as the wave frequency shown in Equation 2.9.

Gyroscopic moments induced by rotor rotation on a floating turbine can occur in both the yaw and pitch motions of a floating wind turbine structure. It is important to replicate these effects during basin model testing to acquire accurate test data. Gyroscopic moment, M_G, of a fixed wind turbine is a function of angular velocity, ψ, and angular momentum of the rotor, H_o, (Manwell, et al., 2002) and is of the form

$$M_G = \psi H_o,$$

(2.12)

where rotor angular momentum is computed as

$$H_o = J\Omega,$$

(2.13)

where J is the mass moment of inertia of the rotor about the rotor shaft axis. By applying scale factors from Table 2.1 to rotor angular velocity ψ, rotor rotational frequency Ω, and rotor mass moment of inertia J, the following relationships are prescribed

$$\psi_m = \sqrt{\lambda} \psi_p, \qquad \Omega_m = \sqrt{\lambda} \Omega_p, \qquad J_m = \frac{1}{\lambda^5} J_p.$$

(2.14 – 2.16)

Substituting Equations 2.14 through 2.16 in Equation 2.12 gives

$$M_{Gm} = (\sqrt{\lambda}\psi_p)(\sqrt{\lambda}\Omega_p)(\frac{1}{\lambda^3}m_p)(\frac{1}{\lambda}r_p)^2,$$

yielding

$$M_{Gm} = \frac{1}{\lambda^4}M_p. \qquad (2.17)$$

Therefore, if the gyroscopic and mass properties of the rotor are scaled correctly yielding a Froude scale consistent value for *J*, the gyroscopic moment scales consistently with the scale factors listed in Table 2.1 and is maintained in a Froude scaled model.

Proper scaling of structural deformation modes and vibration characteristics are of particular importance in order to accurately model key structural dynamics behavior. By following established scaling relationships and the scale parameters listed in Table 2.1, the frequency of structural vibration scales as

$$\omega_m = \sqrt{\lambda}\omega_p. \qquad (2.18)$$

Delving further, the frequency of lateral vibration for a homogenous prismatic Euler-Bernoulli beam (e.g. see Rao, 2004) is of the form

$$\omega = \beta_n L\sqrt{\frac{EI}{L^3 m}}, \qquad (2.19)$$

where β_n is dependent on beam end boundary conditions, *L* is the member length, *E* is the modulus of elasticity, *I* is the cross-section area moment of inertia, and *m* is the member mass. By following the mass, length, and frequency scaling requirements given in Table 2.1 the scaling relationship for the bending stiffness, *EI*, can be determined by rearrangement of variables which is shown as

18

$$\omega_m = \sqrt{\lambda}\,\omega_p = \sqrt{\frac{(EI)_m}{L_m{}^3 m_m}} = \sqrt{\lambda \frac{E_p I_p}{(\lambda^3 L_m{}^3)(\lambda^3 m_m)}}\,,$$

yielding

$$(EI)_m = \frac{1}{\lambda^5} E_p I_p\,.$$

(2.20)

The same procedure was applied for determining the scaling relationship for other

stiffnesses, such as axial stiffness, *EA*, and torsional rigidity, GJ_T, which were found to

scale by λ^3 and λ^5 respectively. The aforementioned procedures for scaling stiffness

quantities is outlined because achieving a Froude scale stiffness involves a combination

of scaling dimensions and also scaling material moduli. This is difficult as often times the

materials used for model fabrication have similar material densities and moduli as the

prototype materials. Therefore, the combination of material density, stiffness and

geometry are usually tuned together to achieve the gross dimensions, mass properties,

and stiffness of the model component in design. This method was used to design the

model tower discussed in Chapter 3.

2.1.3. Reynolds Number Effects

While many quantities scale consistently with Froude number scaling, there are

limitations due to Reynolds number effects. Reynolds number quantifies the viscous and

inertial qualities of fluid flow and is expressed as (e.g. see Çengal and Cimbala, 2006)

$$\mathrm{Re} = \frac{\rho v L}{\mu}\,,$$

(2.21)

where ρ is the fluid density, v is the mean velocity of the object relative to the fluid, μ is

the dynamic viscosity and *L* is the fluid length of travel of interest. Reynolds number is

19

typically employed in aerodynamic modeling and wind tunnel testing of airfoil sections, wings, wind turbines, and more (Çengel & Cimbala, 2006) where maintaining the viscous and inertial properties of fluid flow is critical. As this model test utilized Froude number similitude, Reynolds number similitude is not maintained. Therefore, forces heavily reliant on Reynolds number such as lift and drag on wind blade airfoils would not scale properly during basin model testing. As a fully functional wind turbine was desired for basin testing, the effect of Froude scaled wind on the performance of the turbine needed to be understood so that corrections could be made to improve testing procedures.

Under Froude scaled conditions, the wind speed and blade Reynolds number were reduced from prototype to model scale. For the $1/50^{th}$ scale model test a full scale 11 to 12 m/s wind speed reduced to less than 2 m/s and the Reynolds number at 70% blade radius found with Equation 2.21 decreased from 11.5×10^6 (turbulent flow) to 35×10^3 (laminar flow). The drastic change in Reynolds number resulted in a significant change in the lift and drag behavior for airfoil sections of the geo-sim wind blade employed during basin model testing. The model blade emulated the geometry of a full scale 5 MW wind blade designed for high-Reynolds number turbulent flow as opposed to the low-Reynolds number flow experienced during the wind/wave basin. Note that a full description of the blade geometry is provided in Chapter 3. During basin model testing, generated torque and thrust were lower than required. Therefore, wind speeds during basin testing were increased to ensure proper thrust forces. However the power coefficient, which depicts the power captured by the turbine relative to the available power in the wind flow, was still low. In this section, an aerodynamic analyses of a NACA 64-618 airfoil at 70% the blade length of the NREL 5 MW blade, used for the

model wind turbine and detailed in Chapter 3, was performed to clarify the Reynolds number effects on a Froude scaled wind turbine model. A full description of wind turbine performance results from basin testing is presented in Chapter 4.

Fluid flow behavior analysis over the NACA 64-618 airfoil was performed with XFOIL (Drela, 1989) under full scale and model operational conditions. XFOIL is freely available high-order panel code incorporating a fully-coupled viscous/inviscid interaction method designed specifically for airfoil analysis. At full scale conditions, an operational wind speed of 11.4m/s and a rotor speed of 12.1 rpm was used yielding a Reynolds number of 11.5×10^6. Model conditions consisted of a wind speed of 20.8 m/s and rotor speed of 12.7 rpm (2.94 m/s 90 rpm model scale) which yielded a Reynolds number of 35×10^3. In XFOIL the laminar to turbulent transition effect log factor, N_{crit}, was set to 9 at both full and model scale for consistency as this is the number used for standard wind tunnels analysis (Drela, 1989). Figure 2.1 displays some of the results from the XFOIL
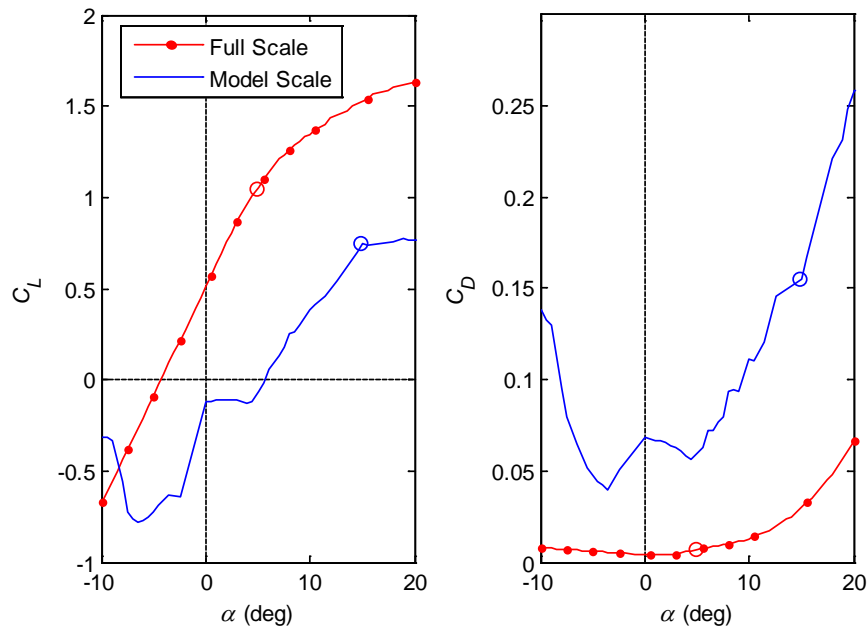
Figure 2.1.   Lift and drag coefficient as a function of angle of attack for a NACA 64-618 airfoil section at r/R = 0.7 at model and full scale wind conditions.

21

analysis through lift and drag coefficients over a range of angles of attack, α. As can be seen in this figure, the relatively thick NACA 64-618 airfoil section exhibits low lift and high drag in model conditions as opposed to full scale conditions.

The resulting forces per unit length of the wind blade using information from the XFOIL analysis are illustrated with airfoil force diagrams in Figure 2.2 at full scale conditions and model conditions transformed to full scale. The top diagram is generic with exaggerated magnitudes for axial and tangential induced velocities, u_a* and u_t*, as well as the angle of attack, α, for clarity. Induced velocities were found with an AeroDyn analysis using the lift and drag coefficient inputs from the XFOIL analyses. AeroDyn utilizes Blade Element Momentum (BEM) theory (e.g. see Moriarty & Hansen, 2005) to calculate wind turbine aerodynamic loads. To calculate induced velocities, BEM theory assumes a pressure loss, or momentum loss, through the rotor plane on the blade elements. The momentum loss and resulting wake creates induced velocities which effect the magnitude and angle of attack of the resulting inflow, $V*$, on the airfoil. In Figure 2.2 the induced velocities are shown as vectors, which contribute to the actual wind flow magnitude and direction experienced by the airfoil, $V*$. The resulting lift and drag forces per unit of blade length, F_L and F_D, are the major forces of interest in airfoil and hydrofoil analysis as they produce the final torque and thrust forces, F_Q and F_D, shown in Figure 2.2. Lift and drag forces are found with the following equations:

$$F_L = \frac{1}{2}\rho V^2 c C_L, \tag{2.13}$$

$$F_D = \frac{1}{2}\rho V^2 c C_D, \tag{2.14}$$
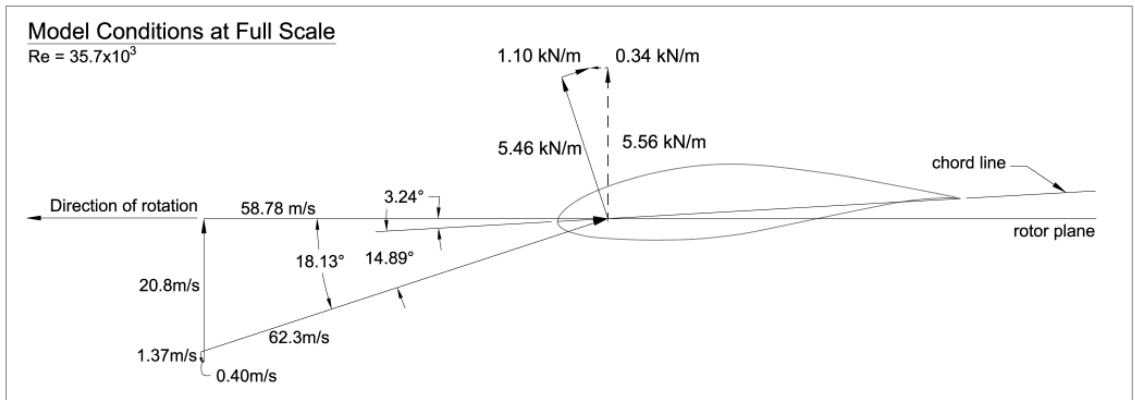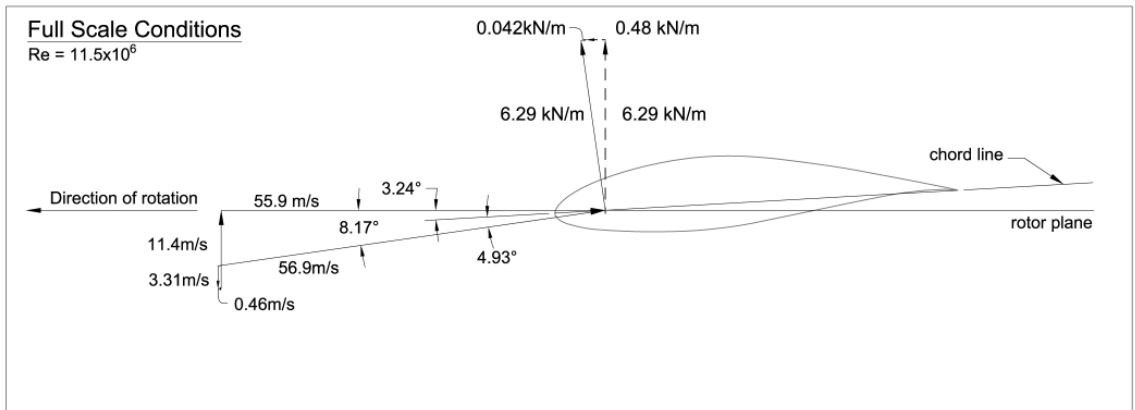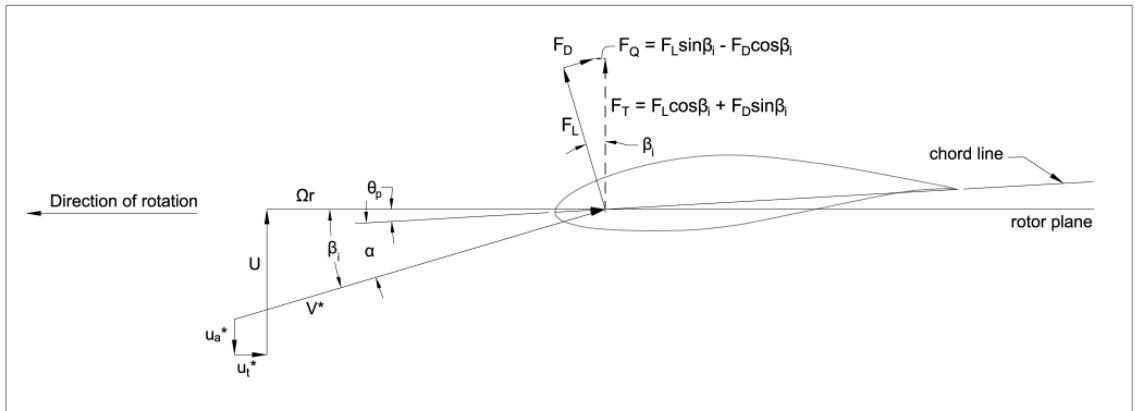
Figure 2.2.   NACA 64-618 airfoil force diagrams at full and model conditions at 70% blade length.

where ρ is the density of air, V^* is final inflow, c is the airfoil chord length, and C_L and C_D are the lift and drag coefficients respectively at the angle of attack under consideration. The lift and drag forces identified in Figure 2.2 were calculated with lift and drag coefficients identified in Figure 2.1 at angles of attack of 4.93 degrees at full conditions and 14.89 degrees at model conditions. These lift and drag coefficients were 1.04 and 6.96×10^{-3} at full scale and 0.757 and 0.152 at model scale respectively. The model scale angle of attack was larger primarily due to the increase in wind speed relative to the rotor tangential speed required at model conditions to achieve comparable rotor thrust forces. The torque and thrust forces, F_Q and F_T, are found as the sum of the axial and tangential components of the lift and drag forces with the equations given in Figure 2.2. From Figure 2.2 it can be seen the model conditions produced similar torque and thrust forces at full scale. The force contributions to torque were 0.48 kN/m and 0.34 kN/m for full and model conditions, respectively while the resulting thrust forces for the full and model conditions were 6.29 kN/m and 5.56 kN/m respectively. Even though the airfoil aerodynamic analysis performed particularly for the model condition was very sensitive to Reynolds number and the transition log effect factor, the results were representative of the performance expected at model scale and demonstrate that similar turbine performance can be achieved as long as the wind inflow velocity is substantially increased for blades with thick airfoil sections. If the wind flow was not increased, the combination of lower angle of attack and high drag at model scale would have yielded a situation where the viscous drag swamped any positive contribution by the lift force in the tangential direction leading to a zero, or more likely, negative net torque contribution, i.e. power would have been required to spin the turbine even under modest wind inflow

speeds. While increasing the wind speeds 'tuned' the net thrust and torque forces somewhat, this was not an ideal situation since the available power from the model wind inflow, at least for the example given, is six times greater than available power from the full scale inflow. Therefore, the geo-sim model rotor power efficiency will be approximately an order of magnitude lower due to the inability to achieve the target levels of torque at the right environmental conditions.

Figure 2.3 provides some insight into the low lift and high drag airfoil coefficients at the model scale Reynolds numbers which lead to poor turbine performance. The figure compares the displacement thickness of the boundary layer, as well as the laminar to turbulent transition and separation location along the NACA 64-618 airfoil for the full
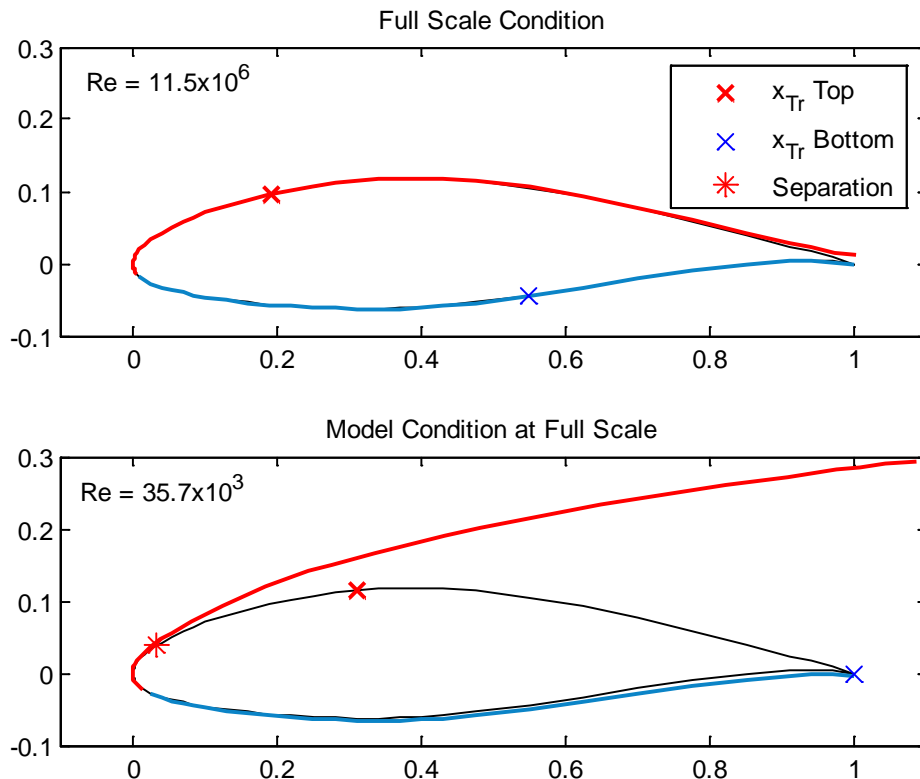
Figure 2.3. Comparison of fluid flow effects at full and model scale conditions.

and model condition Reynolds numbers. As shown in Figure 2.3, at the full scale condition the boundary layers are very thin with a majority of the upper and the last 45% of the lower surface boundary layers turbulent. No separation of the flow occurs at full scale and the total displacement thickness at the trailing edge is quite small, leading to low drag. At model sale, the displacement thickness is drastically larger, especially on the suction side of the airfoil.   In addition, the plot in Figure 2.2 indicates that the flow is separated in the laminar region near the top leading edge of the blade. The end result is an enormous wake for the model scale airfoil which creates a large, virtual projected area perpendicular to the inflow field which drastically increases the drag of the airfoil.   In addition, the poorly organized flow does not yield an optimal pressure distribution about the airfoil perimeter resulting in a diminished lift coefficient for a given angle of attack. As noted earlier, the low lift and high drag coefficients resulting from the flow field changes shown in Figure 2.3 necessitate higher wind inflow velocities in order to create properly scaled thrust and torque values for typical megawatt-scale wind turbine rotors with thick airfoil sections required to achieve adequate structural bending stiffness.

Reynolds number dependent phenomena do not apply to wind turbine aerodynamics alone. Hydrodynamic drag forces on submerged bodies due to currents and waves are also function of Reynolds number. In small Froude models simulated waves and currents will have a lower Reynolds number than the prototype conditions causing the model drag coefficient to increase. This problem, for both the hydrodynamic and aerodynamic instances can be improved by "tripping" the laminar flow to become turbulent at the bow of the structure or leading edge of a wind blade for example. A common and effective approach to trip the fluid flow is to place studs or roughened

material along the aforementioned areas (Chakrabarti, 1994). In general, this technique

can remedy most hydrodynamic issues experienced in Froude scale wave basin tests.

While improvements are made to wind turbine performance with this technique, testing

results given in Chapter 4 will later demonstrate that the method is insufficient by itself to

completely correct wind turbine performance.

A final Reynolds dependent quantity is the Strouhal number which characterizes

vortex shedding of fluid flow past an immersed body (White, 1999). Due to a

dependency on Reynolds number, Strouhal number is also not precisely modeled in a

Froude scaled model (Chakrabarti, 1994). However, according to White (1999), for bluff

bodies the Strouhal number is a weak function of Reynolds number and is approximately

0.2 for cylinders over a wide range of Reynolds numbers. With respect to

hydrodynamics, the spar-buoy, semi-submersible and TLP models tested consist

primarily of cylinders near the water surface where wave particle motion is the largest.

In general, Strouhal number similitude for wave based tests and for this test program is

not a concern.

2.1.4. Overview

The aforementioned scaling relationships properly maintain the dominant model

characteristics and wave forces that greatly influence rigid body motions and structural

loads of a floating wind turbine model. Utilizing Froude number similitude ensures mass

properties of the model and inertia properties relating to hydrodynamics are maintained.

By producing high fidelity Froude scaled wind in the basin the ratio of wind and wave

forces acting on the structure are maintained from full to model scale as long as Reynolds

dependence of airfoil coefficients is weak, which is not always the case and must be

corrected if found to be true. Also by maintaining *TSR* in conjunction with Froude scaled winds, the rotor frequency and any resulting excitations are scaled properly. These relationships ensure that global response of the floating model wind turbine will be well captured in wind/wave basin model testing.

As noted earlier, certain forces reliant on Reynolds number are not maintained using this methodology and require special attention when performing these tests. It is important to note that Reynolds number discrepancy is a common occurrence with wave basin testing of offshore structures. Certain corrections can be used to overcome Reynolds number effects such as the use of turbulence inducers on the model where drag forces are more prominent, such a wind blade's leading edge, a tower face and platform hull. In addition alterations to blade or hull geometry may be required to better simulate the full scale response in the model test. For example, it is not uncommon for ship lifting bodies to be altered in size at the model scale to emulate the full scale drag and lift force condition in a Froude scaled towing test.

For this model test program a geo-sim of the NREL 5 MW wind turbine blade was used for basin model testing. Performance results presented in Chapter 4 show that a geo-sim was not an ideal means of achieving the desired performance for torque and thrust, the latter more critical to capture properly in order to simulate the global motion response of the floating system. The previous sections gave insight into the physical reasons which produce the lack of turbine performance of a geo-sim blade. As discussed in previous sections, the low model condition Reynolds numbers drastically alter the flow characteristics around the thick wind turbine airfoil sections yielding poor lift and drag coefficients as compared to full scale. For future model testing it would be beneficial to

design a model wind blade to better emulate the full scale performance at the low

Reynolds number condition of the Froude scale model test. A basic example of a low-

Reynolds number condition blade is presented in Chapter 4 for comparison against the

performance results of the geo-sim model blade subjected to Froude scaled winds. Even

considering the Reynolds number dependent pitfalls, the wave and wind turbine thrust

forces that control global motions and loads of a floating wind turbine model can be

maintained with a Froude scaling architecture, albeit often with a bit of tuning.

2.2. TARGET SCALE MODEL PARAMETERS

This section provides the basis and method used to establish target parameters or

characteristics of the model wind turbine used to guide the design of the final model. The

subsequent paragraphs provide discussion on the selection of the full scale wind turbine

emulated during wind/wave basin testing, determination of the appropriate scale factor,

and establishment of the final scale mechanical properties and dimensions of the model.

The scale model wind turbine is based on the commercial scale 5 MW reference

wind turbine from the National Renewable Energy Lab, NREL, (Jonkman, et al., 2009).

The NREL 5 MW reference wind turbine is a theoretical three bladed HAWT, a common

commercial wind turbine configuration, that has been established for the purpose of

offshore wind turbine analytical studies. This wind turbine was chosen because it is an

open-source design and has been heavily utilized in coupled numerical modeling of

various floating wind turbine concepts similar to those this test program is aiming to

validate. However the NREL 5 MW wind turbine is only theoretical and not all

dimensions and specifications required for fabrication were readily available posing an

interesting challenge to the model design and fabrication effort.

All the model wind turbine components, such as the wind blades, nacelle and hub are based on descriptions of the NREL 5 MW wind turbine. The model tower is based on the OC3 Hywind tower (Jonkman, 2010) which is 10 m shorter than the reference NREL 5 MW tower to account for the increased freeboard of the OC3 Hywind spar-buoy floating platform. The OC3 Hywind tower base was located 10 m above the still water line (SWL) also allowing for the semi-submersible and TLP to have a reasonable 10 m of freeboard at the tower-platform interface. Model testing and fabrication was simplified by using one turbine and tower model for all three platforms.

A model scale factor of $1/50^{th}$, or $\lambda = 50$, was chosen based on basin capacity and construction feasibility. Using a scale factor greater than 50 would have severely reduced the feasibility of building properly scaled wind turbine blades due to tight weight constrictions which is discussed in detail shortly. Also, using smaller models in a basin model test would reduce the accuracy of the test as most wave basins have difficulty creating the diminutive waves required for experiments of a very small scale. While a larger model would potentially perform better, a scale factor less than 50 would greatly increase the model rotor size as well as the size and cost of wind machine specially designed and built to deliver high quality winds in the basin for this test program. Lastly, model design and early fabrication commenced prior to wave basin selection. At that time, a larger model would have severely restricted the number of potential wave basins world-wide that could perform the model tests due to basin dimension limitations. Overall, a $1/50^{th}$ scale factor was found to be a suitable choice.

Utilizing the scaling relationships and parameters previously discussed, the target model parameters given in Table 2.2 were established. While certain design parameters

Table 2.2. Full scale NREL 5 MW properties and target model scale properties.

Property	Full Scale	1/50th Scale
Power	5 MW	5.7 W
Blades mass	17,740 kg	0.14 kg
Blade length	61.5 m	1.23 m
Hub mass	56,780 kg	0.45 kg
Nacelle mass	240,000 kg	1.92 kg
Tower top mass (hub, 3 blades and nacelle)	350,000 kg	2.80 kg
Hub radius	1.50 m	0.03 m
Rotor diameter, D	126 m	2.52 m
Tower mass	249,718 kg	1.998 kg
Tower height	77.6 m	1.55 m
Tower CG (% from tower base)	43.0 %	43.0 %
Tower 1st bending natural frequency	0.478 Hz	3.378 Hz
Tower top diameter	3.78 m	0.08 m
Tower base diameter	6.5 m	0.13 m

were straight forward to achieve physically, several presented interesting engineering

challenges. The NREL 5 MW full scale wind blade is 61.5 m in length with a mass of

17,710 kg. When scaled by 1/50th the blade was reduced to 1.23 m in length with a mass

of 0.14 kg, which was extremely light relative to its size. Selection and use of

appropriate materials and fabrication techniques was critical in order to ensure the model

wind blade emulated the appropriate geometry and ultra-light mass requirement while

possessing adequate strength to resist loading during wind/wave basin model testing.

Design of the nacelle was also a unique engineering challenge as a motor assembly, all

necessary sensors and components and a durable housing needed to collectively weigh

1.92 kg at the 1/50th scale. Detailed discussion of the design, component selection,

and fabrication methods for the 1/50th scale model wind turbine used to overcome these design challenges and others is provided in Chapter 3.

In order to size the sensors and motor needed for the model turbine, reasonable estimates of the range of forces, moments, and the rotor torque needed to be established. To do so extreme values of these reactions were taken from a suite of numerical simulations performed with the NREL 5 MW wind turbine mated to the ITI Energy Barge platform model (Jonkman, 2007). Simulations of the ITI Energy Barge floating wind turbine exhibited the highest internal force and moment reactions due to poor platform stability and excessive wave loads as compared to the OC3 Hywind Spar and MIT/NREL TL, (Jonkman & Matha, 2009). Thus, the barge internal reactions were used to identify appropriate instrumentation as the magnitudes of these reactions would have been the maximum expected during basin model testing. Table 2.3 shows the internal forces and moments at the tower top as well as the rotor torque at full and model scale used to appropriately select the model motor and sensors. Specifics on the sensors, motor, and controls utilized on the model wind turbine is discussed in Chapter 3.

Table 2.3. Maximum internal reactions of NREL's ITI Energy Barge at full and model scale, used to select model instrumentation.

Maximum Reaction	Full Scale	1/50th Scale
Rotor Torque	10,700 kN·m	1.710 N·m
Power	6.05 MW	6.84 W
Force – tower top – x (surge)	8,560 kN	68.5 N
Force – tower top – y (sway)	1,880 kN	15.0 N
Force – tower top – z (heave)	6,080 kN (compressive)	48.6 N (compressive)
Moment – tower top – x (pitch)	11,900 kN·m	1.90 N·m
Moment – tower top – y (roll)	38,900 kN·m	6.22 N·m
Moment – tower top – z (yaw)	21,600 kN·m	3.46 N·m

The values from Tables 2.2 and 2.3 provided the target parameters used to base the design of scale model wind turbine. Throughout the design process, these target design values remained constant and used to judge accuracy by which the model wind turbine emulated full scale characteristics. Many of these target values provided many technical challenges throughout the design process which is presented in the following chapter.

CHAPTER 3. MODEL WIND TURBINE DESIGN AND FABRICATION

This chapter details the design and fabrication of a 1/50th scale model HAWT

based on target parameters of the NREL 5 MW reference wind turbine established in

Chapter 2. In addition to meeting the target parameters that control global motions and

dynamic such as system mass, inertia, etc., this model design included a fully-functional

turbine and rotor with rotational speed and pitch control capability. The structure of this

chapter is as follows: key components and sensors located in or near the wind turbine

nacelle will be presented first followed by the design of the nacelle enclosures that

housed sensors and served as a connection point for the motor, turbine drive shaft, rotor,

pitch control components and tower. Selection of the blade pitch control equipment and

the final rotor hub design will then be presented followed by a description of the data

acquisition system and control software wired to the model wind turbine during basin

testing. A detailed description of the final blade geometry and wind blade fabrication

process developed to manufacture ultra light yet stiff composite model wind blades will

then be discussed. Finally, the final model tower design will be presented as well as final

adjustments and modifications made to the fully assembled model wind turbine.

3.1. NACELLE AND HUB

Similar to a typical full scale upwind HAWT, the model nacelle included the

enclosures/housings, sensors, components and motor assembly located at the top of the

tower and downwind of the wind turbine rotor. The hub provided a connection between

the blades and main drive shaft and was designed to incorporate pitch control. A major

design challenge was meeting the nacelle target weight of 1.92 kg model scale, which

needed to include the motor assembly, sensors, pitching mechanism, rotor drive shaft and supportive enclosures. Another challenge was meeting the hub weight requirement of 0.45 kg model scale. This section will present instrumentation selection, enclosure or housing design, pitch control design and rotor hub design.

3.1.1. Instrumentation and Housings

Considerations for selection of instrumentation included data input range and accuracy as well as physical size and weight of the sensor. Data necessary to collect during basin model testing included generated torque, rotor rotational position, nacelle accelerations and tower-top forces and moments. The model wind turbine was also designed to function as a fixed-speed, fixed-pitch machine. During model testing at MARIN the rotor speeds and blade pitch were set to prescribed values based on the wind environment being tested. To maintain rotor speed a small gearbox and servo-motor with an internal encoder was included on the model. The pitch control mechanism which could vary the blade pitch range approximately 90 degrees is detailed in the following section. The sensors and components chosen were compact, light weight and provided high resolution data rates. Sensors and components are identified in Figure 3.2 and additional information including individual weights can be found in Table 3.1. Further specifications are provided in Appendix A.

The nacelle enclosure was designed to satisfy the connection requirements for the selected sensors and components. The final nacelle enclosure consisted of two housings: the bearing housing and the torque tube as shown in Figure 3.1. The bearing housing, upwind of the torque tube, was designed to house the rotor position encoder and pitch actuator. The analog encoder was to be placed up-wind of the torque transducer to ensure

Table 3.1.   List of nacelle sensors and components with individual weights.

Component	Manufacturer	Mass (g)
MA3 Analog Encoder	US Digital	10
L12 Linear Actuator	Firgelli Inc.	34
T2 Precision Rotary Torque Transducer	Interface Inc.	180
6-Axis Force and Moment Sensor	Advanced Mechanical Testing Inc. (AMTI)	100
Gyro Enhanced Orientation Sensor (6-axis accelerometer)	MicroStrain	74
Parker Rotary Servo Motor	Parker Motion	712
20:1 Gearhead	Parker/Bayside	385

rotor position data was captured with little interference from the torque transducer. The

analog encoder was chosen due to its light weight and high resolution output, however

the single shaft design could not be placed directly on the main drive shaft. Therefore, the

bearing housing was designed to support the encoder externally while accommodating

1:1 acetyl miter gears to transfer the rotational speed from the main drive shaft to the

encoder as shown in Figure 3.1. In an effort to keep weight down, the bearing housing

was made of aluminum and four large holes were bored on each face parallel to the

centerline of the drive shaft to reduce weight. The downwind face of the bearing housing

hosted a welded aluminum flange to provide a mechanical connection to the torque tube.

The torque transducer required isolation from any axial, lateral or angular

motions which resulted in the unique housing for the sensor, coined the torque tube. The

stiff torque tube supported the torque transducer with bellows couplings to ensure clean

torque data was collected. As an extra precaution to protect the torque transducer from

thrust, thrust bearings and shaft collars were placed before and after the bearing housing

prior to the upwind bellows coupling.   The two shaft collars also held the rotor drive

Figure 3.1. Rendering of model nacelle and internal components with dimensions given at model scale.
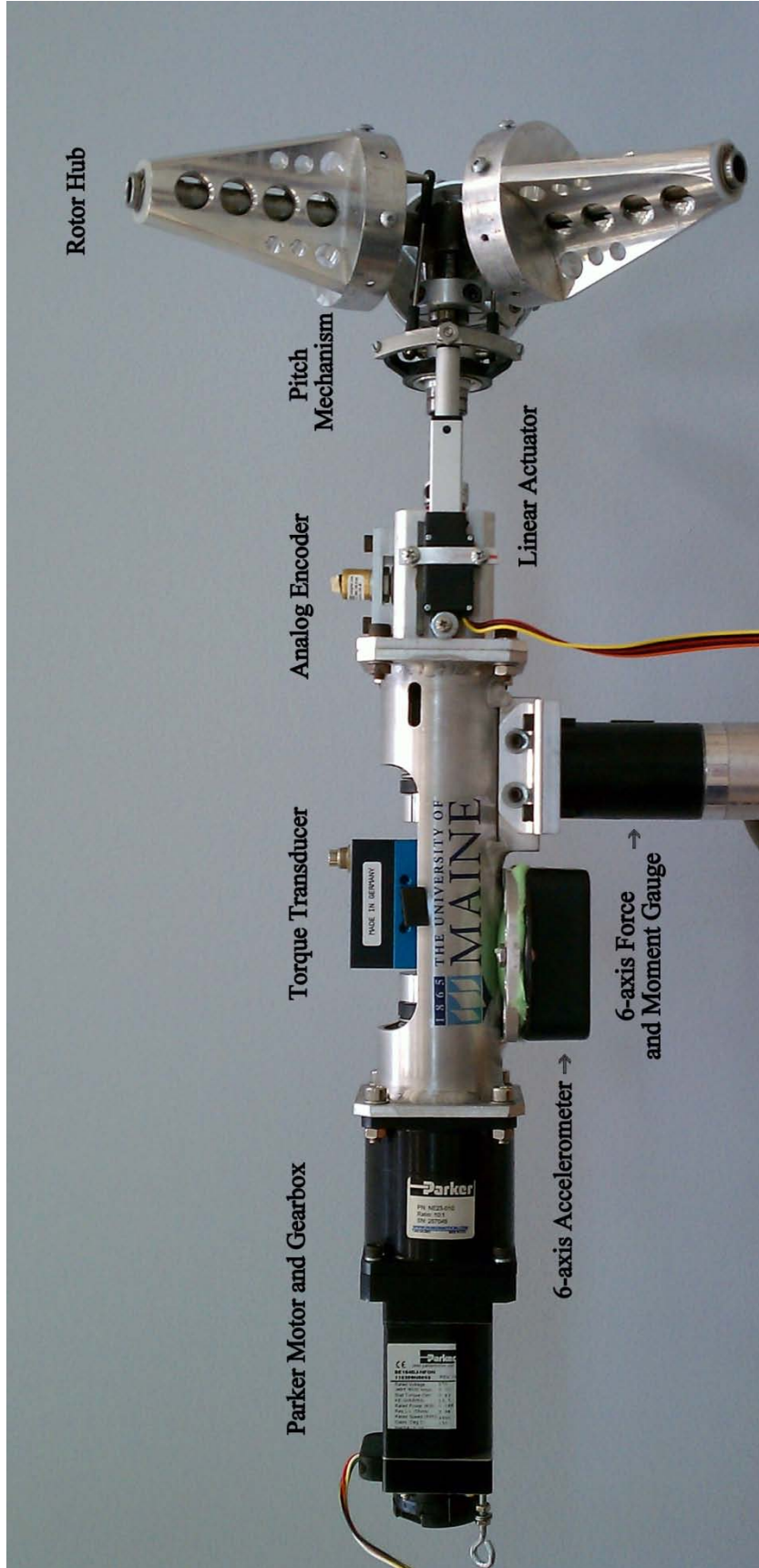
Figure 3.2.   Image of fully instrumented model nacelle.

shaft in place which facilitated mechanical disassembly and assembly of the unit. Internal bearings and couplings for the torque tube arrangement are shown in Figure 3.1.

The torque tube itself was designed as a hollow aluminum cylinder to house the torque transducer and bellows couplings and to ensure proper alignment with the motor and rotor drive shafts as well as provide a stiff and light weight enclosure. Aluminum flanges with bolt attachments were welded on either end of the torque tube to provide mechanical connections for the motor/gearbox combination and the bearing housing. Bolted connections were used throughout the model design, as opposed to welded or epoxy bonds, to allow for assembly and disassembly of the model nacelle and provided access to internal sensors components as needed. Detailed drawings of the bearing housing and torque tube can be found in Appendix B.

The nacelle's tower attachment point was located such that the vertical center line of the tower and 6-axis force gauge intersected the CG of the model nacelle along the drive shaft axis. Balancing the nacelle and rotor on the tower was important to ensure the entire model did not tilt due to weight imbalance when placed on a floating platform during basin model testing. Also, the nacelle and rotor were not angled atop the tower in the pitch axis during basin testing, as is often done in commercial wind turbines to facilitate greater blade to tower clearance. However if an angled nacelle and rotor is desired, the model could be easily modified to accommodate the change. The tower attachment bracket consisted of an aluminum channel with the web welded flush to the bottom of the torque tube and a set of slotted bolt holes in either flange. Two aluminum angles with standard bolt holes had one face mated with positioned with one face mated to either side of the channel and one face flush with the 6-axis gauge mouthing plate. The

channel slotted bolt holes allowed for lateral adjustment of the tower center line upwind and downwind of the nacelle.

3.1.2. Pitch Control

The ability to control blade pitch on the model wind turbine was important to more accurately model real wind turbine performance. For basin model testing at MARIN, remotely adjusting pitch between tests and fixing pitch during tests was the immediate goal. Remote pitch adjustment was desired as manual adjustment would disrupt the floating wind turbine test set up and take up valuable and costly time in the wave basin. Even though the model had remote adjustment of pitch between test the model was also designed to incorporate active pitch control for future model testing.

The pitch control assembly, shown in Figure 3.3, partially consisted of a L12 Firgelli mini linear actuator connected to a modified RC helicopter swash plate. The swash plate translated along the drive shaft with a retrofitted linear bearing and permitted independent rotation between the rotor and actuator with a ball bearing. The swash-plate outer bearing was connected to the linear actuator while the inner bearing was connected to three rigid links that spun in sync with the rotor. To remove rotational slack between the rotor and swash-plate inner bearing from the rigid link ball connections, a linkage arm was pinned to the hub shaft collar and the inner bearing. Each rigid link was connected to a ball pin on the bottom of each blade bearing cup as shown in Figure 3.3. As the swash plate actuated in a linear path along the main turbine shaft, the rigid links would translate the motion into an angular rotation to adjust the pitch angle on each blade equally. The radial position of the ball pin on the blade support hubs was chosen to ensure that the blades were able to pitch from zero to ninety degrees with the actuator
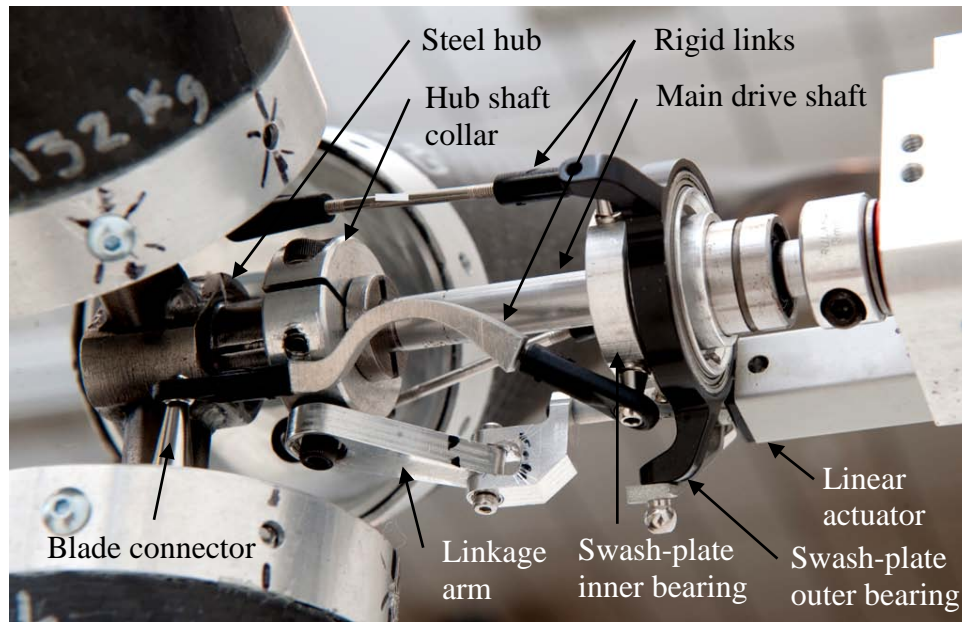
Figure 3.3.   Image of the pitch control assembly.

stroke length available. The blade pitch angle was calibrated with the linear actuator

stroke length prior to wind-wave basin testing. Pitch calibration consisted of measuring

blade pitch manually from the blade tip and correlating the angle with the stroke length of

the actuator. During basin testing, a certain pitch angle was reached by commanding the

actuator to a certain stroke length using the information established from pre-basin testing

calibration.

The pitching mechanism was successful for the purpose of this basin model test

program, however it is important to note there were difficulties with this pitch design.

Due to extensive testing, the small actuator did experience difficulties resisting thrust

loads on the wind blades. A small plastic female sleeve for the actuator worm gear

deformed during testing and caused slack in the system. Due to the created slack the

actuator needed to be fully retracted and then actuated in the upwind direction for every

pitch adjustment to remove slack and to ensure the correct pitch angle was achieved.

Also, the small rigid links between the swash plate and blade ends were not as durable as

desired. In general, it is recommended this pitch mechanism design be revisited and improved for future testing, especially if active pitch control is pursued.

3.1.3. Rotor Hub

The model rotor hub supported three model blades and permitted each blade the freedom of rotation about each blade pitch axis. The rotor hub consisted of three aluminum bearing cups, three hollow steel rods, and a steel central hub as shown in Figure 3.4. Steel was chosen for the rods and hub to provide extra rigidity while aluminum was chosen for the bearing cups to reduce weight. The steel hub incorporated a female connection to the rotor drive shaft and was fixed with an aluminum shaft collar as shown in Figure 3.3.
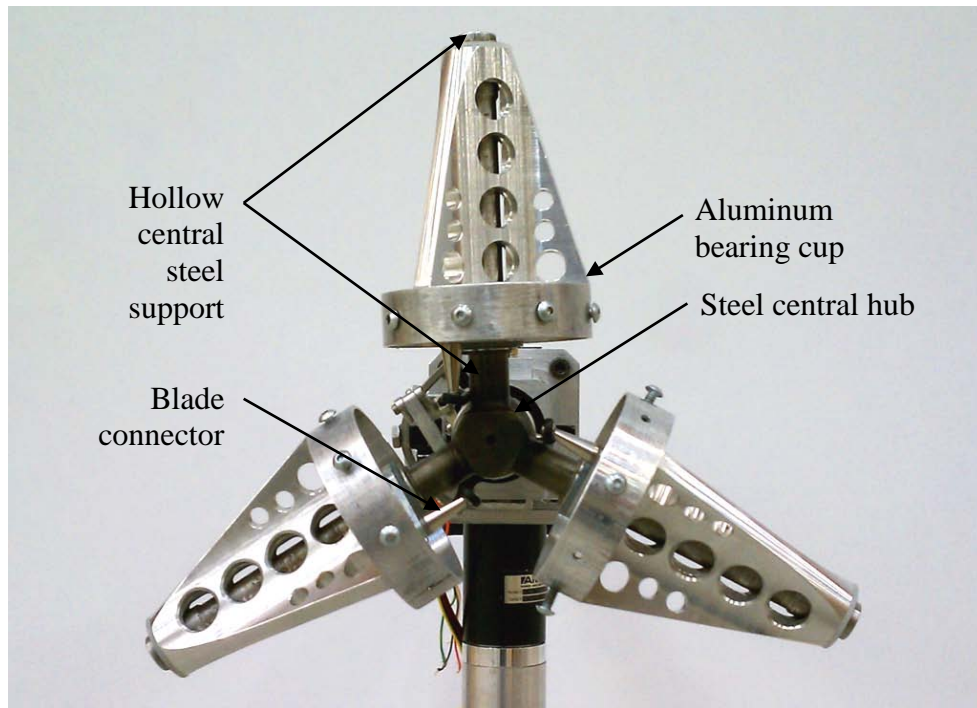
Figure 3.4. Image of the rotor hub.

Each bearing cup was held on the hollow steel supports with retaining rings positioned above and below the cup. Nylon flanged bushings provided a bearing surface

42

between the bearing cups and the steel supports to allow for low friction rotation about the blade pitch axes. The base of each bearing cup included a blade connector for the attachment of the rigid links connected to the inner bearing of the swash plate. The large outer diameter of the bearing cup was designed to fit tightly within the composite blade root end with allowances for blade base aluminum band thickness and blade material thickness. Specifics on the blade material composition will be discussed in Section 3.3. Detailed drawings of the rotor hub are provided in Appendix B.

3.1.4. Mass

The final masses of the model nacelle and hub are listed in Table 3.2. The nacelle mass includes hardware, enclosures, the motor assembly, pitch control components, and sensors excluding the 6-axis force gauge. The 6-axis force gauge is included in the mass distribution of the tower . The hub mass includes the hub assembly described previously.

Table 3.2. Final mass of model nacelle major components, excluding blades.

Component	Full Scale Mass (kg)	1/50th Scale Mass (g)
Nacelle	274,900	2,200
Hub	72,880	583.0
Total	347,800	2,783

The final total nacelle and hub mass was higher than the target sum mass of 296,780 kg given in Table 2.2. At model scale, the final nacelle mass was 2.78 kg which was found to be acceptable after removing all excess material possible and considering the amount of equipment and capability included in the nacelle. To accommodate the heavy nacelle, alterations were made to the final tower design and are detailed in section 3.4.

3.2. DATA ACQUISITION AND CONTROLS

All data acquisition hardware and controllers were fastened in an industrial control panel enclosure, or control box, separate of the floating model. Major equipment consisted of a power supply, a data acquisition system, motor controller, and pitch actuator circuit board. Figure 3.5 labels the major components of the control box. Further details on the control box hardware can be found in Appendix A. UMaine and MMA collaborated to select the hardware and controllers while R.M. Beaumont Inc. built and wired the control box.

Data acquisition
4-slot Chassis
and input
modules

Rhino 24 V,
5 V, and 12 V
Power Supply

Merlin Gerin
Protection
Circuit Breaker

Copley Xenus
XTL Digital
Servo Drive

EMI Filter

Linear
Actuator
Control Circuit
Board
(Encased)

Power switch
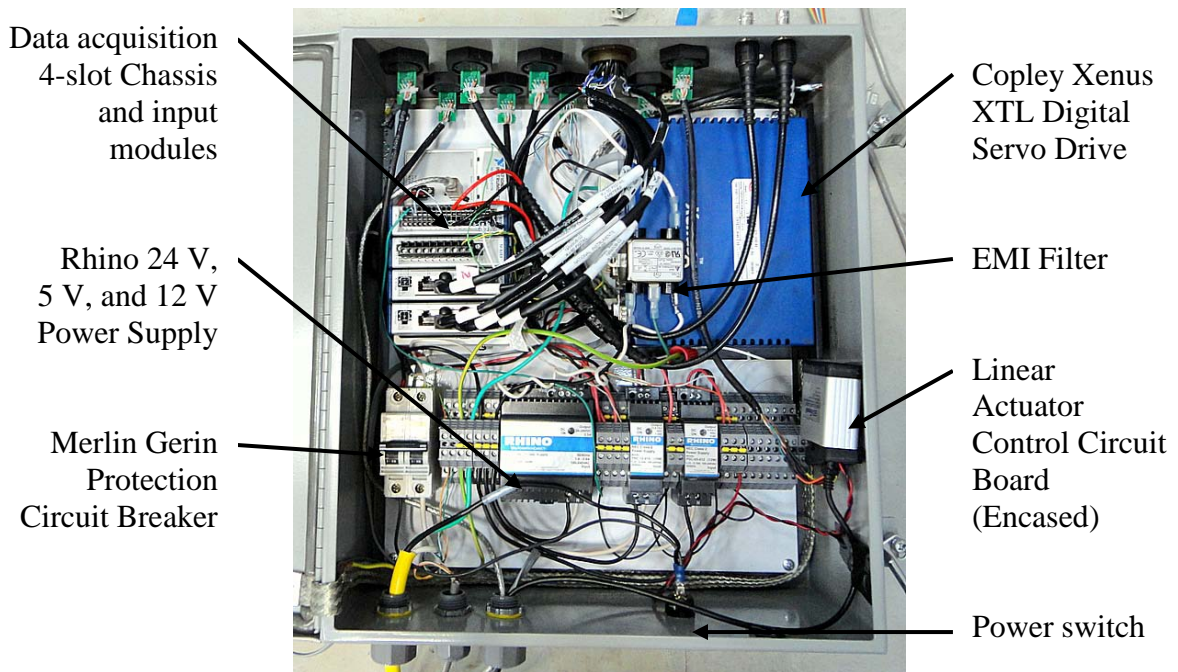
Figure 3.5. Control box with data acquisition and control equipment.

The torque sensor, 6-axis force gauge, accelerometer, analog encoder and linear actuator were connected to the control box via CAT5e shielded cable. The motor was connected by 4-wire cable with braided shielding. The selected cabling worked appropriately for transmitting signals, however the cables selected were physically robust adding unwanted stiffness and mass to the system. To correct for cable addition, the

cable stiffness was quantified from data collected from basin tests and will be included in later numerical code validation efforts. While the cables worked adequately for basin testing it is recommended that slender, flexible basin specific cables be identified as early as possible in the development of a scale model to maximize test quality.

Cables included along model tower.
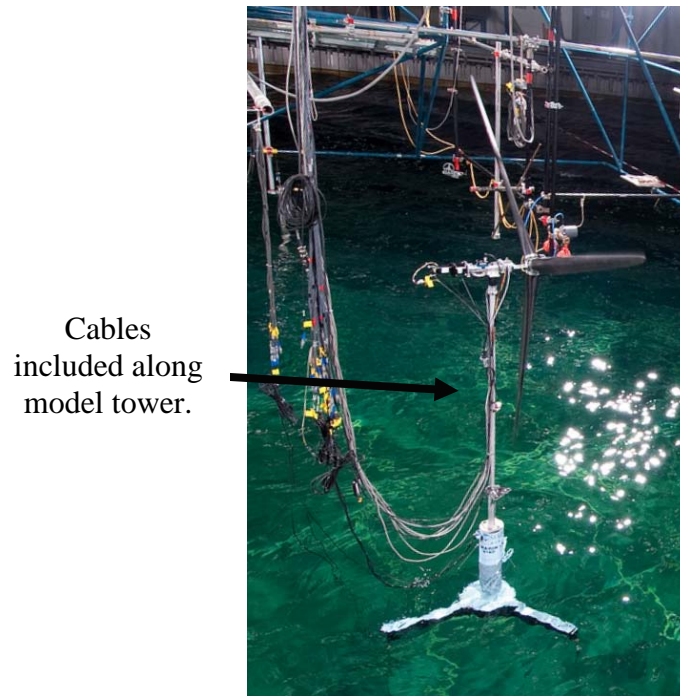
Figure 3.6.   Image of cabling from the floating wind turbine model to the basin carriage.

Labview was used to collect, filter, and record data from the NI CompacDAQ data acquisition chassis as well as send command signals through the DAQ to the Copley motor controller. The Copley Xenus motor controller maintained an RPM set-point by changing the input power to the motor based on feedback from the motor position encoder. The controller accepted a RPM set-point from an analog command signal. The controller was configured to accept a command signal from ±10 V, where 0 V = 0 RPM, and ±10 V = max rated RPM, in opposite directions. The NI9263 output module sent the analog controller command signal based on the slider setting in a custom VI. The pitch linear actuator was controlled by a separate computer program, Firgelli's LAC

Configuration Utility (2011). A screen shot of the Labview VI is shown in Figure 3.7.

R. M. Beaumont Corp. wrote and calibrated the Labview interface with all hardware.

Figure 3.7.   Labview GUI for data acquisition and controls.

The control computer running Labview and the LAC utility was positioned near

the control box on a basin carriage near the floating model to reduce the length of the

USB connection. User control was performed in the basin control room approximately 20

m away from the control box and basin carriage. This was facilitated with an Ethernet

cable that ran from the main computer to the control room computer to allow for Remote

Desktop control of the main computer. This set up allowed the data acquisition system to

be close to the model without lengthening sensor and power cables.

Data was collected from the turbine and platform instrumentation in parallel by

UMaine and Marin respectively. To synchronize the two data streams, a simple 0-5 V

saw-tooth signal was generated by Marin and collected by both systems in addition to a

start and stop signal. A more robust challenge was removing noise and interference

46

between the Marin and UMaine electrical systems. Electromagnetic interference (EMI) generated in the sensors by the motor was eliminated by connecting the motor Copley Zenus motor controller, shields, and enclosure to earth ground with a flat braided grounding strap. In addition, high-density polyethylene (HDPE) washers and sleeves were used to electrically isolate Marin sensors from the motor chassis. Finally, a line filter was used to eliminate noise on the 220 V/50 Hz supply to the Copley Xenus. Once the systems were collecting data cleanly all data acquisition ran smoothly for the full five weeks of the test program. For simplicity a single data acquisition system is recommended for future tests to reduce set-up time and ease troubleshooting and calibration complications.

3.3. BLADE DESIGN

The model blade geometry and mass properties are based on the NREL 5 MW reference wind turbine blade. Accurate representation of the full scale blade geometry was chosen due to initial views that alteration of the geometry would come under scrutiny from the wind turbine scientific community. Scaled mass properties were maintained to capture proper inertial and gravitational effects during wind/wave basin model tests. The following sections detail the formation of the blade geometry, structural design, fabrication method and qualitative analysis of structural response.

3.3.1. Geometry

The model blade is a geo-sim, or a geometric copy, of the 5 MW NREL reference wind turbine blade. A geo-sim from full to model scale was chosen as the NREL blade geometry was publicly available and utilized for simulations in the NREL coupled

floating wind turbine simulator. This allowed for a greater impact of the floating turbine tests on the scientific community as this particular blade geometry was familiar to many in the floating wind turbine research field. However, gathering blade geometry data was not entirely straightforward as the NREL blade was well documented with regard to aerodynamic characteristics, yet there were information gaps related to the physical blade geometry. Much of the blade geometry work involved finding valid information from appropriate sources, such as Delft University (Timmer, 2009), and using appropriate interpolations to generate an accurate and fair wind blade.

Information used from the NREL 5 MW wind turbine documentation (Jonkman, et al. 2009) included the hub and rotor diameters, chord length, c, blade section structural twist or pitch angle distribution, θ_p, and airfoil type distribution along the blade span. At model scale the rotor diameter, D_r, was 2.52 m and the hub diameter, D_h, was 0.06 m yielding a model blade length at 1.23 m model scale or 61.5 m full scale. Information on blade tip geometry beyond 61.33m from the hub center was not specified except for section pitch angle. Aside from the cylindrical blade root all non-dimensional 2D airfoil geometries and blade pitch axis locations were obtained through other sources and is detailed in following paragraphs.

All DU and NACA 64-618 airfoil surface coordinates were shared by Delft University (Timmer, 2009) as Cartesian coordinates. An iterative numerical method, illustrated by a flow chart shown in Figure 3.8, was used to calculate mean-line and thickness information from each airfoil as only the Cartesian surface coordinates were available. Airfoil mean-line and thickness information allowed for thickness adjustments as needed without severely disrupting the aerodynamic properties of the airfoils.
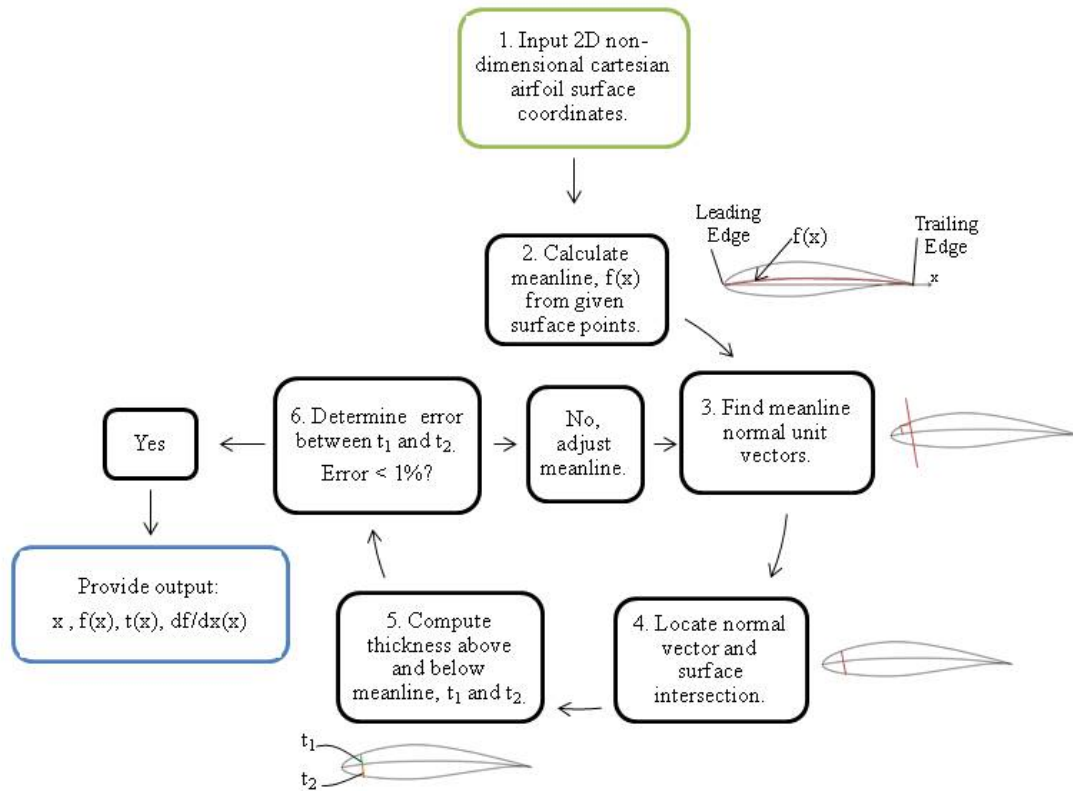
Figure 3.8. Flow chart of iterative method used to determine 2D airfoil geometry.
Adjustments to thickness necessary for creating a manufacturable blade geometry,
especially near the trailing edge are discussed below. There were 200 sets of Cartesian
surface points for the NACA 64-618 airfoil and 400 sets for the DU airfoils. To reduce
upload time and processing power needed to generate a digital model blade surface, 25
sets of mean line and thickness data was generated per airfoil. Cosine spacing along the
airfoil chord length was used to preserve curvature at the leading and trailing edges. The
resulting non-dimensional meanline and thickness data sets and plots for each airfoil can
be found in Appendix C.

The final geometry of the NREL 5 MW blade is provided in Table 3.3 in non-
dimensional terms. Information provided in Table 3.3 includes all interpolations and

Table 3.3.   Final non-dimensional geometry of NREL 5 MW reference wind blade.

Source	Section Number	Airfoil	r/R	c/D	θ_p	t/c	x_p/c
NREL documented sections	1	Cylinder1	0.024	0.028	13.308	1.000	0.500
	2	Cylinder1	0.031	0.028	13.308	1.000	0.500
Extracted sections from UCDavis model.	3	Cylinder2	0.054	0.029	13.302	0.930	0.478
	4	Cylinder3	0.088	0.031	13.308	0.780	0.449
	5	Cylinder4	0.137	0.033	13.308	0.610	0.423
NREL documented sections	6	DU 40	0.187	0.036	13.308	0.477	0.375
	7	DU 35	0.252	0.037	11.480	0.383	0.375
	8	DU 35	0.317	0.035	10.162	0.331	0.375
	9	DU 30	0.382	0.034	9.011	0.290	0.375
	10	DU 25	0.447	0.032	7.795	0.260	0.375
	11	DU 25	0.512	0.030	6.544	0.238	0.375
	12	DU 21	0.577	0.028	5.361	0.219	0.375
	13	DU 21	0.642	0.026	4.188	0.202	0.375
	14	NACA 64-618	0.707	0.024	3.125	0.180	0.375
	15	NACA 64-618	0.772	0.022	2.319	0.180	0.375
	16	NACA 64-618	0.837	0.020	1.526	0.180	0.375
	17	NACA 64-618	0.892	0.018	0.863	0.180	0.375
	18	NACA 64-618	0.935	0.017	0.370	0.180	0.375
	19	NACA 64-618	0.978	0.011	0.106	0.180	0.375
Interpolated sections (tip geometry)	20	NACA 64-618	0.983	0.010	0.082	0.180	0.375
	21	NACA 64-618	0.988	0.009	0.060	0.180	0.375
	22	NACA 64-618	0.992	0.008	0.040	0.180	0.375
	23	NACA 64-618	0.995	0.006	0.023	0.180	0.375
	24	NACA 64-618	0.998	0.005	0.010	0.180	0.375
	25	NACA 64-618	0.999	0.003	0.003	0.180	0.375
	26	NACA 64-618	1.000	0.002	0.000	0.180	0.375

extrapolation information discussed in subsequent paragraphs. The non-dimensional terms detailing the blade geometry consist of the local radius over total rotor radius, r/R, airfoil chord length over total rotor diameter, c/D, airfoil structural twist angle, θ_p, maximum airfoil thickness over airfoil chord length, t/c and airfoil pitch axis location over airfoil chord length, x_p/c.

Another useful source of information was the UC Davis NREL 5 MW 3D surface plot (van Dam, 2010). This accurate surface plot was not solely used as the model blade basis due to unrealistic sharp trailing edge geometry and an inability to easily control airfoil thickness adjustments. However, three UC Davis airfoil sections between the circular blade root and first DU airfoil, DU40, were extracted from the UC Davis plot and used in the final model blade geometry. These sections, though different, are labeled as Cylinder2 through Cylinder4 in Table 3.3. These sections are named as such since the model for the NREL 5 MW wind turbine models this section aerodynamically as a cylinder, even though the geometries are not cylindrical. These three sections were used over this particular region to ensure accurate geometry was preserved between the cylindrical and airfoil sections near the blade root. The UC Davis blade was also used to numerically extract airfoil blade pitch axis locations, x_p/c. Extracted values for the pitch axis location were found to be very similar to the DOWEC 6MW blade pitch axis (Kooijman, et al. 2003), which formed the basis of the NREL 5 MW reference wind blade. The final blade pitch axis values are detailed in Table 3.3.

The chord length and structural twist angle of the blade tip sections 20 through 28 of Table 3.3 were extrapolated. A quadratic curve was used to generate the tip chord distribution to create a rounded blade tip as shown in Figure 3.9. Tip structural twist

angles were interpolated from the NREL structural twist distribution using a cubic

hermite interpolating polynomial (Lancaster & Šalkauskas, 1986). The structural twist

interpolation is illustrated in Figure 3.10. Matlab scripts and functions used to determine

the tip chord and structural twist distributions are located in Appendix C. Through

visual inspection of prototype, 1/130th scale 3D printed blades, it was found that the

original blade thickness distribution as computed from the NREL 5 MW Reference

turbine documentation did not result in a fair, or smooth, blade. Therefore, the final blade

thickness distribution was smoothed using another cubic hermite interpolating
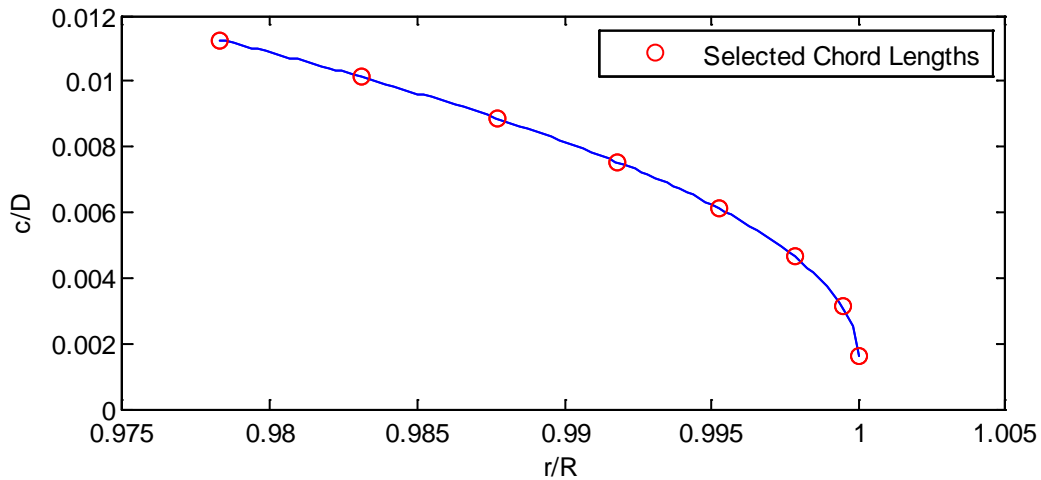
Figure 3.9. Quadratic tip chord distribution.
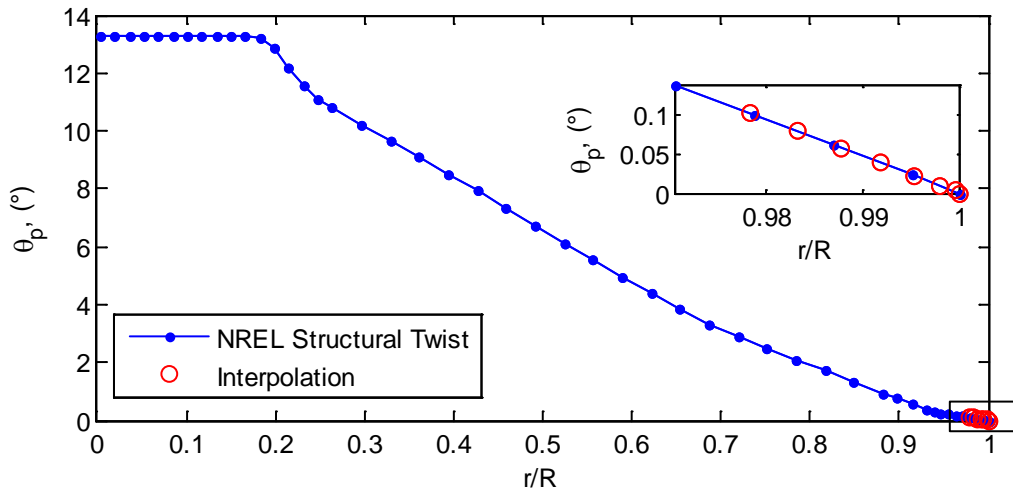
Figure 3.10. Blade structural twist distribution and tip section interpolation.

52

polynomial to obtain a fair blade. Figure 3.11. shows the original thickness distribution

of the NREL blade and the smoothed thickness distribution. Figure 3.11 does not

incorporate trailing edge thickness adjustments which are discussed in the following

paragraph. The smoothed thickness distribution was reviewed and deemed suitable by

NREL research staff and used for the final blade geometry. The thickness smoothing

scripts made with Matlab and inputs can be found in Appendix C.
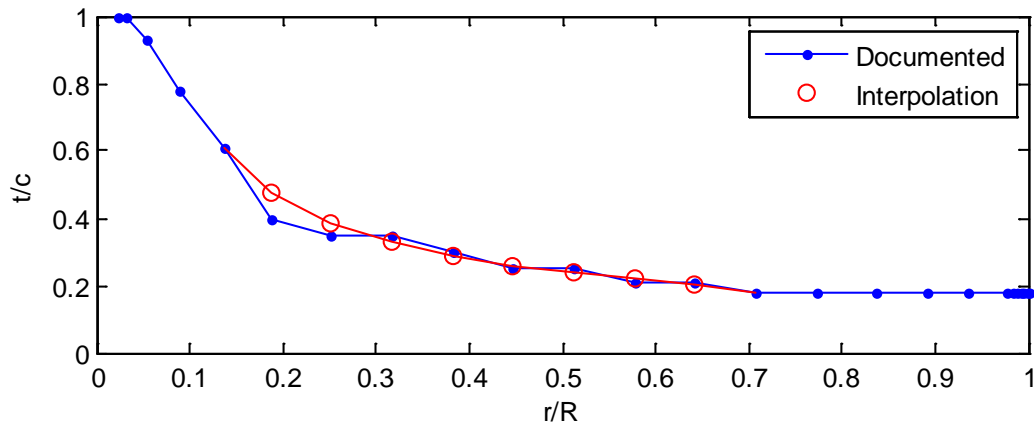
Figure 3.11.   Comparison plot of documented and smoothed blade thickness distribution.

A uniform trailing edge thickness along the blade length was incorporated into the

final geometry as the NACA-64-618 airfoil and DU airfoils possessed sharp trailing

edges making 3D surface generation difficult and model blade fabrication infeasible.

Therefore, a wedge technique was used to increase the thickness of each airfoil linearly,

starting with zero thickness at the leading edge and increasing to maximum thickness at

the trailing edge. The wedge technique allowed increase in trailing edge thickness while

preserving airfoil surface geometry. A thickness of 2 mm was estimated prior to blade

composite material selection to allow for two layers of composite material to meet at the

trailing edge. The trailing edge thickness of blade tip sections were slightly decreased

from the uniform trailing edge thickness in an effort to preserve the small tip airfoil

section geometries. Figure 3.12 shows the blade airfoils sections with structural twist angles of zero to clearly show the uniform trailing edge thickness along the blade length. The final non-dimensional airfoil thickness values, *t/c*, including smoothed thickness and trailing edge thickness are listed in Table 3.3.
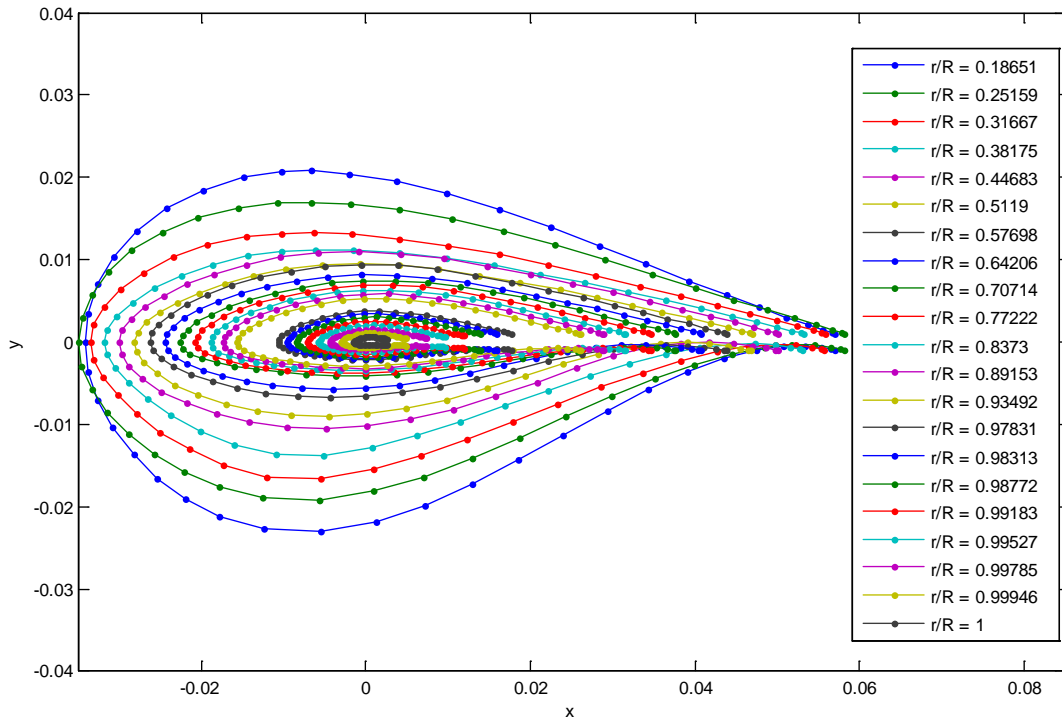
Figure 3.12.   Uniform trailing edge thickness of airfoils along blade span without incorporating structural twist.

Combining all the resources and interpolations previously described resulted in a fair and constructible 1/50th scale NREL 5 MW wind blade, shown in Figure 3.13. OpenProp, an open-source propeller and turbine design software suite (Epps & Kimball, 2010) was used as a guide to write a source code for generating the final blade surface coordinates with all interpolations and thickness adjustments incorporated. MATLAB was used for all interpolation functions and to write all parts of the blade input file needed to create a 3D blade surface in Solidworks (2010). The blade sections were assembled manually to create the final blade input file, SWBladeInput.txt whereas a

SolidWorks import macro available with OpenProp was used to create the 3D blade

surface. Figure 3.13 is a rendering of the final SolidWorks model with called out section

numbers. The geometry generating source code and the final blade input file can be

found in Appendices C.2 and C.3 respectively.
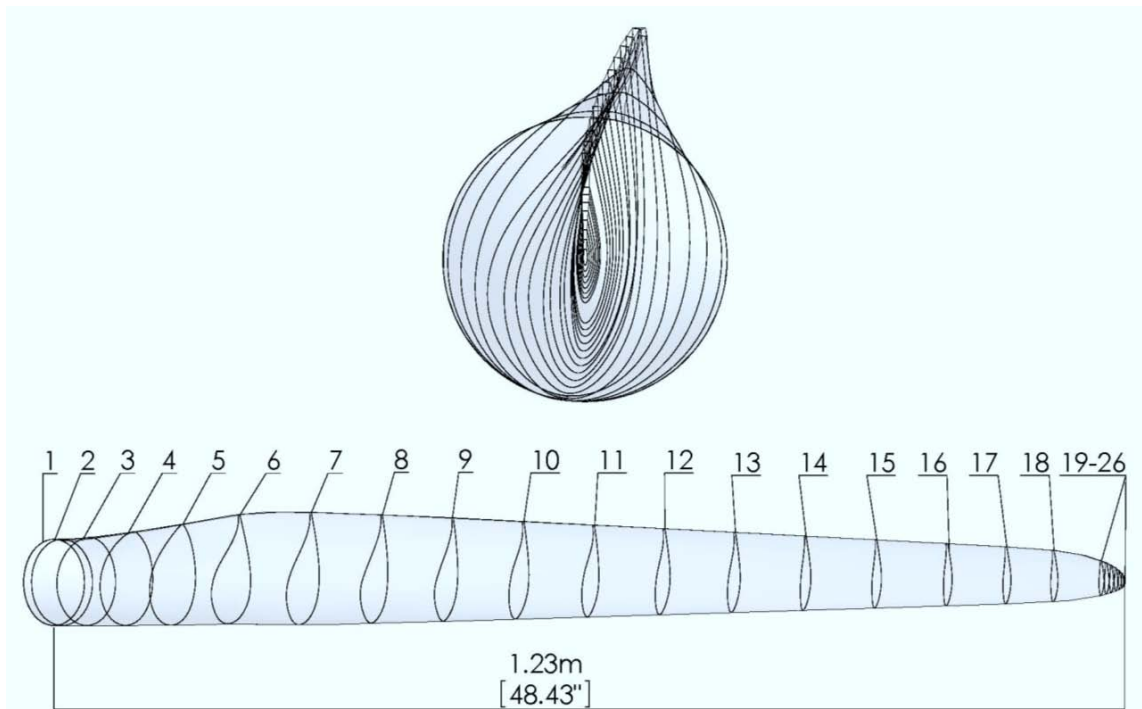
Figure 3.13.   3D rendering of final model blade with sections number in accordance with Table 3.3. Dimensions are model scale.

Throughout the design process, several iterations of the NREL blade were built in

SolidWorks and 3D printed for visual inspection. Most of the interpolations, such as

smoothing of blade thickness were incorporated after these inspections were done. The

SolidWorks model was also used for fabrication of the 1/50th scale clam shell mold used

for composite blade fabrication presented in section 3.3.3.

3.3.2. Structural Analysis

As a precursor to basin model testing, a basic structural analysis was performed

on the composite model blade to ensure low stresses and small deformations would occur

during basin model testing. In addition to ensuring blade strength, elimination of blade

flexibility was desired to reduce the number of variables in model testing. The analysis

to confirm design objectives were met was performed with the loading conditions of a

modified scaled extreme environmental condition. A simplistic loading scenario in the

flap-wise direction (perpendicular to the chord length of the tip airfoil section) was used

as it would produce the largest deflection estimate. This was deemed sensible since the

aerodynamic loads on a wind turbine blade are oriented such that their primary effect is

flap-wise bending. In addition, the area moment of inertia along the blade length in the

flap-wise direction is much less than the edge-wise direction, (except at the blade root)

and therefore flap-wise deflection was considered critical. In an effort to get an estimate

of the blade deflection, a simple cantilever bean analysis using Euler-Bernoulli beam

theory, was performed to estimate maximum stress and deflection as a function of span.

This analysis was performed on a simplified version of the blade geometry, where there

was no structural twist of blade sections along the blade span as shown in Figure 3.11 and

airfoil camber was removed such that the product inertia of the sections were zero.

Nonetheless, the blade geometry was non-prismatic resulting in the use of equations 3.1

and 3.2 from Gere (2006), to perform the analysis.

$$\sigma(x) = \frac{M(x)y(x)}{I(x)}, \tag{3.1}$$

$$u(x) = \iint \frac{M(x)}{EI(x)}. \tag{3.2}$$

The moment as a function of span, $M(x)$, was modeled linearly where maximum

moment occurred at the fixed blade root and there was zero moment at the blade tip. This

bending moment distribution corresponded to a point load at the tip of the cantilever

beam which was not necessarily representative of a realistic wind turbine loading

scenario. However, this approach was conservative and placed a greater internal bending

moment in the outer half of the blade span than would normally be achieved in a real

loading scenario. As the outer sections were the thinnest, they were the most flexible and

yielded larger axial stresses for a given internal moment compared to the thicker, more

robust inner foil sections. For this particular analysis, a maximum blade root moment of

5.44 Nm was used which was scaled down from a full scale maximum blade root moment

of 34,000 kN·m computed from an extreme condition simulation of the NREL 5 MW

reference wind turbine supported by the floating ITI Energy barge (Jonkman, 2007).

Similar to scaled maximum internal forces and moments discussed in section 2.2, results

from the ITI Energy Barge were used as this platform was found to have the worst

performance in fully-coupled simulations of any previously conducted floating wind

turbine foundation concepts, the others being the OC3 Hywind Spar and the MIT/NREL

TLP (Jonkman & Matha, 2009). Therefore, a maximum blade root moment of 34,000

kN·m was seen as very conservative as each of the actual platforms tested in this program

were more refined and better performing than the ITI Energy Barge. The area moment of

inertia, $I(x)$, and the largest distance to the neutral axis, $y(x)$, were based on the simplified

blade geometry described previously with wall thickness equal to 0.55 mm, the

measured final thickness of the model composite blades discussed in the subsequent

section.

The analysis showed the model blade reactions under scaled extreme conditions

to be minimal. The maximum stress located at r/R = 70.7%, or 0.86 m model scale, from

the blade root was 8.55 MPa, which was 0.016% of the Sprint ST-94 compressive

capacity of 53 GPa. The maximum blade deformation at the tip was found to be 5.5 mm

model scale or 0.28 m full scale assuming an axial material modulus of 54.12 GPa, as

given in Table 3.4. The predicted maximum deflection was only 2.0% of the maximum

blade deflection of 13.9 m determined from a fully-coupled simulation of the ITI Energy

barge under sea-state conditions, (Jonkman, 2007). These results gave confidence that the

model blade was very stiff and would easily resist loading during basin model testing.

Therefore, the model blade was predicted to have more than enough strength to resist

failure during basin testing and that deflections during basin testing would be negligible.

To verify the structural analysis results presented here, a point loaded cantilever bending

test was conducted on a model wind blade. The test procedure and a discussion of results

are presented in Chapter 4.

3.3.3. Structural Design and Fabrication

The focus of the model blade structural design was to achieve a very light wind

turbine blade while building a structure that replicated the complicated blade geometry

outlined in section 3.3.1. Due to the strict weight requirement, material choice quickly

steered towards a carbon fiber epoxy resin composite with very light and stiff material

properties. Early in the design process it was decided to not scale blade stiffness.

Scaling blade stiffness would have been extremely challenging due to difficulties with

simultaneously sourcing materials with appropriately scaled stiffnesses that would

emulate full scale construction architectures and fit the target weight budget. Also, as

mentioned previously, manufacturing a stiff blade in lieu of a flexible one reduced the

number of variables to consider during basin model testing. In addition, capturing global

performance was the main priority over blade deformation, rotor dynamics, and higher-

order aeroelastic effects. The chosen material for blade layup was Sprint ST-94/RC200T

(Gurit, 2011), a pre-pregnated woven carbon fiber resin epoxy composite. The material

properties for the chosen composite is given in Table 3.4. This material was selected as it

was designed specifically for composite mold fabrications and its material properties fit

the light weight and high stiffness requirements required of the model blade.

Table 3.4.   Mechanical properties of blade composite material, Sprint ST-94/RC200T.

Material Property	Value
Composite Weight	0.200 kg/m2
Fiber Volume Fraction	0.44
Cure Ply thickness	0.253 mm
Tensile Modulus	54.12 GPa
Compressive Modulus	53.04 GPa
In-Plane Shear Modulus	3278 MPa
Longitudinal ILS Modulus	2980 MPa

Based on a 1/50th scale SolidWorks model of the wind blade described in section

3.3.1, the blade surface area was found to be 0.19 m^2 . Using the surface area and the

composite weight listed in Table 3.4, it was found that two layers of Sprint ST-94

creating the blade surface shell would result in a blade mass under 0.10 kg and

undershoot the target scaled mass of 0.14 kg per blade. A lighter blade was ideal as this

weight allowed room for additional material in complex hub components of the model.

A bladder-mold fabrication method (Lokocz, 2010) was used to build a hollow

carbon fiber model wind blade. The final 1/50th scale SolidWorks blade model was

inverted to design a complex clam-shell aluminum mold containing the model wind blade

profile as shown in Figure 3.14. The mold consisted of three major components: the

major clam-shell halves containing the blade profile, two end plates to close the mold

root end, and a full end plate with an air connection adapter.   Much of the mold design

and all machine tooling was done by the Advanced Manufacturing Center at UMaine.
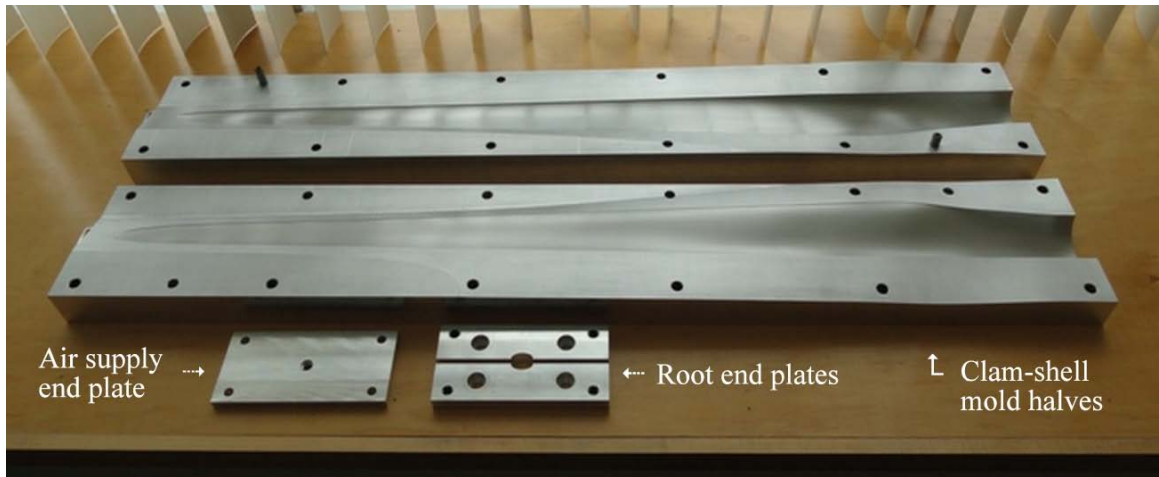
Figure 3.14.   Model blade mold components.

Prior to blade fabrication, the newly-made clam-shell blade mold was treated with

a Frekote Mold Release system (Henkel, 2010) which allowed for the clean removal of a

cured blade. The fabrication procedure is illustrated in Figure 3.15 with the images

numbered by order of operation. Image 1 shows two layers of Sprint ST-94 that were cut
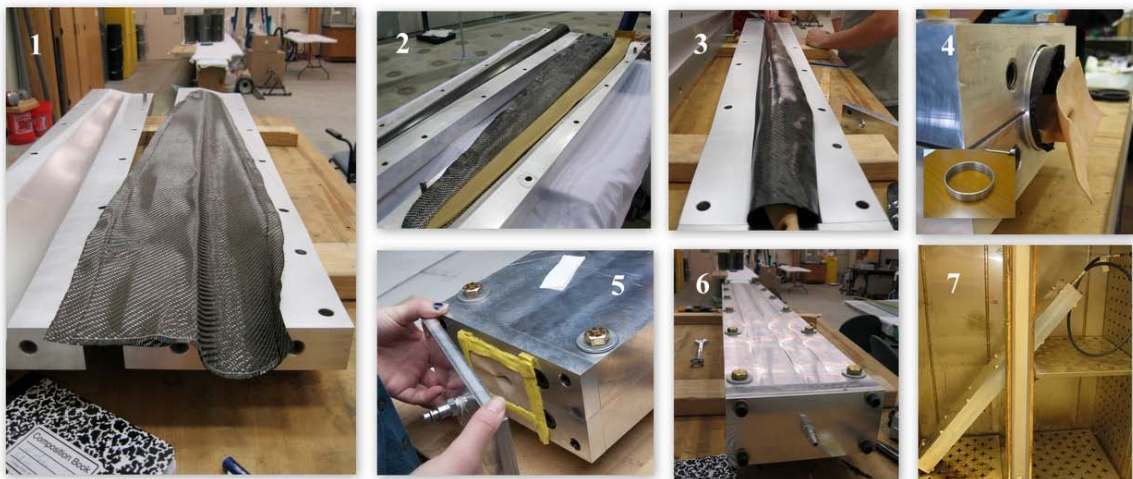
Figure 3.15.   Fabrication procedure for model blade fabrication.

to size and laid one after another in one half of the clam-shell mold's blade profile. Each

layer was cut to start at the trailing edge, wrap around the leading edge and meet back at

the trailing edge along the blade length yielding only one material seam along the trailing

edge. The two laminate layers were oriented in the same manner such that the fibers were

parallel and perpendicular to the flat blade root end as shown in Figure 3.16. In common

composites terminology, the 0/90 woven fabric laminate lay-up can be represented as

$[0/90]_{2f}$.
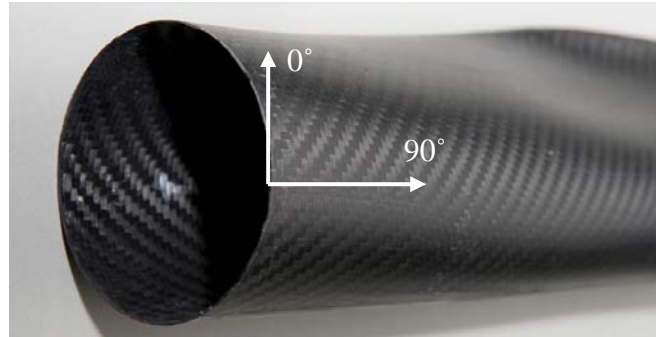
Figure 3.16. Blade laminate orientation.

Referring back to Figure 3.15, a custom latex bladder sized to fit inside the blade

profile and manufactured by Piercan USA Inc. (2010) was then laid on top of the open

composite laminates shown in image 2. The laminate layers were then folded over the

bladder and sealed along the trailing edge as shown in image 3. The second mold half

was then placed on top of the composite/bladder envelope and bolted down. Image 4

shows a 1 mm thick by 1.5 cm wide aluminum ring being slid into the open root end of

the mold with the laminate located between the ring and bladder. The aluminum ring was

machined to closely match the diameter of the blade end designed to provide a rigid

attachment point at the blade root. A set of end plates were then bolted onto the open end

of the mold to close the mold and provide a flush face for the blade root to but up against

while curing. Image 5 shows the end plates bolted to the mold with yellow adhesive

which secured the bladder flange and sealed the air connection once the outer end plate,

with an air supply valve, was attached. The fully closed mold is shown in image 6. After the air connection was inspected and found sealed the mold was then cured for 12 hours at 85 ˚C.

After cure completion the air supply was disconnected and mold allowed to cool. Once the mold was at handling temperature, the end plates were removed and the bladder released. The mold halves were then separated with the built in pry bolts and the blade released. After removal, excess resin and carbon was removed from the blade via scouring and sanding. Finally, through holes were drilled in the blade root aluminum band which allowed for a bolted blade to hub connection. A completed blade is shown in Figure 3.17.

Figure 3.17.   Carbon fiber model blade.

The bladder-mold fabrication procedure proved to be very successful.   Fifteen of nineteen blades produced possessed complete and fair geometries. Out of the fifteen, the average blade weight was 0.130 kg model scale or 16250 kg full scale undershooting the full scale target mass of 17740 kg. The lighter blades helped to reduce the mass of the entire wind turbine model which was beneficial due to the higher weight of the nacelle design and additional mass from data cables, as will be further discussed in Chapter 4.

3.4. TOWER DESIGN

The model tower was designed with intentions of emulating the dynamic behavior of the OC3 Hywind tower (Jonkman, 2010) which is 10 m shorter than the NREL 5 MW

reference wind turbine tower (Jonkman, et al., 2009) . The designs of the TLP, spar-buoy

and semi-submersible platforms each possessed 10 m of freeboard to ensure the rotor

centerline sat at 90m above the SWL for all three platforms.

Through preliminary tower design efforts it was clear that achieving all scaled

structural and dynamic parameters for the model was extremely difficult. Composite

fiber-reinforced nylon was found to have the necessary scaled stiffness, however

extrusion of a custom sized, hollow, non-tapered tower would have been time consuming

and expensive. Therefore, certain tower properties and considerations were prioritized

over others to achieve the most important tower characteristics that would ensure that the

tower emulated the full scale tower dynamic response. These parameters were prioritized

as follows:

1. Length

2. Tower mass

3. First natural bending frequency & mode shape

4. Center of gravity

5. Ease and cost of fabrication

As the overall mass of the entire wind turbine model was considered critical

compared to the individual tower mass and the nacelle and rotor final masses were

already deemed to be as light as possible, the target tower mass was reduced in order to

accommodate the over-weight nacelle. The target tower mass was reduced from 2.0 kg

listed in Table 2.1 to 1.12 kg in order to meet an overall wind turbine mass of 4.80 kg.

The tower material selected was aluminum due to its relatively low cost, light

weight and low stiffness; each of these traits being desirable for the scale model

construction. To determine the final design the tower height was fixed while an iterative method was used to size the tower diameters to achieve the target mass and CG. The tower diameter sizes were chosen from readily available aluminum tubing sizes to lower cost of fabrication. Once a sample design was established, the 1st bending frequency and the associated mode shape were found and compared with the full scale 1st bending frequency and mode using BModes. BModes is an open source NREL beam finite element model (Bir, 2008) used to determine the natural frequencies and associated mode shapes of blades and towers, including towers on floating (compliant) foundations. The tower design process described previously was iterated until a tower design was found with comparable full scale structural and dynamic properties to the OC3 Hywind tower.

The final design consisted of two sections of 2024 aluminum alloy hollow rod. The top section consisted of a 25.40 mm OD and 20.57 mm ID diameter rod at 129.9 cm long with 7.620 cm of length, model scale, dedicated to a fit inside the bottom tower section. The bottom section consisted of a 33.66 mm OD and 25.40 mm ID diameter rod at 24.13 cm in length, model scale. Inside the bottom tower section was a solid 12.70 mm seat to fix the vertical position of the top section starting at 7.620 cm from the tower top. Below the seat the remainder of the bottom section was bored hollow. The base of the bottom section also incorporated a welded base plate with a bolt hole pattern that provided a connection between the tower and floating platforms. Slots were cut at the top of both tower sections which were paired with shaft collars to affix tower sections, allow for manual yaw adjustment, and provide an easy method of assembly and disassembly. Also included in the tower design and analysis was the 6-axis force gauge and its associating aluminum adapter which was made to fit inside the top tower while allowing

access to attach and detach the sensor. Using the shaft collars to fix the nacelle and tower

sections ensured the model was held together securely yet provided a simple method to

remove the entire nacelle and rotor from the tower. A detailed drawing of the tower is

included in Appendix B.

A comparison of the target and final calculated model design parameters are given

in Table 3.5. As can be seen in the table, the achieved values are fairly close to the

desired target values. The lower frequencies and higher CG can be attributed to the

increase in tower top mass relative to the desired scaled rotor and nacelle weights.

Nonetheless, the FA fundamental bending frequency is only 5.4% lower than desired and

the center of gravity is only 3.3% higher than desired.

Table 3.5.   Comparison of target and model tower properties.

	OC3 Hywind Tower	Full Scale Achieved	1/50th Scale Achieved
Length (m)	77.6	77.6	1.552
1st FA fn (Hz)	0.491	0.459	3.247
1st SS fn (Hz)	0.481	0.459	3.247
Mass (kg)	249,718	164,600	1.317
CGz (% from tower base)	43.0%	44.4%	44.4%

Comparisons for the 1st and 2nd order bending mode shapes in both the FA and SS

directions between the model tower and OC3 Hywind tower atop the OC3 Hywind spar

and supporting a turbine are shown in Figure 3.18. As can be seen in Figure 3.18, the

first order FA and SS mode shapes are very similar between the model and full target

towers. The second order mode shapes are less similar, however this is not a concern as

the model tower design objective was to only match the full scale first order response.

Therefore this analysis deemed the model tower suited dynamic tower property goals.
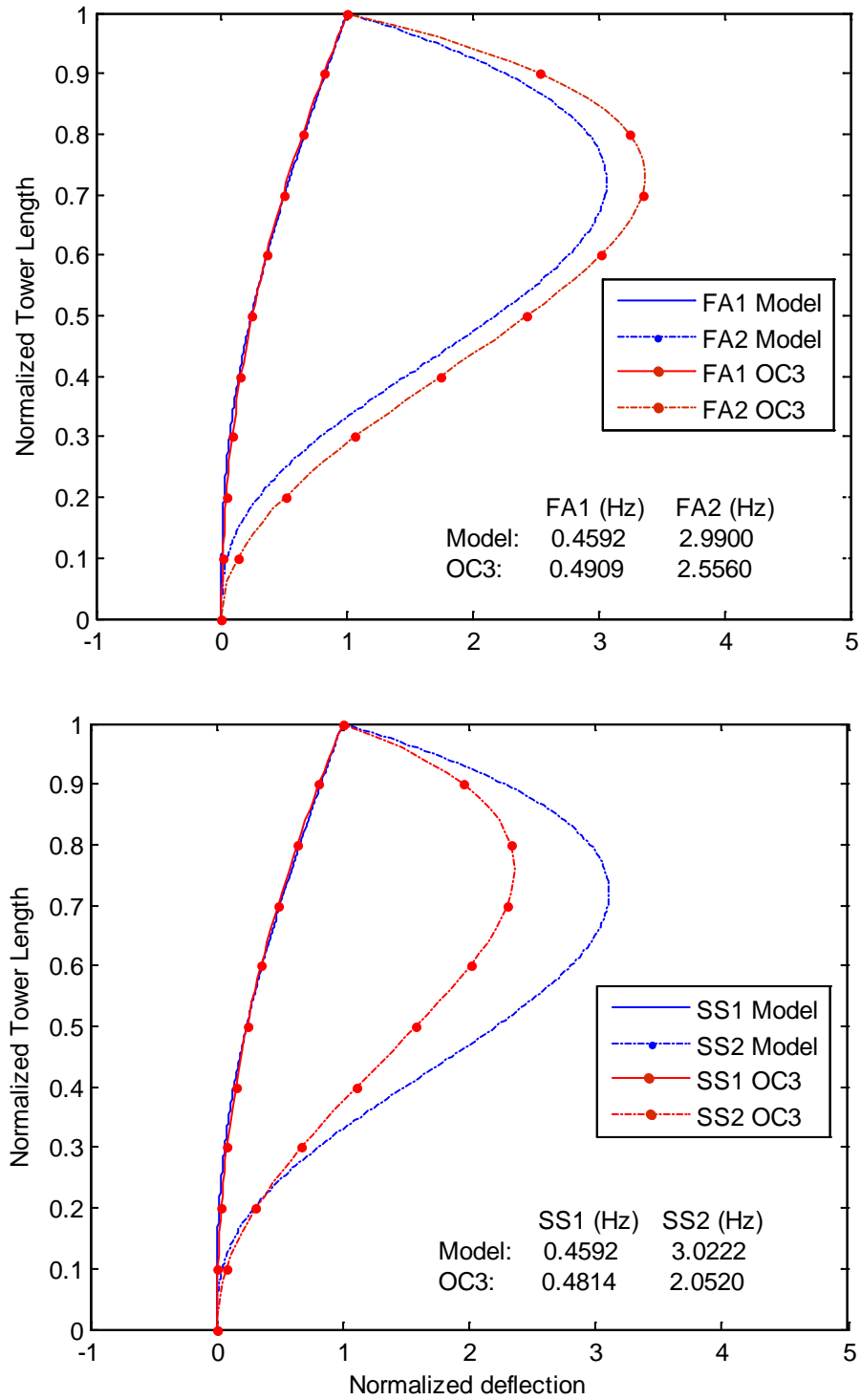
Figure 3.18.   Comparison of normalized tower mode shapes.

A final and important comment refers to the tower diameter which was not properly modeled due to limitations previously discussed. The final model tower diameter was only 26.9% of the largest scaled maximum tower diameter. However, this was deemed to be a minor issue. In fact, it was seen as potentially advantageous. The current NREL simulator does not have a means to simulate the aerodynamic interaction between the tower and the rotor blades as they pass by. Therefore, a smaller tower is desirable as it minimizes this aerodynamic interaction making the data better suited for code validation studies.

3.5. FULL ASSEMBLY

As a precaution in case of damage or failure, two model wind turbines were built in parallel. Both models were shipped to MARIN for basin model testing, however only one was used for the duration of the test program. The fully assembled final model wind turbine, without data cables and a hub cover, is pictured on the following page in Figure 3.19.

Figure 3.19.   Fully assembled fixed wind turbine model excluding cables.

CHAPTER 4. MODEL CHARACTERIZATION AND PERFORMANCE RESULTS

This chapter presents results from physical characterization tests, blade structural tests, and turbine performance data of the fully assembled and functional model wind turbine with a fixed base. First, characterization of the mechanical and mass properties of the model wind turbine will be presented. Second, blade structural testing and results are presented and compared to the predicted values from the structural analysis discussed in Chapter 3. A second analysis of the model tower dynamic response will also be presented as the mass of the system increased from the original design due to the addition of heavy instrumentation cables. Lastly, performance data from fixed-based wind-only basin testing will be presented for the model rotor with original blades and for blades with a roughened leading edge. The collected performance data will then be compared to target performance curves and suggestions for a future model blade design will be given.

4.1.   PHYSICAL CHARACTERIZATION

The final physical properties of the model wind turbine including the data cables with a fixed base and mounted to each of the floating platforms was determined at MARIN prior to floating wind turbine basin model testing. This data, in conjunction with numerical estimates, was used to determine properties pertaining to the tower, turbine and data cables exclusive of a floating platform. For all testing, a consistent reference frame was used to properly identify all model properties and motions. Figure 4.1 illustrates the floating wind turbine reference frame for positive x, y, and z axes as well as the 6-degrees of freedom, these being surge, sway, heave, roll, pitch and yaw. The origin for this

69
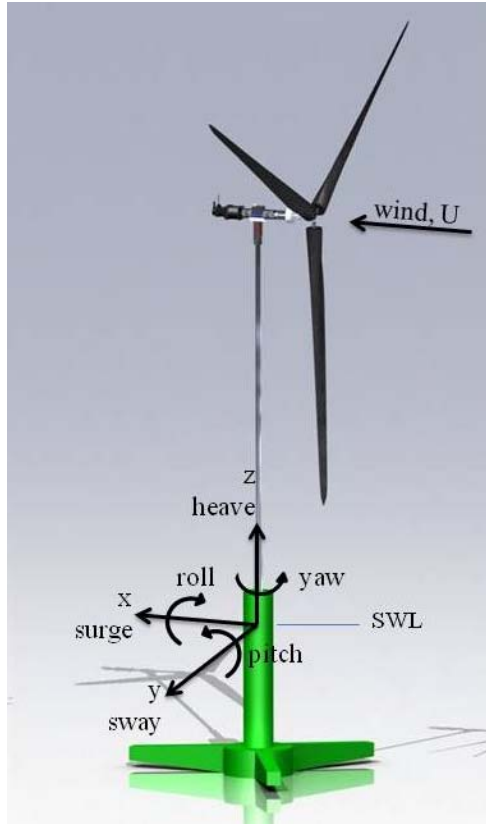
Figure 4.1. Degrees of freedom and reference frame for floating wind turbines.

reference frame was taken at the intersection of the tower centerline and the still water

plane surface or still water line (SWL). The center of gravity of the wind turbine in the x,

y and z axis were determined by string suspension tests. Values for radius of gyration for

the entire wind turbine model including a floating platform were determined using bifilar

swing tests. Radius of gyration for the wind turbine model alone was obtained via a

combination of numerical estimates for the tower, nacelle and data cables and swing tests

for the rotor. The complete mass properties of the wind turbine model were checked

against the difference between MARIN's reported masses of the entire systems and

platforms alone. The final values for mass, CG, and radius of gyration of the model wind

turbine with and without cables is given in Table 4.1.

Table 4.1. Physical properties of the model wind turbine at full scale.

Property	Without Cables	With Cables
Mass (kg)	561,750	699,400
CG_x (m)	0	0
CG_y (m)	0	0
CG_z (m)	76.7	71.2
r_x (m)	27.8	27.3
r_y (m)	27.8	27.3
r_z (m)	9.2	8.2
Rotor mass (kg)	122,225	122,225
r_{rotor} (m)	19.3	19.3

A second analysis of the tower natural frequency and associated mode shapes was

performed due to the additional mass of the data cables employed during basin model

testing. In the analysis, the cable mass was modeled as an even distribution down the

tower length equal to 1,774 kg/m. Similar to the tower analysis discussed in Chapter 3,

the analysis utilized the specialized beam finite element package BModes (Bir, 2008) as a

basis to determine the natural frequency and mode shapes of the OC3 Hywind tower and

model tower. Each tower was modeled using approximately 200 beam finite elements.

The OC3 Hywind tower geometry varied linearly from a wide tower base to a more

narrow tower top and required a unique mass and stiffness matrix for each element. The

model tower, which does not taper but includes uniform sections, utilized nine different

uniform cross-section element, and hence many of the finite elements possessed similar

properties in the analysis of the model tower. The distributed properties used to generate

the segment mass and stiffness matrices for the model tower include segment mass

density, bending stiffness, axial stiffness and torsional stiffness. Tables of the distributed

properties for the model tower with and without cables are provided in Appendix D. For
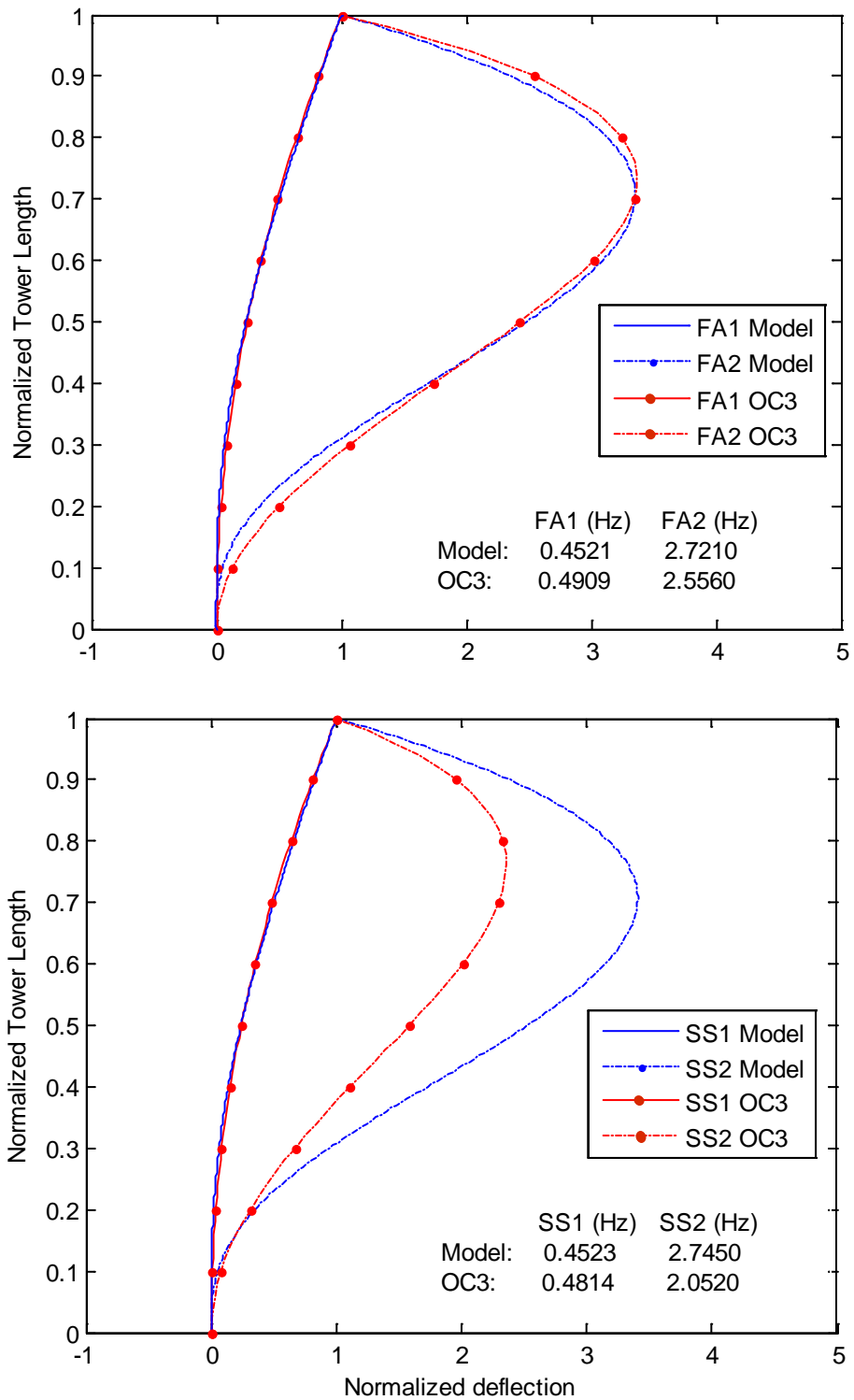
Figure 4.2.   Normalized mode shapes for the model tower with cables and the OC3 Hywind tower with 1st and 2nd order natural frequency values provided at full scale.

comparison, the OC3 Hywind tower distributed properties can be found in Jonkman, (2010). The analyses modeled the model tower top with a free boundary supporting a mass and inertia representing the nacelle and rotor and the tower base supporting a mass and inertia emulating the compliant OC3 Hywind spar-buoy as well as a stiffness matrix which represented restoring terms from the mooring system and hydrostatics. These conditions were the same as those chosen in the earlier design efforts of Section 3.4. Analysis results are shown in Figure 4.2. with the first and second order normalized mode shapes for the OC3 Hywind and model towers in both FA and SS directions. By comparing these mode shapes one can see the first order mode shapes between the model and OC3 towers are very similar for both the FA and SS directions. The second order bending mode shapes vary significantly between the model and prototype, much like the results from the original tower analysis discussed in Chapter 3. However, this was not a concern as emulating the second order mode shapes was not a primary goal of this research initiative.

Experimental determination of the tower model natural frequencies was done with hammer tests prior to wind/wave testing. Hammer tests were executed by exciting the model with an impulse force, as shown in Figure 4.3, and recording resulting
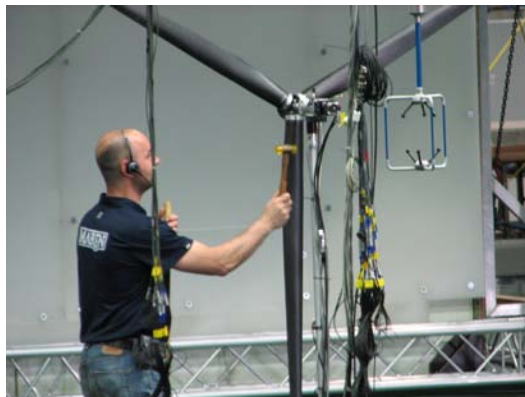
Figure 4.3. Image of a hammer test to determine model natural frequencies.

accelerations at three locations along the tower. These locations were at z = 8.3 m, 49.5 m, and 81.7 m. Excitation was applied in both the x and y directions along the tower length to determine the FA and SS natural frequencies. Figure 4.4 displays the FA time-domain acceleration plots and the frequency-domain power spectral density (PSD)acceleration plots at z = 49.5 m for both the fixed wind turbine model and the floating wind turbine fixed to the spar-buoy. The PSDs were determined by using traditional Fast Fourier transform (FFT) techniques (e.g. see O'Neil, 2003). The peaks on the PSDs identify the system natural frequencies. For the fixed wind turbine the first significant peak indicates a first FA natural frequency of 0.29 Hz. For the floating wind turbine on spar-buoy the first large peak, which is at a very low frequency, represents the rigid body
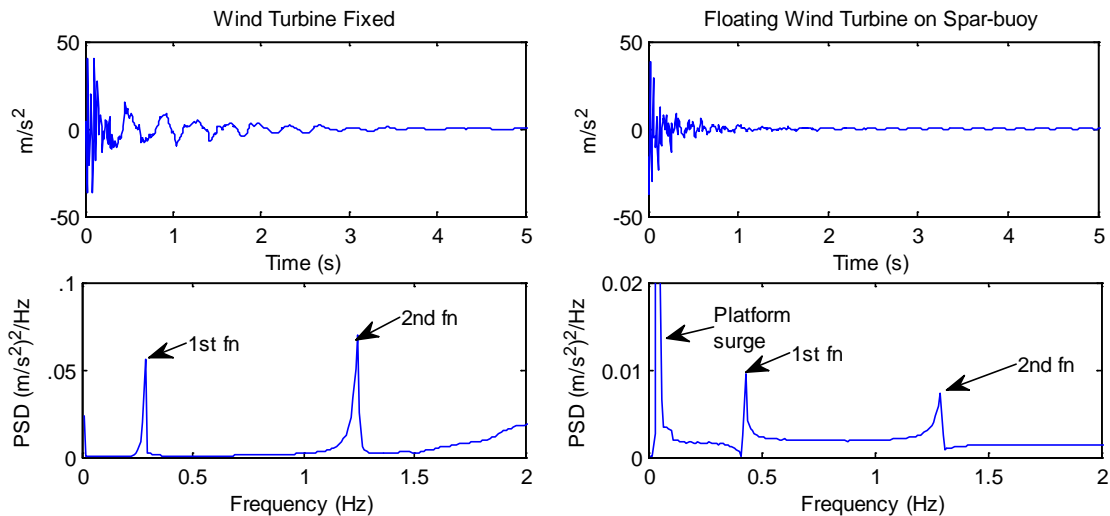
Figure 4.4. Acceleration and PSD plots of a fixed and floating wind turbine on the spar. surge natural frequency for the floating system. The second peak represents the first FA natural frequency of the entire floating system which is 0.43 Hz. The remaining acceleration and PSD plots at mid height (z = 49.5 m) for FA and SS excitations are

given in Appendix D for all the platform types considered. The first and second order FA

and SS natural frequencies for all foundation types considered are listed in Table 4.2.

Table 4.2. Measured tower bending natural frequencies of the model wind turbine with a fixed base and placed on the TLP, spar and semi-submersible platforms at full scale.

	Natural frequency (Hz)		
	1st FA	1st SS	2nd FA
Wind turbine alone	0.29	0.29	1.24
Wind turbine placed on TLP	0.28	0.29	1.16
Wind turbine placed on spar-buoy	0.43	0.44	1.29
Wind turbine placed on semi-submersible	0.35	0.38	1.26

The natural frequency values given in Table 4.2 line up well with analysis results

given in Figure 4. Figure 4.2 provides tower bending natural frequencies for the model

wind turbine tower on the spar only, where the FA and SS first order frequencies were

both 0.452 Hz. These predicted values were 5.1% and 2.7% higher than the measured

values, respectively. The discrepancy, though small, may be attributed to a number of

factors. The finite element analysis assumed rigid tower to platform and tower to nacelle

connections which, in reality, are not perfectly rigid. Also, imperfect characterization of

the tower structural properties and exclusion of gravity effects in the finite element

analysis would yield lower estimates of the bending natural frequencies better aligning

predictions with data. Nonetheless, the model wind turbine and tower yielded similar

physical and dynamic response properties as compared to the target OC3 Hywind tower

design. The total system weight including data cables was a modest 16.6% larger than

the target value and the fundamental FA tower bending frequency with the wind turbine

placed on the spar was 0.43 Hz, or 12.2% lower than the target value of 0.491 Hz. The CG of the model tower including cable weight was at 46.9% the total tower height resulting in a 9.1% difference between the final and target CG location of 43%.

4.2.   BLADE STRUCTURAL TESTING

To complement the structural analysis presented in Chapter 3, a cantilever bending test was performed to gather data on deflections and strains along the blade length under loading. The purpose of the structural test was to prove that the model blade possessed significant strength and exhibited minimal deflection under the most severe Froude scaled wind conditions utilized during wind/wave basin model testing. All loads were applied at the tip as it simplified the blade loading logistics during the test and created a more severe shear force and bending moment distribution along the blade length than would be expected in operation for a given blade root moment. Loading conditions used for the test were done such that the resulting blade root moment was equivalent to the resulting blade root moment from theoretical loading scenarios. All tests were conducted such that bending occurred about the compliant, or flap, axis of the blade. In the following discussion, note that all dimensions and loads are given at full scale.

The cantilever test set up is shown in Figure 4.5. Three string-pots were used to measure the transverse deflection along the blade span. String pots were placed at the tip and at the third points of the blade span, i.e. at 20.5 m, 41.0 m, 61.5 m from the root. Six strain gauges were used, three along the top or pressure side and three along the bottom or suction side starting at the blade root and placed at third points along the blade span or at 0 m, 20.5 m and 41.0 m from the blade root. All gauges were oriented such that the only axial strain was recorded.   Load application occurred at 60 m from the blade root

Figure 4.5.   Cantilever bending test set up for 1/50th scale model blade.

and was performed using measured weights for simplicity. Digital control over load application via actuators and load cells would have been the preferred method of load application, however the resolution of available lab equipment was not high enough to apply the small scaled loads needed for the cantilever test. Therefore, weight data was taken manually and paired with strain and deflection data collected with Labview.

Two types of tests were performed: one at operational loads and the other with loads leading to blade failure. For operational testing, mass was added in increments of 15,250 kg up to a total load of 137,250 kg. A mass of 57,776 kg was needed at the load location to create the maximum root moment of 34,000 kN·m which was determined in Chapter 3.   Figure 4.6 illustrates the deflection along the blade span under a blade root moment of 34,000 kN·m from predicted structural analysis results discussed in Section 3.3.2 and structural test data. From this figure it can be seen the test tip deflection of 0.416 m was larger than the predicted deflection of 0.280 m. What is more important is that the test deflection of 0.416 m was only 3% of the maximum tip deflection of 13.9 m

computed by Jonkman from a fully-coupled simulation with the same 34,000 kN·m blade root moment. With this data it was found that the model blade stiffness was over 33 times more stiff than the prescribed NREL 5 MW reference wind turbine blades. Therefore the model blade achieved the high stiffness desired for basin testing as the peak deflections found via analysis and testing were both minimal compared to the NREL result. The discrepancy between the test and the analysis can be attributed to the simplified Euler-Bernoulli analysis model which ignored shear deflection, bend-twist coupling and three-dimensional effects such as ovalization of the blade cross-sections.
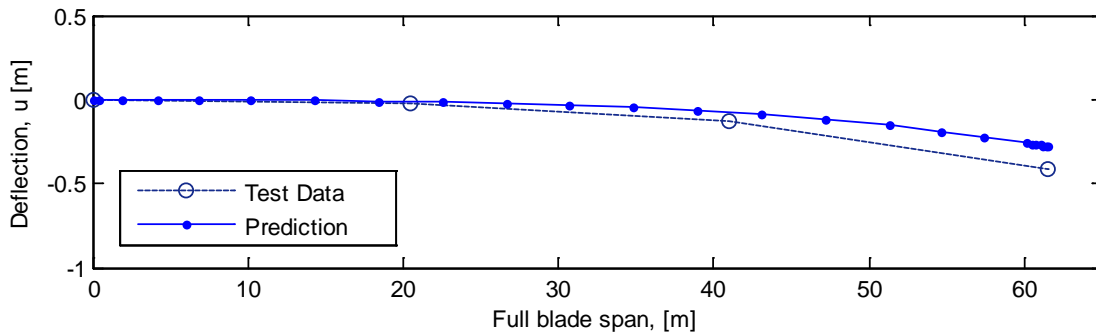
Figure 4.6. Deflection along blade span at full scale under loading to induce a maximum blade root bending moment scenario of 34,000 kN·m from analytical predictions and test results of the model blade.

As noted earlier, a second cantilever test was performed to determine the model blade failure strength. This was done to ensure that the blade strength greatly exceeded the strength required to resist aerodynamic loads during floating wind/wave basin model testing. The results of this test are displayed in Figure 4.7 where tip deflection is plotted as a function of blade root moment. The blade root moment shown in Figure 4.7 was calculated by multiplying the applied load by the load location relative to the root and adding the self-weight of the blade multiplied by the blade CG location which was identified at 38% of the blade length from the root from a knife edge test.
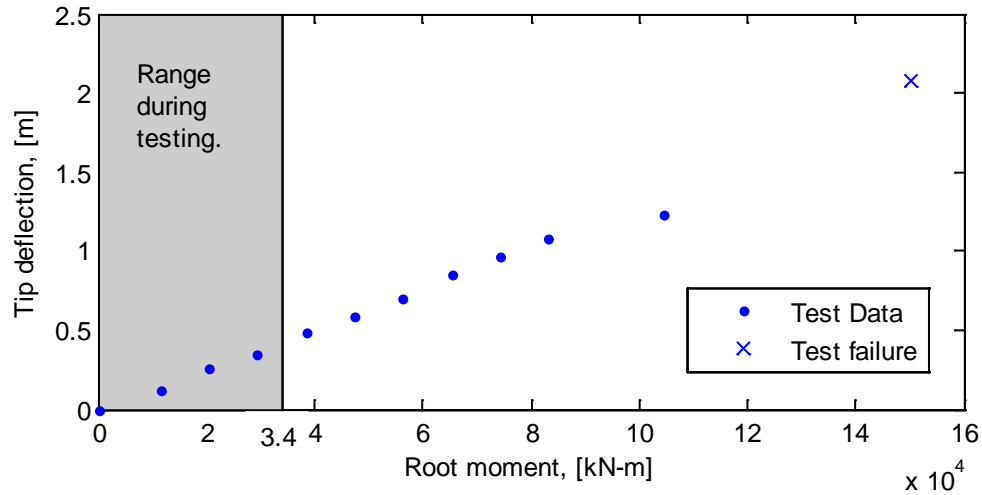
Figure 4.7.   Tip deflection as a function of blade root moment up to blade failure for the model blade at full scale.

The last data point taken prior to blade failure is shown with an "×" in Figure 4.7. Also the gray area of Figure 4.7 represents the range of blade root moments that are expected during basin model testing with the maximum being 34,000 kN·m. As can be seen by this figure, the model blade failure point is well beyond the expected operating range which indicates that the blade is sufficiently strong to endure all wind/wave basin model testing. The second structural test also demonstrated that blade failure was a result of buckling and not material failure. Once the load was removed post failure, the blade restored itself to its original configuration. The location of buckling failure or peak stress occurred at a relatively thin blade section, at least for the NREL blade, at approximately two-thirds of the blade length from the blade root under a load of 2,506 kN.

The location of buckling failure was found to be in close proximity with the location of maximum stress under operational conditions determined from test data and predicted stress values from the analysis discussed in Section 3.3.2. Strain gauge data taken along the bottom, or compressive side, of the blade is shown in Figure 4.8 and compared to predicted stress values determined from the structural analysis provided in
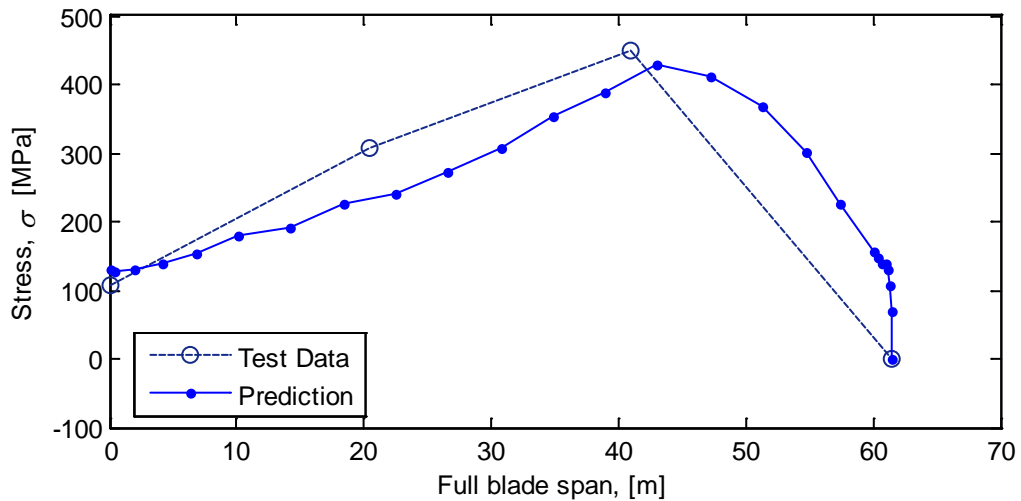
Figure 4.8. Induced stress along blade span at full scale under loading to induce a maximum blade root bending moment scenario of 34,000 kN·m from analytical predictions and test results of the model blade.

Section 3.3.2. Stress values from strain data were computed simply with Hooke's law by multiplying the recorded axial strain by the composite compressive elastic modulus of 54.10 GPa. Analysis results showed a maximum stress of 427.7 MPa at 43.0 m from the blade root while test data reported a maximum stress of 450.4 MPa at 41.0 m from the blade root. While no strength information is available for this material from the manufacturer, no material failure is expected during operation since typical strength values in compression for woven carbon epoxy composites are expected to be approximately twice the maximum stress values from Figure 4.8 (e.g. see Daniel & Ishai, 2006).

The differences of the predicted and test values given in Figure 4.8 are due to the crude analysis method used in Section 3.3.2 where anisotropic material properties were not considered and a simplified blade geometry was modeled. In addition, the information recorded by the strain gauges may be mildly altered by the presence of the woven material structure. Additionally test strain data was limited as data was collected

at three discrete points along the blade span and the maximum stress most likely occurred in a location not equipped with a strain gauge. As a result, the information provided n Figure 4.8 has considerable room for error due to the test and analysis procedures. However, the purpose of the analysis and test was to prove beyond a reasonable doubt that the model blade possessed high stiffness and adequate strength to resist deflection and failure during basin model testing. The information provided in both the analysis and test data has achieved this purpose even with the simplified procedures employed. Overall, it is evident that the model blade met not only the design goals of a very high bending stiffness, but also exhibited sufficient strength to easily resist any wind loading during basin model testing.

4.3. WIND TURBINE PERFORMANCE

In addition to building an accurately scaled model wind turbine to achieve proper dynamic response during basin model testing, the fully functional model wind turbine was also built to emulate the functions of a real wind turbine and produce power and thrust from Froude scaled winds during basin model testing. As discussed in Chapter 3, the model blade geometry was scrutinized to produce a clean and accurate geo-sim of the NREL 5 MW reference wind blade. During assimilation of the blade geometry, it was anticipated that the geo-sim blade would perform comparably with the full scale blade performance. This was predicated on the notion that the primary lift forces, for small angles of attack, were not heavily reliant on Reynolds number and that the increase in drag would be moderate and in line with flat plate calculations. However, the discussion on Reynolds number effects in Chapter 2 clearly indicates that the lift and drag coefficients are significantly affected by Reynolds number, especially for the thick foil

sections used for the model blade. The performance data taken during basin model

testing reflects the influence of low Reynolds number wind airflow on airfoil behavior,

and therefore, wind turbine performance. The remainder of this section will present and

discuss the performance data taken during fixed-based wind turbine testing.

Performance data collected during initial wind/wave basin model testing showed a

lack of generated torque and thrust when compared to expected values. While not

completely understood at the time, laminar separation was suspected as the cause of the

altered airfoil performance which was later confirmed with the analysis presented in

Chapter 2. Therefore, during basin model testing a decision was made to increase the

wind speeds to help increase model turbine performance and more specifically match full

scale and model scale thrust values which significantly influence the coupled motions of

the floating wind turbines. An example of the effect of the increased wind speed is

detailed Chapter 2 where wind speed was increased from 11.4 m/s to 20.8 m/s, these

speeds corresponding to the rated thrust condition.

Performance data is presented in subsequent text as the power coefficient, C_P, and

thrust coefficient, C_T, which are computed as

$$C_P = \frac{P}{\frac{1}{2}\rho U^3 A},$$
(4.1)

$$C_T = \frac{T}{\frac{1}{2}\rho U^2 A},$$
(4.2)

where ρ is the density of air, U is the wind inflow speed and A is the total swept area of

the HAWT rotor. P is the generated power determined from model torque data

multiplied by the rotor rotational speed and T is the generated thrust determined by x-axis

force data taken at the tower top. The power coefficient is a ratio of the generated power to the available power of the wind inflow. Similarly the torque coefficient is the ratio of generated thrust to a basic quantity representing potential wind force (Manwell, et al., 2002). The power and thrust coefficients were used to provide a clean and concise way to analyze the performance of a wind turbine design.

Figure 4.9 provides the normalized power and thrust coefficient curves generated from the fixed-based model wind turbine performance data. These performance curves were generated with a blade pitch setting of 6.4 degrees as this pitch angle was found to produce the highest power response for the turbine during basin model testing. As is
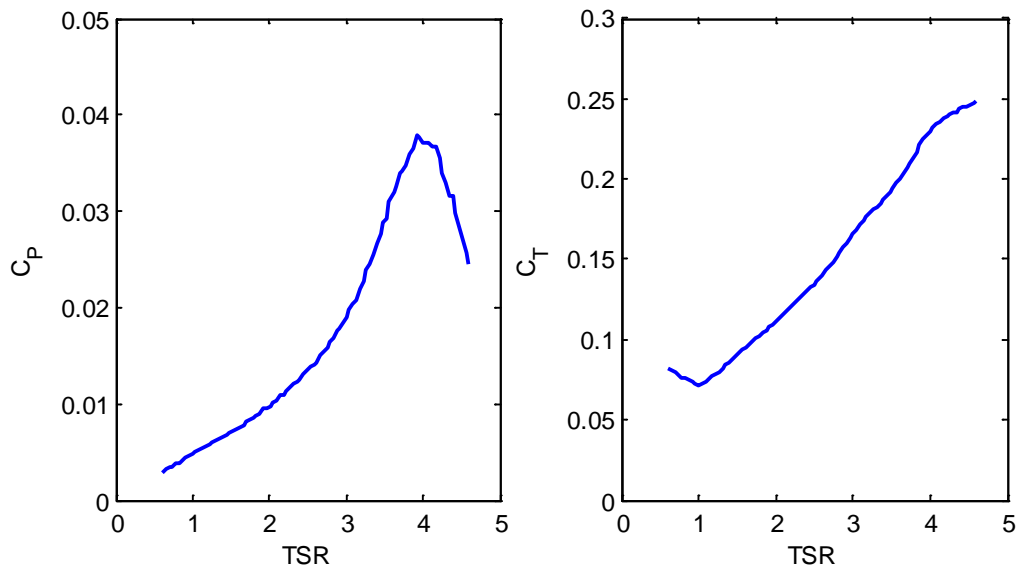
Figure 4.9.   Model wind turbine power and thrust coefficient performance curves from fixed-base wind-only basin model testing data.

shown by Figure 4.9 the peak values for C_P and C_T were very low at 0.038 and 0.25 respectively. Typically a full scale peak value of C_P would be approximately 0.45 and a full scale value of C_T around 0.9 at an operational *TSR* of roughly 7. For this performance test, data was collected up to a *TSR* of 4.6 as maximum C_P was achieved at a *TSR* of 3.9. In addition, since the wind speed was increased while rotor speed was

maintained, the range of possible *TSR* values the model could operate through was

diminished. Due to rotor speed safety limitations, the aforementioned maximum *TSR* of

4.6 could not be surpassed to collect data at an ideal full scale *TSR* of roughly 7. The

range of tested *TSR*s aside, these low C_P and C_T values were attributed to low lift and

high drag coefficients for the model blade airfoil sections due to the low Reynolds

number conditions experienced during wind/wave basin model testing. As detailed in

section 2.1.3, the geo-sim model blade utilized thicker high-Reynolds number airfoils

which performed poorly at model scale wind inflow and rotor speeds.A comparison of

the data performance curves from Figure 4.9 and the desired performance curves are

shown in Figure 4.10. The desired full scale performance curves are provided for a blade

pitch angle of zero and 6.4 degrees and are labeled as Full 0 and Full 6.4 respectively.

Note that the target turbine blade pitch angle was zero degrees as this yields the
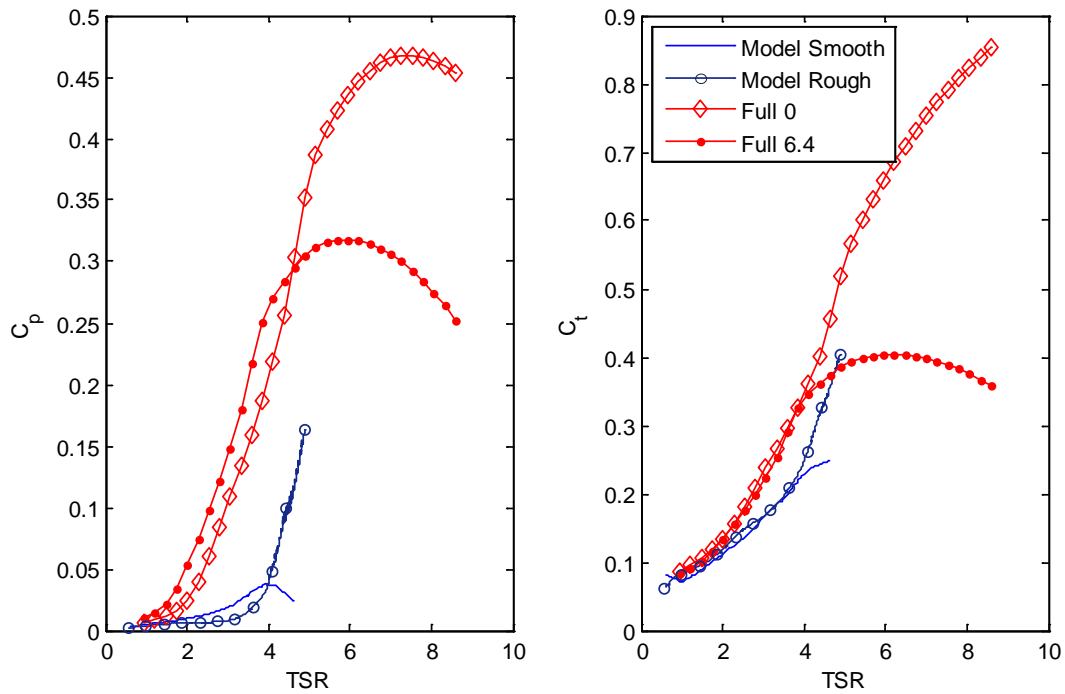
Figure 4.10.   Performance curves for the NREL 5 MW wind turbine and model turbine.

maximum performance coefficient under full scale conditions.. However, the model

achieved maximum performance at a blade pitch of 6.4 degrees. Hence the full scale

performance curve of 6.4 degrees is shown to illustrate the maximum achievable

performance for this blade at that pitch angle. The result for the shift in maximum

performance of the model blade from the expected zero degrees to 6.4 degrees is a result

of drastically altered lift and drag coefficients at the low Reynolds number, as discussed

in Section 2.1.3. Referring back to Figure 4.9, the model performance curve is labeled as

Model Smooth, which will be elaborated upon in subsequent text. By comparing these

performance curves, it can be seen that the model wind turbine did not produce the torque

and thrust behavior desired during basin model testing. Note that the model thrust

coefficient curve was significantly closer to desired behavior than the power performance

curve and hence required a modest increase in wind speed (see Equation 4.2) to maintain

full scale thrust. The very low power coefficient lends evidence to the fact that the model

did not yield sufficient torque to create properly scaled power, even when wind speeds

were increased by 80% to match the desired thrust. Nonetheless, the thrust and not the

torque, is the main aerodynamic load which contributes to the floating system global

motions and dynamics and was the more important parameter to maintain. In addition to

closely modeling the appropriate thrust forces, the proper model wind turbine rotor

rotational speed was utilized during basin model testing which when coupled with the

near target rotor inertia, yielded the correct gyroscopic dynamic effects. Aside from the

thrust correction and achieving the correct gyroscopic dynamic effects, the increased

wind speed could have negative effects and reduce the representative accuracy of the

model wind turbine as compared to the expected full scale behavior. For example,

alterations that could have occurred as a result of increased wind speed include

misrepresenting the aerodynamic damping forces resulting from motion of the floating

structure. Nonetheless, the model wind turbine captured the correct mean thrust forces

and gyroscopic moments which were representative of full scale behavior. The higher

order discrepancies from the expected performance, such as aerodynamic damping, are

being addressed in ongoing research efforts.

After the three floating platforms described in Chapter 1 were tested, additional

performance testing of the fixed base wind turbine model was done in hopes of better

understanding the diminished rotor performance. For these performance tests the model

wind turbine was modified with roughness added to the leading edge of each blade. The

roughness consisted of calibrated carborundum grains with diameters ranging between

250 to 290 μm applied with an adhesive strip 2 cm wide, all dimensions model scale.

The leading edge roughness was used to trip the flow transition along the chord from

laminar to turbulent which effectively increased the local Reynolds number and created a

more efficient, attached flow pattern around the blade. With the flow attached and not

separated as described in Chapter 2 for the geo-sim model blade, the blade section drag

force diminished due to the smaller effective frontal area of the blade. Also, the lift

increased as a result of diminished pressures on the suction side of the blade. The end

result was an increase in generated torque and thrust.

The performance curves generated from the test data of the wind turbine with the

roughened leading edge system are presented in Figure 4.10 and labeled "Model Rough".

It is clear by comparison to the original model performance curve that the roughened

leading edge significantly increased the power and thrust performance of the model wind

turbine, primarily above a *TSR* of 4. The drastic jump in performance around this *TSR* is likely a result of the changing Reynolds number. As the rotor speed, or *TSR*, was the dominant contributor to airfoil section speed, and hence Reynolds number, the low *TSR* regions possessed a blade that was almost entirely experiencing laminar separation. At the higher *TSR*s, or higher Reynolds number, the flow began to reattach on the outer blade airfoil sections which produced appreciable lift and low to moderate drag and resulted in drastically increased rotor performance. Even though it would have been desirable to do so, *TSR* values beyond 4.9 were not tested as a result of a rotor speed limit of 15.5 rpm (110 rpm model scale) set on the control system for safety purposes. As the C_P curve was still increasing at the largest tested *TSR* it is very likely peak C_P was in excesses of the 0.16 value shown. Even so, a C_P of 0.16 was still 420% higher than the turbine performance with a smooth blade leading edge. As a result of this testing, it is clear that careful attention should be made to model blade surface treatment in order to maximize turbine performance in the Froude scaled environment of a wind/wave basin model test.

Even though leading edge roughness helped increase performance, future wind turbine testing under Froude scaled winds will benefit by using a low-Reynolds number specific wind blade geometry. While the blade geometry will likely not represent the full scale architecture, the blade should be designed to increase torque output, match full scale C_T curves, and if possible closely match the change in total blade lift force with respect to blade pitch. The first two points will ensure that the global mean forces on the structure are maintained in a Froude scale environment, while the second will help maintain the effect of turbine damping forces due to either changing wind speeds or

global motion of the floating wind turbine structure. In the following paragraphs an example of a Froude scale specific model wind turbine blade geometry is presented. To simplify the design process, emphasis was placed only on creating a simple geometry that matched the C_T curve in the vicinity of operational *TSR* (approximately 7) and maximized the peak value of the C_P curve.

The example redesign of the model wind blade began with the selection of a low-Reynolds number airfoil which for this example is the Drela AG04 low-Reynolds specific airfoil (Drela, 1995). The AG04 geometry is provided in Figure 4.11 where it is clearly evident that the airfoil is very thin and therefore not as susceptible to laminar separation
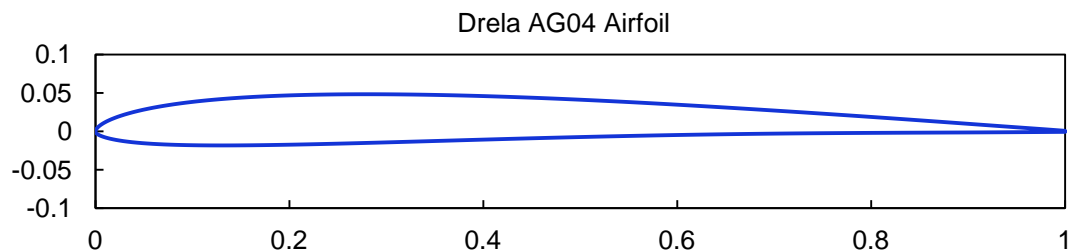
Figure 4.11. Drela AG04 low-Reynolds number airfoil.

as many of the NREL 5 MW blade thick airfoil sections at the low model scale Reynolds numbers. Lift and drag coefficients of the Drela AG04 and NACA 64-618 airfoils determined by an XFOIL analysis are provided in Figure 4.12. As can be seen in Figure 4.12 it is clear that the AG04 airfoil showed significantly larger lift coefficient and lower drag coefficient than the NACA 64-618 airfoil at the low Reynolds number of 35.7×10^3 for operational angles of attack between zero and ten degrees. This was a drastic improvement, however it is important to note that is difficult to create an airfoil that will achieve the same high lift and very low drag of the full scale high Reynolds number condition at these low Reynolds numbers.
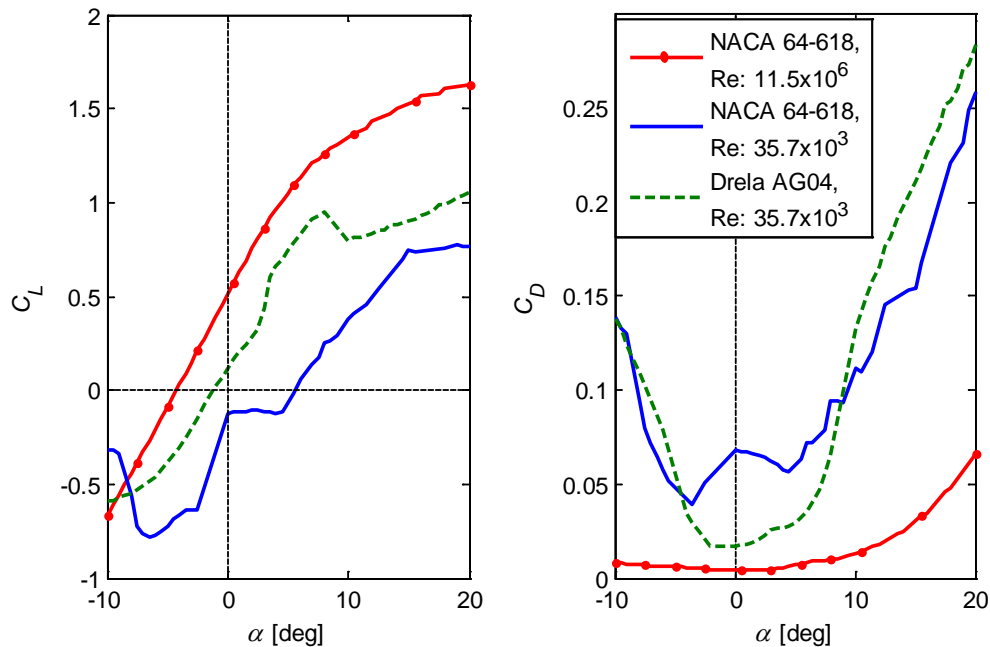
Figure 4.12. Lift and drag coefficients of the NACA 64-618 airfoil under high and low-Reynolds number conditions and of the Drela AG04 airfoil under low-Reynolds number conditions.

Using the AG04 lift and drag information of Figure 4.12 in the NREL FAST package and manually adjusting the blade chord and twist distributions, a reasonably well performing low-Reynolds number blade was achieved. A description of the blade is given in Table 4.1. Comparing the new blade and the blade of Table 3.3, one can see that the new blade had some unique differences as compared to the NREL 5 MW blade. First, the inner sections, which are now airfoils instead of cylinders, were rotated a great deal further so that the root sections produced lift and would not stall. Also, note that the chord is 25% longer along the entire length of the blade as compared to the original configuration of Table 3.3. This is to make up for the diminished lift force resulting from the slightly smaller lift coefficient. The increase in chord raises the lift force to nearly the same value as expected at full scale. Lastly, it is evident that the new blade is very thin throughout the length of blade and does not possess any thick sections which will

Table 4.3. Non-dimensional geometry of a simple low-Reynolds number wind blade.

Section Number	Airfoil	r/R	c/D	Θ_p	t/c	x/c
1	Drela AG04	0.046	0.035	42.712	0.064	0.375
2	Drela AG04	0.089	0.038	31.187	0.064	0.375
3	Drela AG04	0.132	0.041	23.109	0.064	0.375
4	Drela AG04	0.187	0.045	16.389	0.064	0.375
5	Drela AG04	0.252	0.046	11.475	0.064	0.375
6	Drela AG04	0.317	0.044	8.502	0.064	0.375
7	Drela AG04	0.382	0.042	6.523	0.064	0.375
8	Drela AG04	0.447	0.040	5.052	0.064	0.375
9	Drela AG04	0.512	0.037	3.878	0.064	0.375
10	Drela AG04	0.577	0.035	2.939	0.064	0.375
11	Drela AG04	0.642	0.032	2.216	0.064	0.375
12	Drela AG04	0.707	0.030	1.673	0.064	0.375
13	Drela AG04	0.772	0.027	1.245	0.064	0.375
14	Drela AG04	0.837	0.025	0.844	0.064	0.375
15	Drela AG04	0.892	0.023	0.497	0.064	0.375
16	Drela AG04	0.935	0.021	0.235	0.064	0.375
17	Drela AG04	0.978	0.014	0.064	0.064	0.375

severely degrade performance resulting from laminar separation at low Reynolds

numbers. The performance curve and thrust curve from analysis for the low-Reynolds

number blade described in Table 4.3 is shown in Figure 4.13 and compared to the actual

performance of the NREL 5 MW blade and the model scale achieved test results. The

low-Reynolds blade was operated at a pitch angle of 0.5 degrees as this yielded the best

match to the desired full scale C_P and C_T curves. Figure 4.13 shows that the C_T curve is

very similar to the desired full scale behavior especially near operational *TSR* values of

approximately 7. This indicates that the model scale blade will produce the correct thrust

in a proper, and unaltered, Froude scale environment. The C_P curve, while much better, is still not the same as the full scale curve. This is due primarily to the inevitable increase in airfoil drag at low Reynolds numbers which detracts almost directly from the wind turbine power generation, or torque. Achieving a peak final value of over 0.35, especially with peak efficiency occurring at the correct *TSR*, is most likely the best one can expect under Froude scaling circumstances.
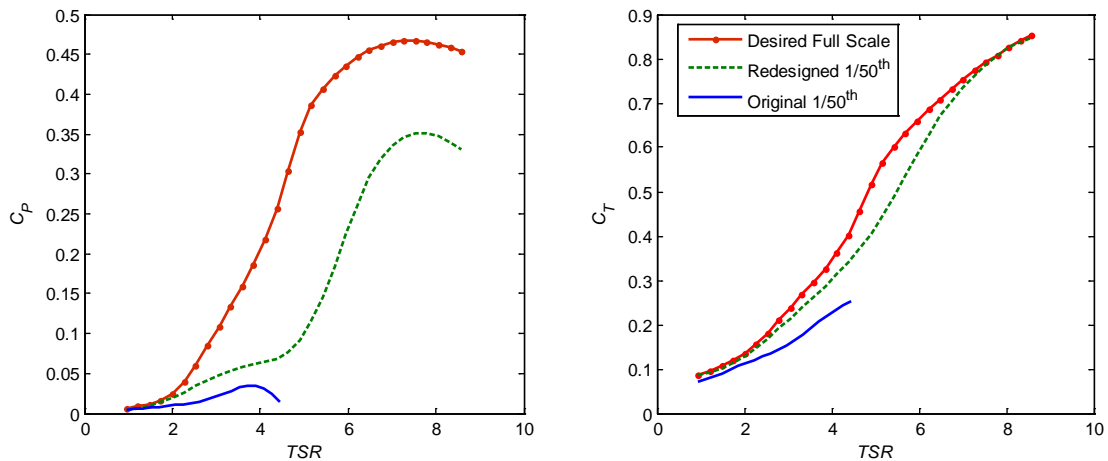
Figure 4.13.   Power and thrust coefficient curves for the full scale, achieved geo-sim at 1/50th scale, and redesigned 1/50th scale blade.

Overall, the performance of the geo-sim model wind blade did not closely match the desired performance values due to Reynolds number dependent alterations in airfoil section lift and drag coefficients. The addition of roughness along the geo-sim blade leading edge helped increase performance drastically, however data collection did not cover the range of desired *TSR* values due to instrumentation limitations and the maximum C_P was not believed to be achieved.   Nonetheless, it is advised for future model tests to treat the leading edge of model blades in addition to designing a low-Reynolds number specific wind blade to best match the desired performance results in a Froude scale test. The previous design example presented is a good starting place from

which to further optimize the blade geometry to best achieve scaled aerodynamic performance. Even though the NREL 5 MW geo-sim did not yield the correct turbine performance under strictly Froude scale winds, the additional testing results and design efforts presented here indicate that a suitable wind turbine can be constructed to more closely match the target performance values under Froude scaled winds.

CHAPTER 5. CONCLUSION

The purpose of this work was to design, build and characterize a fully-functional 1/50th scale model wind turbine based on the NREL 5 MW reference wind turbine for the purpose of wind/wave basin model testing of commercially viable offshore floating wind turbine concepts.   Unlike other known floating wind turbine wind/wave basin model tests, this program subjected the floating model wind turbine to fully characterized Froude scaled wind with the goal to produce torque, thrust, and gyroscopic forces that a real wind turbine would experience. Aside from turbine performance, the functional scale model wind turbine was designed to be mounted to three scale floating platforms via a flexible tower which experienced additional forcing from scaled wave environments in order to study the global motions and dynamic response of the entire system. The end goal of the scale model development testing program was to collect data for validation of fully-coupled servo-aero-hydro-elastic simulation codes, such NREL's fully-coupled simulator, as no such data currently exists. This goal was ultimately met in large part due to the work outlined in this thesis which details and characterizes the fully functional scale model wind turbine and tower utilized in wind/wave basin testing.

5.1. OVERVIEW OF DESIGN AND RESULTS

Overall, the physical model performed well throughout the duration of the model test program. More specifically, the model nacelle, hub, sensors, and components suited their purpose and met the needs of the basin model test program. No part of the bearing housing, torque tube or hub malfunctioned throughout the five week basin model test program. Nonetheless, improvements could still be made in future design iterations.

One design improvement involves the use of materials better suited to resist a humid and dynamic environment for manufactured components. Mid-way through basin model testing, the nacelle was disassembled and certain components cleaned of potentially harmful rust accumulation. This can be avoided in future testing if rust resistant materials or coatings were used for critical components, particularly those possessing mating surfaces with other parts . For the wind turbine model described in this thesis, not all components of the hub and nacelle were manufactured from these types of materials in order to keep project costs in check. The blade pitch control assembly also satisfied the needs for this model test program, however the linkages and the actuator were not as durable as desired in order to resist the accumulation of joint slop caused by continuous loading throughout five weeks of double shift basin model testing. As a result, these components were periodically checked and replaced as needed throughout the test program. In short, there is appreciable room for improvement of the pitch control assembly design if the system is to be employed for future testing. This is especially true if active blade pitch control would be a major part of future testing. For the wind/wave basin test program, just the periodic remote operation of the blade pitch system in between tests was enough to develop the aforementioned slop issues, therefore continuous actuation of the system will be far more demanding, requiring an increase in system robustness. Lastly, the final nacelle weight was still higher than the target weight. Further reduction of the nacelle weight would be another area suitable for improvement. Potential ways to reduce weight further would be truncating the torque tube and/or removing more material from the bearing housing. However, the majority of the nacelle and hub mass was located in the motor and gearbox assembly. Therefore, finding an

alternate, smaller motor with the similar capability as the Parker Motion BE164D may be the cleanest and best weight loss solution for the nacelle.

Regarding the physical properties of the entire model wind turbine, the total mass of the model was 16.5% larger than the target value which was primarily due to the additional mass from the chosen instrumentation cables. Even though the model tower weight described in Chapter 4 was 34% less than the target weight in order to accommodate the heavy nacelle, the inclusion of the instrumentation cables affixed to the length of the tower caused the final tower mass to be 21% greater than the target tower mass which was not ideal. Nonetheless, the model tower dynamic response analysis, which included the additional cable mass, mass from the model nacelle and inertia and stiffness of the floating spar-buoy, yielded dynamic characteristic results very near the target values. The fundamental bending frequencies and mode shapes for FA and SS motion of the model tower were within 12.4% of the full scale target values, a discrepancy deemed suitable for the needs of the wind/wave basin model testing program.

Aside from the blade aerodynamic performance, the quality and stiffness of the carbon fiber model blades exceeded design goals. The bladder-mold fabrication produced high quality, ultra-light hollow composite model blades consistently and reliably. Due to these successes, it is highly recommended that the bladder-mold fabrication method be used for future composite model blades and other lightweight model components. The structural analysis results and accompanying test data proved that the model blade possessed the desired high stiffness and more than adequate strength to resist deflections

under extreme wind/wave basin loading conditions meeting the established blade design goals.

Due to the difficulty of achieving target performance of a model wind turbine under Froude scaled winds, much of this research effort was focused on understanding and identifying the most appropriate method to capture appropriate aerodynamic forces. During the pre-basin testing design efforts, crude flat plate viscous flow calculations led to the assumption that the model turbine performance would represent full scale wind turbine performance at low angles of attack with a geo-sim of the NREL 5 MW blade under Froude scaled wind. However, the geo-sim blade utilized thick high-Reynolds number airfoils which are required in real machines to provide adequate bending strength. As the Froude scaled wind conditions in the basin were of a very low-Reynolds number relative to the full scale wind conditions, the performance of the high-Reynolds number airfoil geometries used in the blade design suffered resulting in a model rotor performance that was much poorer than expected with low thrust and power generation. Therefore, basin wind speeds were increased by 80% as a result of the diminished thrust coefficient of the rotor. While this adjustment captured the correct thrust vital for properly modeling the coupled global response of the floating wind turbine system, the generated power and torque were still low.

Further investigation with XFOIL analyses of the NACA 64-618 airfoil sections utilized in the model blade showed that the diminished performance was due to laminar separation of the fluid flow near the leading edge of the suction side of the airfoil at the low model scale Reynolds numbers. This laminar separation caused the formation of a large wake in the rotor plane perpendicular to the wind inflow which decreased lift

96

coefficients and increased drag coefficients, resulting in low aerodynamic thrust and torque. To gather performance data on the model wind turbine as a function of *TSR*, fixed-base wind only tests were performed with Froude scaled winds increased by 80% to match full scale rated thrust conditions. Data from these tests confirmed the XFOIL analysis and characterized the model turbine with low thrust coefficients and severely low power coefficient as a function of *TSR* compared to target performance.

Due to suspicion of laminar separation over the blade surface, a second round of fixed-based wind only basin model testing was performed with roughness added to the leading edge of each blade to trip the flow over the airfoil sections from laminar to turbulent to prevent laminar separation. The performance data presented from these tests showed power and thrust generation was greatly improved with the simple addition of leading edge roughness, especially at higher *TSR* values. However, the test could not be performed over the range of desired *TSR*s due to instrumentation limitations, and hence, the incomplete test was unable to record the maximum power coefficient.

In addition to adding leading edge roughness it was found through analysis that improved performance could be achieved through a redesign of the model blade geometry by incorporating low-Reynolds number airfoils. By utilizing low Reynolds number airfoils, such as was done in the example blade provided in Chapter 4, the model wind turbine performance has the potential to achieve closer performance values under Froude scaled winds as compared to the desired target performance from the full scale wind turbine. The provided redesigned Froude scale blade illustrated the great potential of using a modified turbine geometry to replicate full scale turbine performance, particularly in the magnitude and shape of the thrust coefficient curve in the vicinity of

the turbine operating range. However, while not ideal, the geo-sim blade used for this model test did attain the appropriate thrust forces that greatly affect the critical system global responses of the entire floating wind turbine model by increasing wind inflow velocities.

5.2.   FUTURE WORK

The work described in this thesis is hoped to provide a foundation for the development of future floating wind turbine basin model tests. That said, there is certainly room for future improvements and additional model testing. A first suggestion for future work is to complete the performance curves of the wind turbine model with leading edge roughness by performing another fixed-base wind-only test and removing system rotational speed limitations such that the model would operate at higher *TSR*s. A completed performance curve would help characterize the extent to which leading edge roughness can help improve the model wind turbine performance under Froude scale winds. In addition, another series of performance testing with varying grain size of the roughness material would also be useful information to help establish recommendations for ideal blade leading edge treatments for future model testing.

Another area of future work would involve a re-design of the model wind blade geometry to closely achieve target performance values, especially those for thrust. Unlike the wind blade used for this model, using low-Reynolds number airfoils for the blade design will help improve wind turbine performance under Froude scaled winds, likely more than can be achieved by the addition of leading edge roughness alone. This is not to suggest that a revised blade geometry should ignore leading edge roughness, as the optimal model scale blade designs will likely make use of both strategies. The low-

Reynolds number wind blade design given in Chapter 4 illustrated potential blade redesign techniques and provided a starting place for a new blade design. However, it is important to note the example redesigned blade has not been fully optimized with regard to best mimicking the performance behavior of the NREL 5 MW reference wind turbine blade under Froude scale winds. Once a more optimal blade has been established and built, another round of fixed-base wind only testing should be performed to capture performance data and generate new power and thrust coefficient curves. Subsequently, target and collected performance curves can be compared and further iteration of the design procedure executed until no further improvement can be realized.

While beyond the scope of the initial floating wind turbine model test program, future wind/wave basin model tests may want to include active blade pitch control functionality to the model wind turbine as the effect of active pitch control on global system response is an important research topic. To do so, the current nacelle design should be retrofitted to accommodate new hardware for active pitch control as the actuator and components used for this test program do not exhibit as much durability as initial estimates would expect for this type of application. One design suggestion is to incorporate separate mini-servo motors on the nacelle or within the blade roots which receive command signals in parallel to actuate pitching of the wind blades. This arrangement has the potential to be more robust and creates greater test flexibility, such as the possibility to study cutting edge individual blade pitch schemes. However, three mini servo motors are likely to be heavier than the small L12 Firgelli actuator employed in the design outlined in Chapter 3. However, this could be compensated for with weight reduction in some of the other nacelle and blade components. In addition to different

actuators, it is highly recommended that thicker, more stiff linkages or another more robust manner of connecting the blades to the actuator or servo motors be used to make the pitch control assembly more durable.

A final but important improvement in future model wind turbine designs is the inclusion of lighter, less stiff cables to connect the model sensors and motor to the control box. It is advised to specify and obtain cables well in advance of basin model testing as specialty cables may need to be ordered and/or created. Having the appropriate cables and including them in the original wind turbine design would reduce complications related to testing and analysis.

5.3. CONCLUSIONS

In conclusion, the 1/50th scale wind turbine model met the critical design requirements to execute a successful wind/wave basin floating wind turbine model test. In retrospect, the chosen scale factor of 50 was an appropriate scale factor. A larger scale factor was not desirable as it would have been difficult to create the small wave environments, would have worsened Reynolds number dependent issues with the wind turbine, and created near impossible model weight targets to achieve during design and fabrication. A smaller scale factor would have increased the model size and improved test accuracy, however mooring line length would have become a limiting factor with respect to the basin size. Also, a smaller scale factor would have increased the size and cost even more so of the wind machine built for this test program. Therefore, a scale factor of 50 was suitable for this test program.

The forces and turbine properties that dictate the global motions and structural response of the wind turbine model were in the vicinity of target values. The model

turbine power generation target was not ideally attained, however achieving the appropriate power generation was considered secondary to achieving the appropriate thrust forces which affect the global motions and structural response of the entire turbine. The performance data presented here was for a fixed wind turbine and it would be likely that performance of the floating wind turbine model would have diminished slightly due to changes in the relative turbine wind inflow angle resulting from the moving rotor plane. Maximizing energy capture for a moving turbine is a significant reason to pursue future floating wind turbine basin model testing with active pitch control.

The test data taken from the wind/wave basin model test can now be compared to outputs from fully-coupled numerical simulations employing the wind turbine model characterized in this thesis for various code calibration and validation efforts. The information provided in this thesis is intended to help refine the science of basin model testing of floating wind turbine systems and guide future testing endeavors. Overall, it is believed that the planned numerical code validation efforts which utilize data generated from this model wind turbine will help boost future development and commercialization of floating wind turbine technology in the United States and aid in ensuring future energy security with a sustainable, renewable and abundant domestic resource: offshore wind.

APPENDIX A. INSTRUMENTATION AND CONTROLS SPECIFICATIONS

Component	Manufacturer	Part Number	Signal Type	Notes
Analog Encoder	US Digital	MA3-A10-125-B	10-bit Analog	Absolute output
Linear Actuator	Firgelli Inc.	L12-30-210-P L12-30-100-P	USB/RS232	210 &100 gear ratios used for comparison
T2 Precision Rotary Torque Transducer	Interface Inc.	T2-10Nm	TTL Signal	
6-Axis Force and Moment Sensor	Advanced Mechanical Testing Inc. (AMTI)	FS6-500	Analog	
Gyro Enhanced Orientation Sensor (6-Axis Accelerometer)	MicroStrain	3DM-GX1	16-bit Analog Output	
Parker Rotary Servo Motor	Parker Motion	BE164D-J-NFON	Encoder TTL	
10:1 Gearhead	Parker/Bayside	NE23-010	N/A	

Table A.1. Nacelle sensor and component specifications.

Component	Manufacturer	Part Number	Notes
CompactDAQ data acquisition 4-slot chassis	National Instruments	NI cDAQ-9174	Collect and distribute signals
32-Ch Analog Input Module	National Instruments	NI 9205	Torque and encoder input
4-Ch Analog Output Module	National Instruments	NI 9263	Motor controller output
(2) 4-Ch Simultaneous Bridge Modules	National Instruments	NI 9237	6-axis gauge inputs, module 1: forces, module 2: moments
Xenus XTL Digital Servo Drive (Motor controller)	Copley Controls	XTL-230-40	Motor controller
Linear Actuator Control Board	Firgelli	LAC	
24V, 12V, 5V Power Supplies	Rhino	PSC-24-060 PSC-12-015 PSC-05-012	24 V: Motor, motor controller, CompactDAQ and modules, 12V: torque transducer, 6-axis accelerometer 5V: linear actuator and MA3 encoder
Protective Circuit Breaker	Merlin Gerin	Multi 9 System C60a	
EMI Filter	Delta Electronics, Inc.	03DBAG5	

Table A.2. Data acquisition and control equipment specifications.
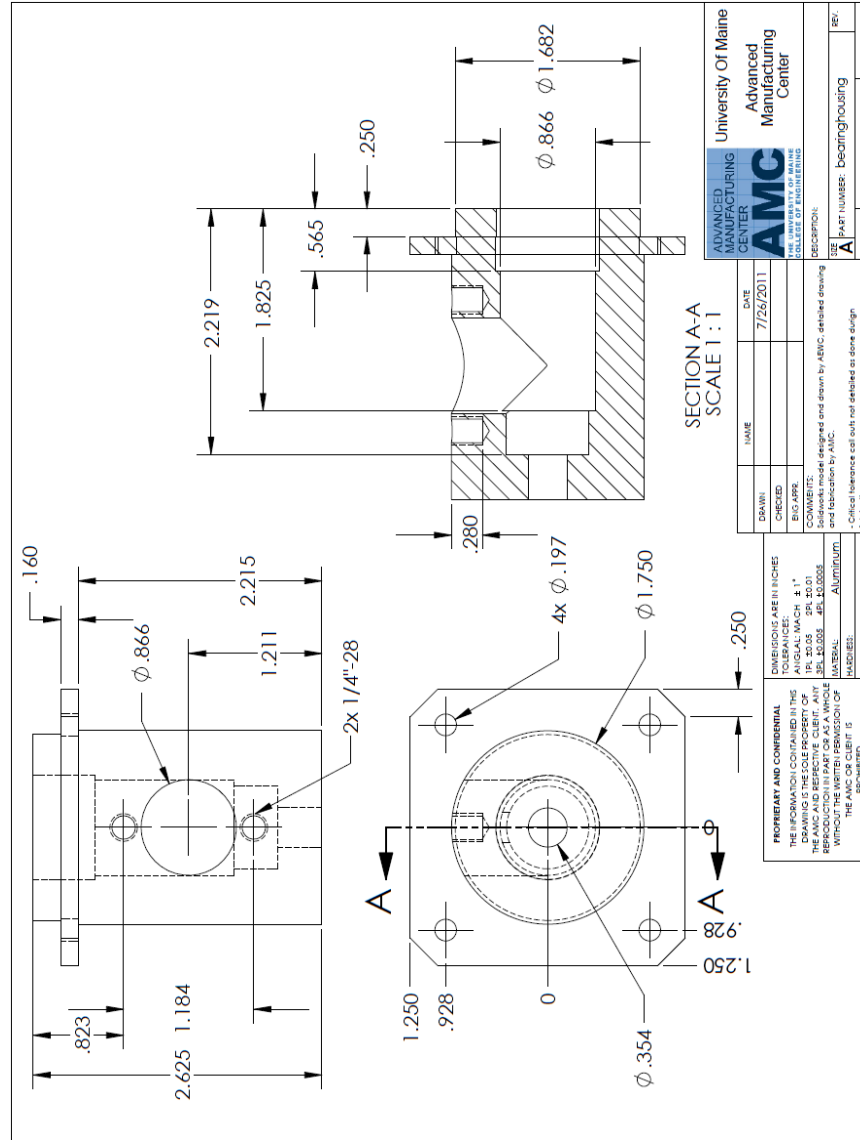
Figure B.1. Nacelle, hub and tower shop drawings.

Figure B.1. Nacelle, hub and tower shop drawings.

Figure B.1. Nacelle, hub and tower shop drawings.

Blade Cup

0.468"ID Snap Ring

Nylon Flanged Bearing
1/2"ID, 5.8"OD

0.468"ID Snap Ring

1/2" Hollow steel shaft,
ID: 0.37"

Rotor Central Steel Hub

[4.54in]
115.235mm

[0.81in]
20.472mm

[0.38in]
9.525mm

[1.18in]
30mm

Radial symmetry about
hub center @ 120deg.

UNLESS OTHERWISE SPECIFIED:			NAME	DATE
DIMENSIONS ARE DISPLAYED	DRAWN		HM	2/20/11
TOLERANCES:	CHECKED			
FRACTIONAL±	ENG APPR.			
ANGULAR: MACH± BEND ±	MFG APPR.			
TWO PLACE DECIMAL ±	Q.A.			
THREE PLACE DECIMAL ±	COMMENTS:			
INTERPRET GEOMETRIC	Final Bearing cups have			
TOLERANCING PER:	holes for blade removal.			
MATERIAL				
FINISH				

AEWC Advanced Structures
& Composites Center

TITLE:

Rotor Hub

SIZE **A** | DWG. NO. RotorAssemblyDWG | REV **0**

SCALE: | WEIGHT: | SHEET 1 OF 1

DO NOT SCALE DRAWING

NEXT ASSY | USED ON
APPLICATION

Figure B.1. Nacelle, hub and tower shop drawings.

107
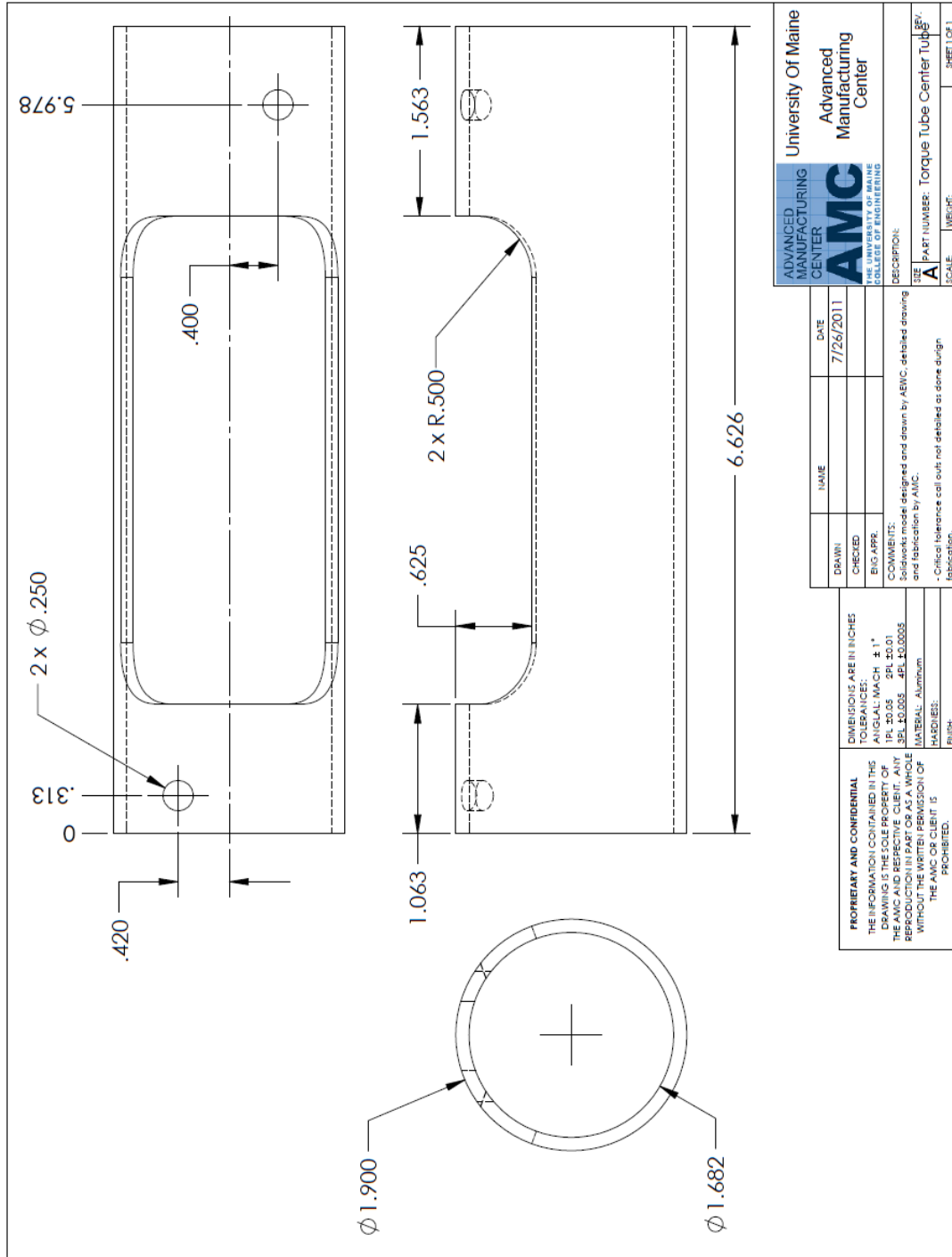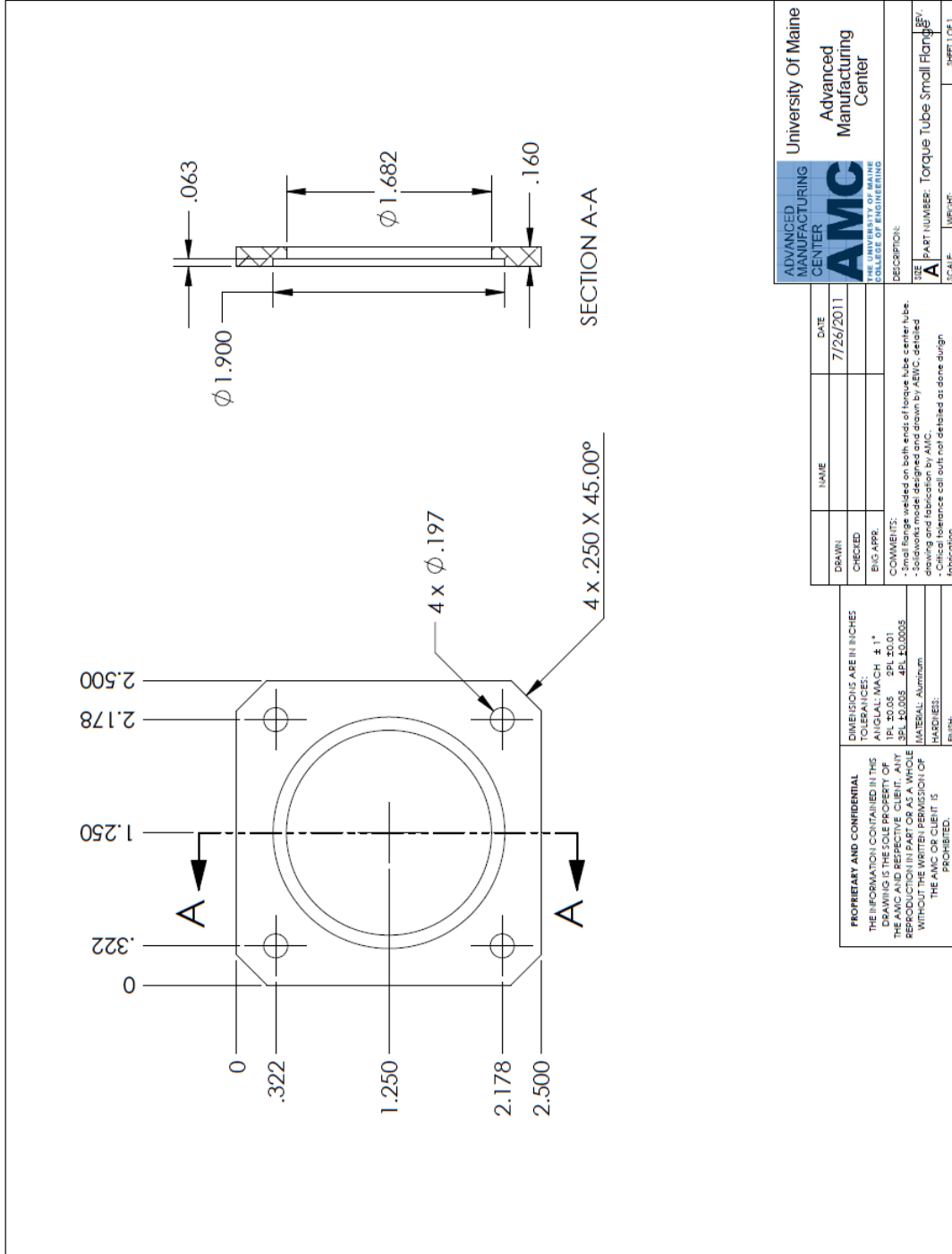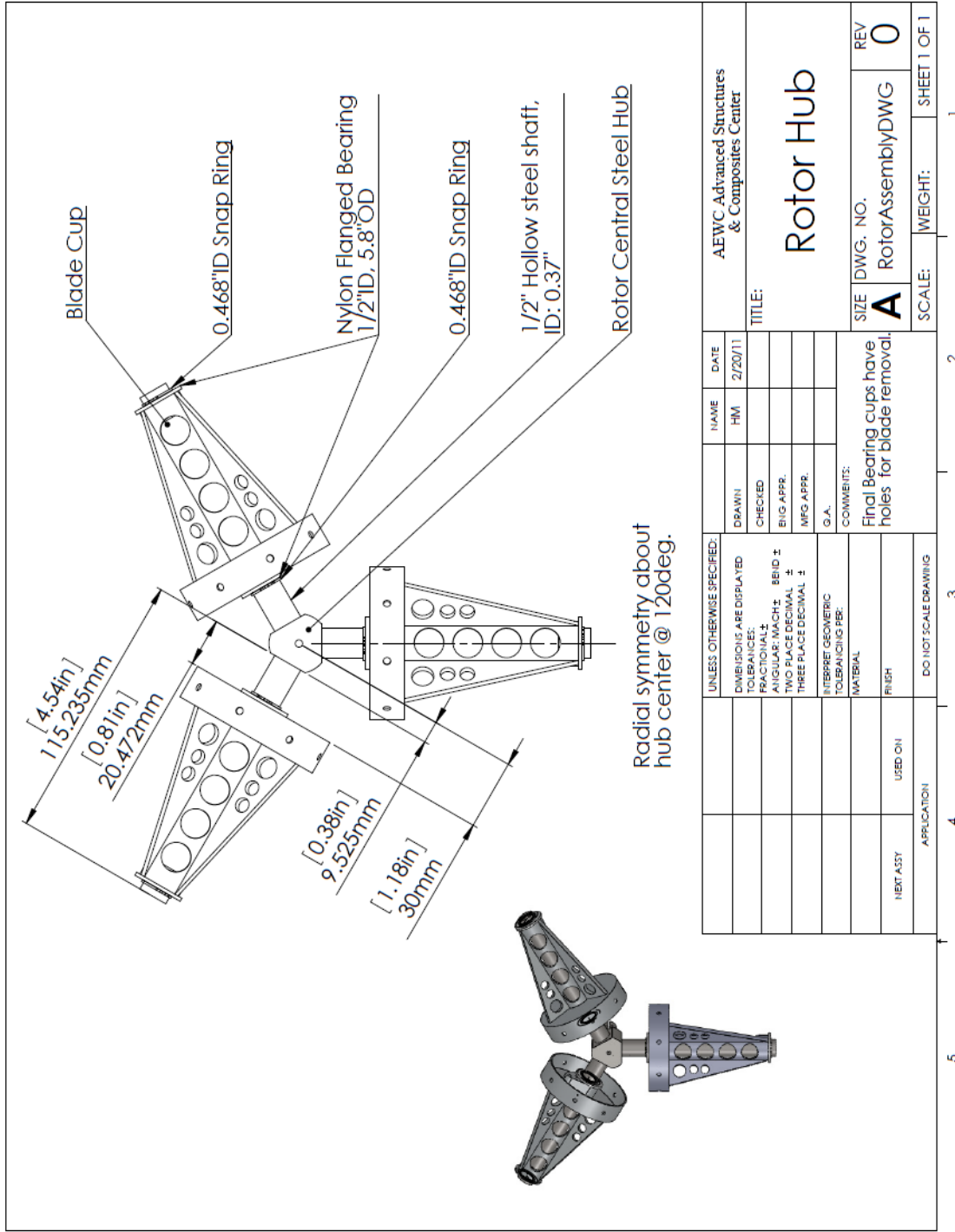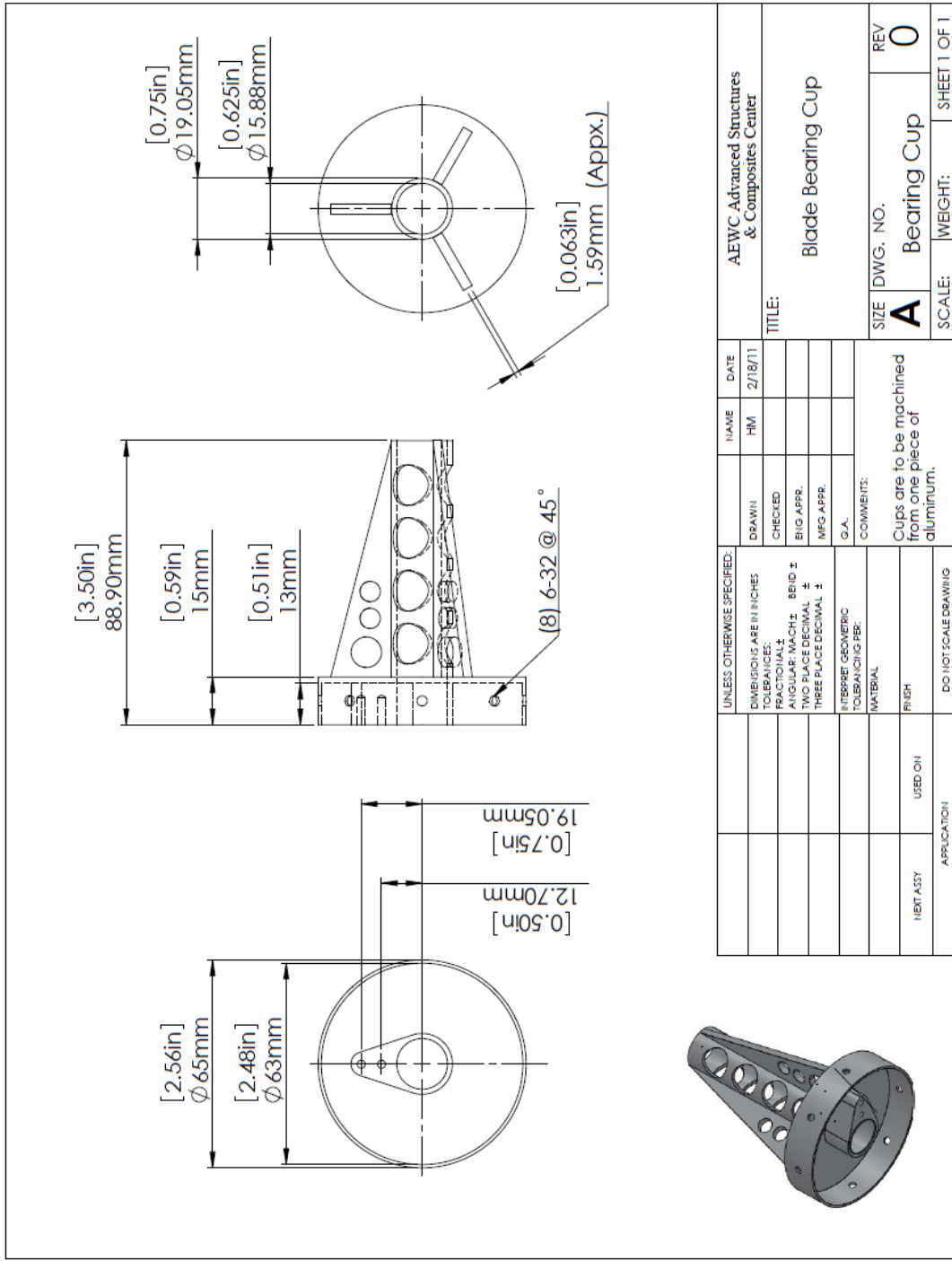
Figure B.1. Nacelle, hub and tower shop drawings.
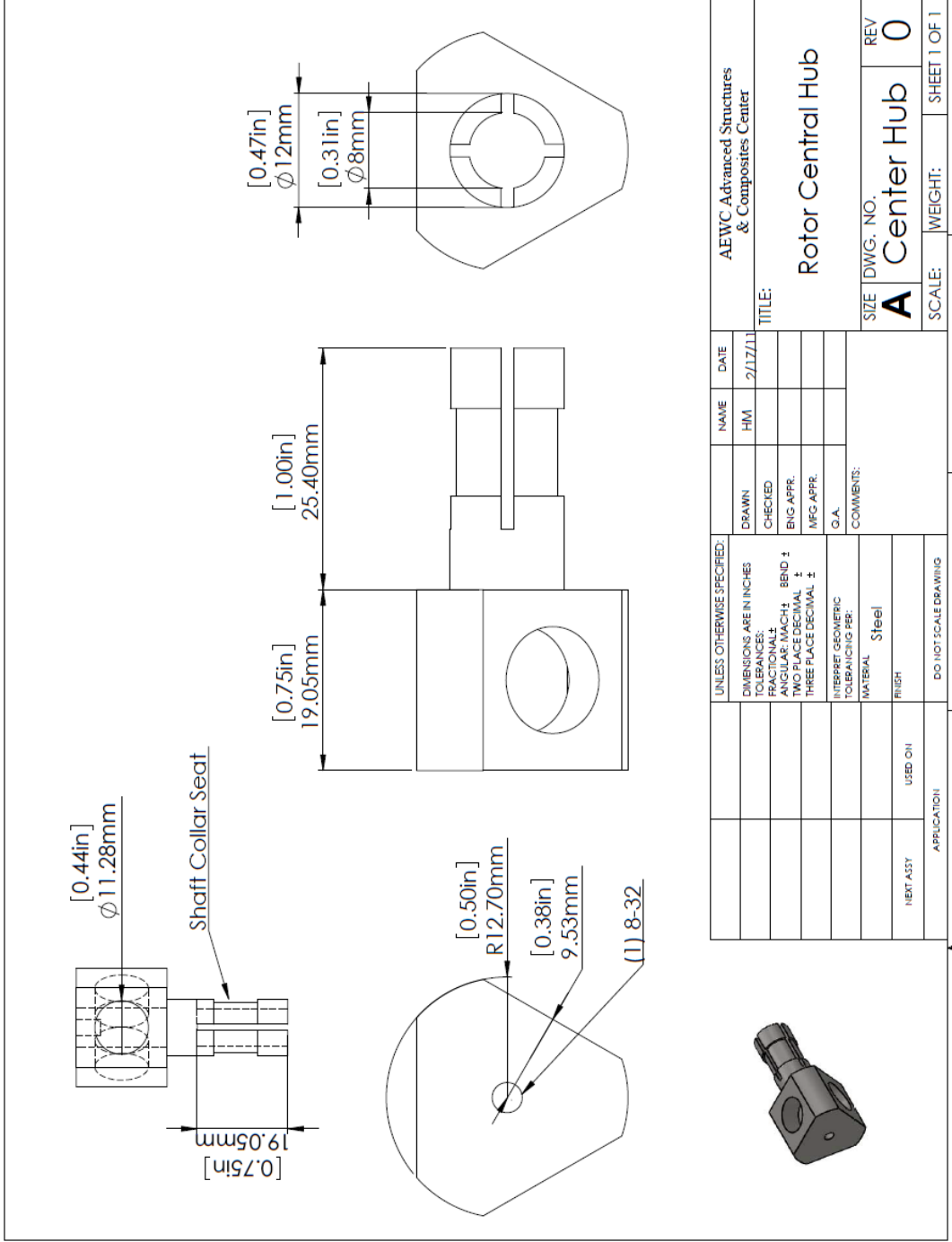
Figure B.1. Nacelle, hub and tower shop drawings.
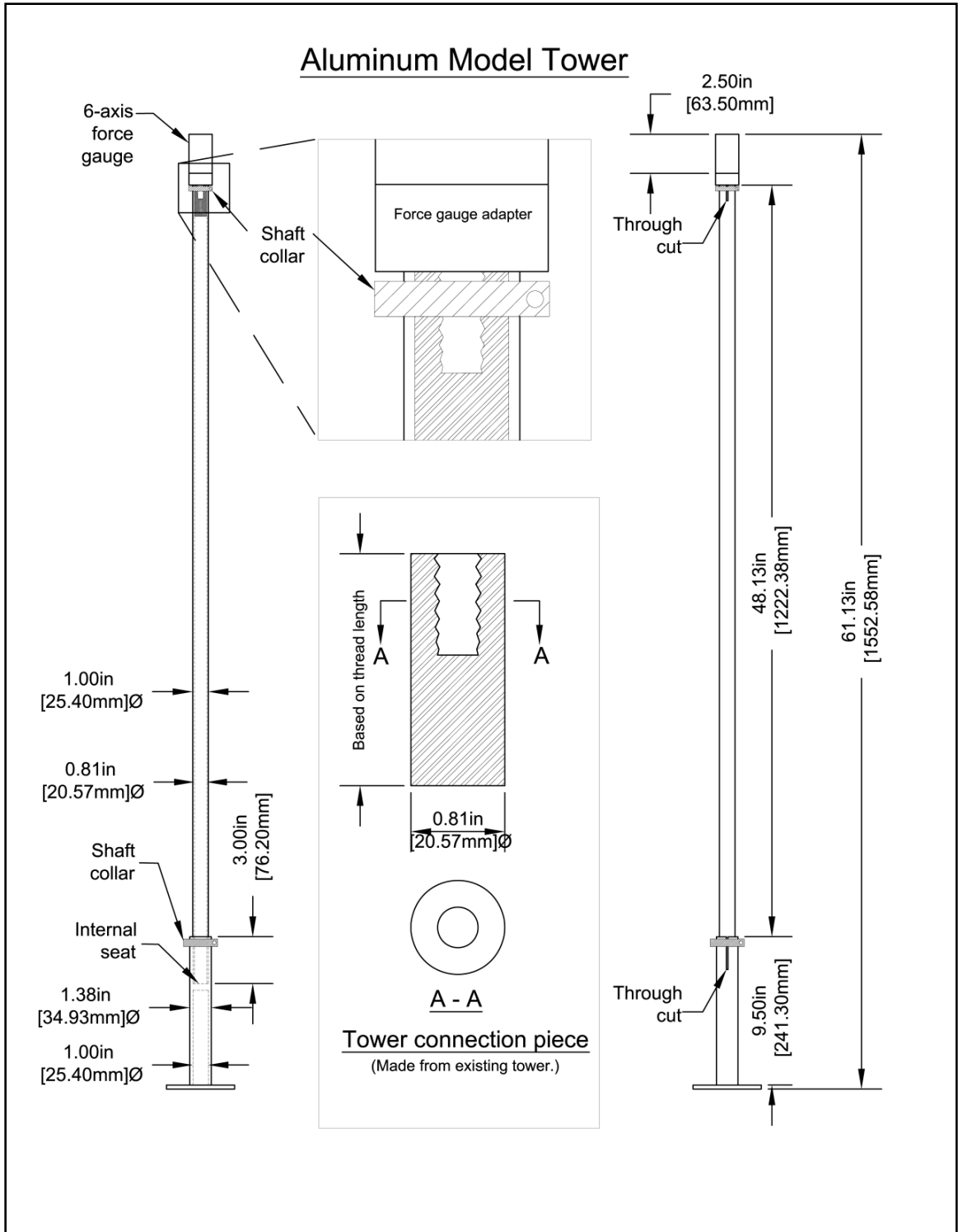
Figure B.1.   Nacelle, hub and tower shop drawings.

APPENDIX C. BLADE GEOMETRY, SCRIPTS AND INPUT FILES

Airfoil 2D Geometry
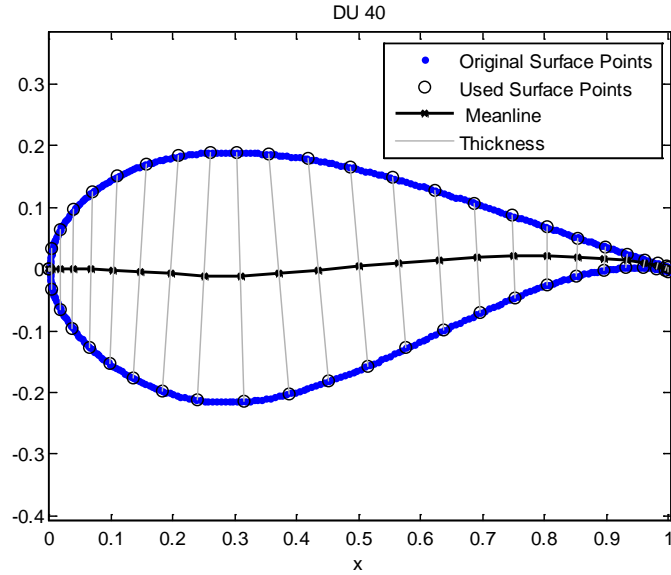
Figure C.1.   2D geometry of model blade airfoil sections.

```
DU40_ft.txt
x/c                t(x)/c             f(x)/c             df/dx(x)
0.0000000e+000     0.0000000e+000     0.0000000e+000     0.0000000e+000
4.2775693e-003     6.5574565e-002    -2.1947304e-005    -5.2558510e-003
1.7037087e-002     1.3030746e-001    -9.3769328e-005    -6.1730149e-003
3.8060234e-002     1.9257545e-001    -2.4239301e-004    -6.1551191e-003
6.6987298e-002     2.5140694e-001    -3.8404680e-004    -1.3437045e-002
1.0332333e-001     3.0411757e-001    -1.2620890e-003    -3.7250904e-002
1.4644661e-001     3.4795068e-001    -3.5382102e-003    -5.8231119e-002
1.9561929e-001     3.8119878e-001    -6.7071413e-003    -6.9467781e-002
2.5000000e-001     4.0118076e-001    -1.0786923e-002    -4.8887020e-002
3.0865828e-001     4.0383509e-001    -1.2000894e-002     2.4752771e-002
3.7059048e-001     3.8946486e-001    -7.4960820e-003     8.1475871e-002
4.3473690e-001     3.6147338e-001    -1.6891405e-003     9.1424304e-002
5.0000000e-001     3.2266322e-001     4.3371165e-003     8.8714308e-002
5.6526310e-001     2.7636500e-001     9.8904004e-003     7.9057419e-002
6.2940952e-001     2.2684946e-001     1.4581258e-002     6.5330014e-002
6.9134172e-001     1.7793445e-001     1.8161053e-002     4.7751685e-002
7.5000000e-001     1.3256259e-001     2.0403724e-002     2.4641268e-002
8.0438071e-001     9.3162842e-002     2.1058515e-002    -5.8035382e-003
8.5355339e-001     6.1468238e-002     1.9979716e-002    -4.3141196e-002
8.9667667e-001     3.8095720e-002     1.7317499e-002    -8.4759338e-002
9.3301270e-001     2.2307767e-002     1.3532745e-002    -1.3239803e-001
9.6193977e-001     1.2861082e-002     9.0525666e-003    -1.8959529e-001
9.8296291e-001     8.4015601e-003     4.5362428e-003    -2.4378830e-001
9.9572243e-001     6.8818589e-003     1.2013367e-003    -2.7605560e-001
1.0000000e+000     6.7328195e-003    -5.7549180e-007    -1.2433734e-001
```
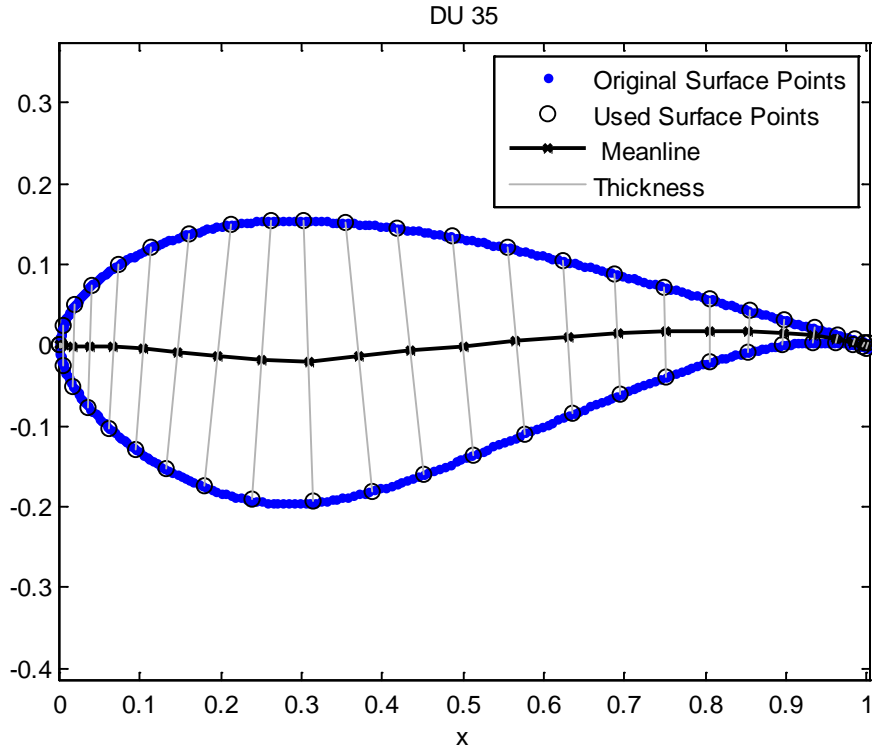
Figure C.1. 2D geometry of model blade airfoil sections.

DU35_ft.txt

x/c	t(x)/c	f(x)/c	df/dx(x)
0.0000000e+000	0.0000000e+000	0.0000000e+000	0.0000000e+000
4.2775693e-003	4.8927993e-002	9.1954304e-006	2.9659318e-004
1.7037087e-002	9.9531343e-002	-5.7549326e-005	-9.8170325e-003
3.8060234e-002	1.5124297e-001	-4.2278906e-004	-2.5697786e-002
6.6987298e-002	2.0267030e-001	-1.4974896e-003	-4.7526594e-002
1.0332333e-001	2.5082022e-001	-3.6979376e-003	-7.1347353e-002
1.4644661e-001	2.9300639e-001	-7.3268356e-003	-9.1164110e-002
1.9561929e-001	3.2647609e-001	-1.2202809e-002	-1.0172065e-001
2.5000000e-001	3.4726079e-001	-1.7888436e-002	-6.4674839e-002
3.0865828e-001	3.4930360e-001	-1.9159013e-002	3.2568070e-002
3.7059048e-001	3.3359988e-001	-1.3596048e-002	9.7913620e-002
4.3473690e-001	3.0607222e-001	-6.7777316e-003	1.0450527e-001
5.0000000e-001	2.7080946e-001	-7.6098097e-005	9.7164152e-002
5.6526310e-001	2.3106279e-001	5.9047352e-003	8.4510896e-002
6.2940952e-001	1.8971897e-001	1.0876206e-002	6.9655969e-002
6.9134172e-001	1.4913949e-001	1.4721010e-002	5.3165636e-002
7.5000000e-001	1.1129800e-001	1.7344308e-002	3.2898225e-002
8.0438071e-001	7.8030057e-002	1.8537255e-002	5.6866081e-003
8.5355339e-001	5.0975388e-002	1.8094335e-002	-2.9255421e-002
8.9667667e-001	3.0942875e-002	1.6067005e-002	-6.9628890e-002
9.3301270e-001	1.7434329e-002	1.2844518e-002	-1.1739099e-001
9.6193977e-001	9.5777834e-003	8.7876940e-003	-1.7814122e-001
9.8296291e-001	6.2487983e-003	4.4635663e-003	-2.3728206e-001
9.9572243e-001	5.4281400e-003	1.1912642e-003	-2.7295846e-001
1.0000000e+000	5.5022424e-003	5.6982911e-009	-1.2332963e-001

112

Figure C.1. 2D geometry of model blade airfoil sections.

DU30_ft.txt

x/c	t(x)/c	f(x)/c	df/dx(x)
0.0000000e+000	0.0000000e+000	0.0000000e+000	0.0000000e+000
4.2775693e-003	3.7041889e-002	8.1015611e-006	-4.6049904e-003
1.7037087e-002	7.6120742e-002	-2.9800761e-004	-2.9450453e-002
3.8060234e-002	1.1886290e-001	-1.1062690e-003	-4.4301956e-002
6.6987298e-002	1.6289490e-001	-2.6208662e-003	-5.7911742e-002
1.0332333e-001	2.0552560e-001	-4.9785828e-003	-6.9039506e-002
1.4644661e-001	2.4413292e-001	-8.1683385e-003	-7.4742832e-002
1.9561929e-001	2.7561296e-001	-1.1887072e-002	-7.0195904e-002
2.5000000e-001	2.9573339e-001	-1.5377807e-002	-3.0746791e-002
3.0865828e-001	2.9905848e-001	-1.5065289e-002	4.4426199e-002
3.7059048e-001	2.8666265e-001	-9.7572763e-003	9.3009282e-002
4.3473690e-001	2.6301000e-001	-3.3058899e-003	9.9364728e-002
5.0000000e-001	2.3218412e-001	3.0987442e-003	9.3910684e-002
5.6526310e-001	1.9736391e-001	8.9519141e-003	8.3689438e-002
6.2940952e-001	1.6091538e-001	1.3942232e-002	6.9904979e-002
6.9134172e-001	1.2508289e-001	1.7799778e-002	5.1860153e-002
7.5000000e-001	9.1932451e-002	2.0262538e-002	2.7380904e-002
8.0438071e-001	6.3383650e-002	2.1015272e-002	-5.2195415e-003
8.5355339e-001	4.0824815e-002	1.9911075e-002	-4.4712933e-002
8.9667667e-001	2.4609131e-002	1.7141173e-002	-8.7957078e-002
9.3301270e-001	1.4090995e-002	1.3218776e-002	-1.3433622e-001
9.6193977e-001	8.1651951e-003	8.7251310e-003	-1.8612875e-001
9.8296291e-001	5.5636416e-003	4.3417621e-003	-2.3445172e-001
9.9572243e-001	4.7845628e-003	1.1493143e-003	-2.6405823e-001
1.0000000e+000	4.7901264e-003	-8.4435508e-008	-1.1898120e-001

Figure C.1.   2D geometry of model blade airfoil sections.

DU25_ft.txt

x/c	t(x)/c	f(x)/c	df/dx(x)
0.0000000e+000	0.0000000e+000	0.0000000e+000	0.0000000e+000
4.2775693e-003	3.4202940e-002	-5.1153001e-005	-2.0608527e-002
1.7037087e-002	6.7728247e-002	-6.4333267e-004	-4.7436786e-002
3.8060234e-002	1.0333986e-001	-1.6761413e-003	-4.1954312e-002
6.6987298e-002	1.3825644e-001	-2.6042565e-003	-2.2440996e-002
1.0332333e-001	1.7122747e-001	-2.9795108e-003	-3.2085344e-003
1.4644661e-001	2.0069533e-001	-2.7535452e-003	1.1492139e-002
1.9561929e-001	2.2474636e-001	-1.8378837e-003	2.5032065e-002
2.5000000e-001	2.4156278e-001	-9.1079363e-005	3.7469316e-002
3.0865828e-001	2.4941372e-001	2.4451586e-003	4.4108090e-002
3.7059048e-001	2.4657077e-001	5.2337957e-003	4.6189699e-002
4.3473690e-001	2.3281770e-001	8.2739319e-003	5.4141844e-002
5.0000000e-001	2.0955174e-001	1.2255468e-002	6.5244563e-002
5.6526310e-001	1.7915448e-001	1.6790056e-002	6.9455134e-002
6.2940952e-001	1.4468295e-001	2.1243682e-002	6.3497902e-002
6.9134172e-001	1.0963617e-001	2.4821597e-002	4.5123127e-002
7.5000000e-001	7.7652377e-002	2.6765732e-002	1.3034267e-002
8.0438071e-001	5.1442631e-002	2.6460741e-002	-3.0403919e-002
8.5355339e-001	3.2203996e-002	2.3863207e-002	-7.8951308e-002
8.9667667e-001	1.9400121e-002	1.9470511e-002	-1.2774674e-001
9.3301270e-001	1.1930122e-002	1.4036239e-002	-1.7217559e-001
9.6193977e-001	8.0667540e-003	8.5348024e-003	-2.0591094e-001
9.8296291e-001	5.8995410e-003	3.9656019e-003	-2.2585233e-001
9.9572243e-001	4.5493346e-003	1.0179258e-003	-2.3629166e-001
1.0000000e+000	4.1680451e-003	-3.9100670e-007	-1.0536030e-001

114
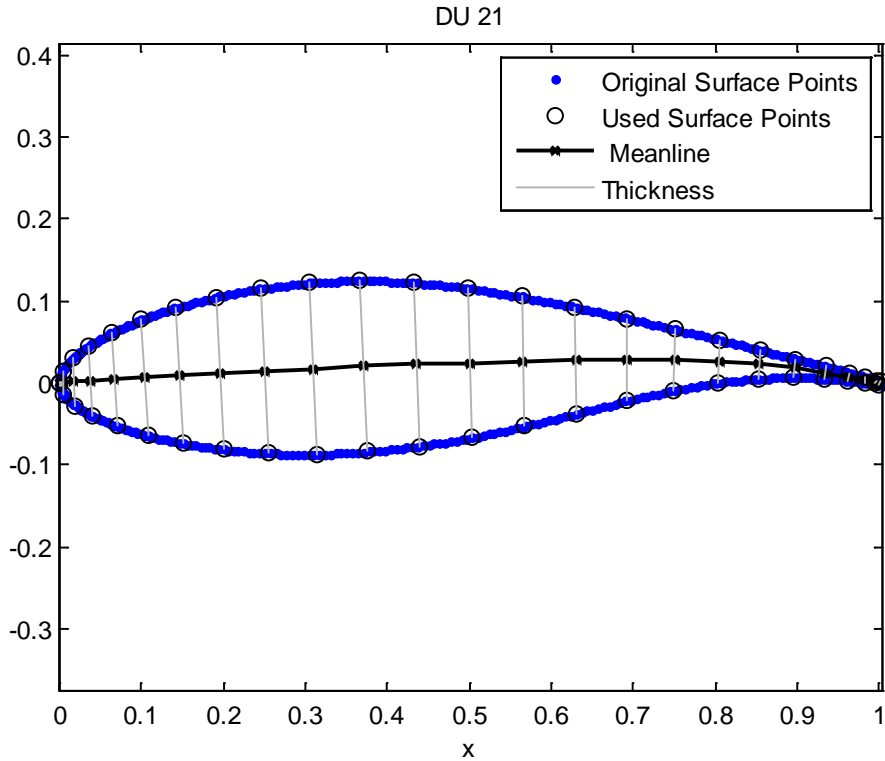
Figure C.1.   2D geometry of model blade airfoil sections.

DU21_ft.txt

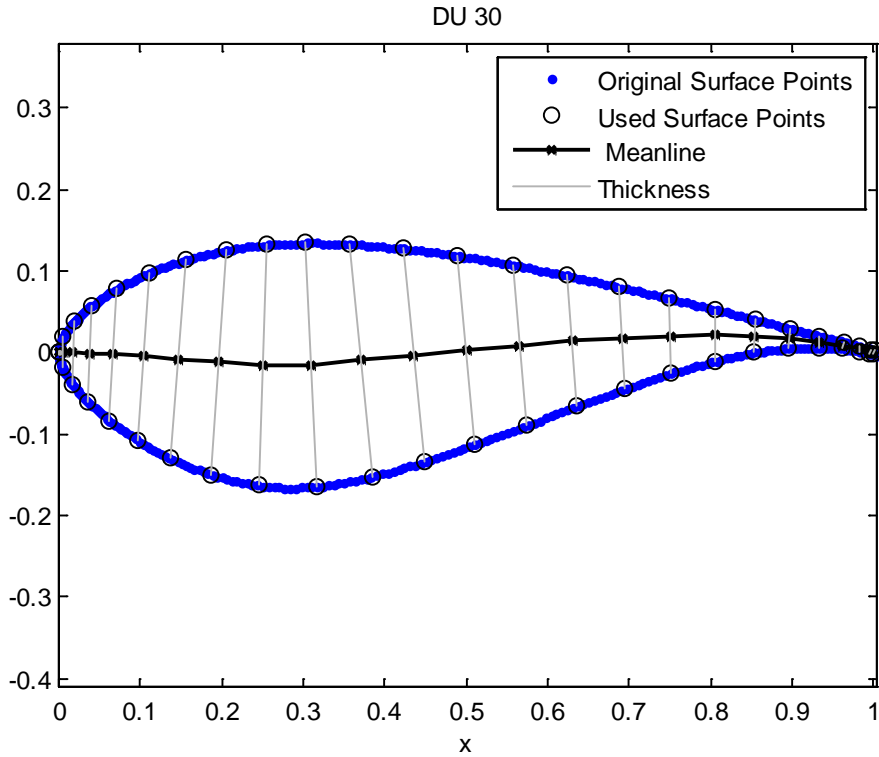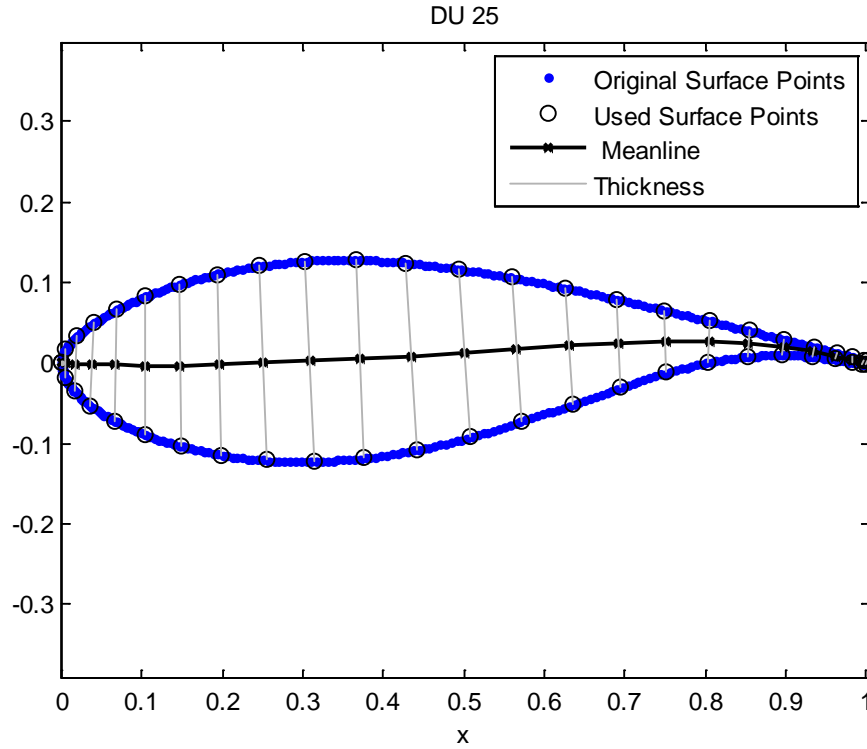| x/c	t(x)/c	f(x)/c	df/dx(x)
0.0000000e+000	0.0000000e+000	0.0000000e+000	0.0000000e+000
4.2775693e-003	2.9290634e-002	2.1645552e-004	5.5713592e-002
1.7037087e-002	5.7171630e-002	1.1218650e-003	6.7369141e-002
3.8060234e-002	8.5786716e-002	2.4138097e-003	6.0580760e-002
6.6987298e-002	1.1421848e-001	4.1314984e-003	5.9850325e-002
1.0332333e-001	1.4135627e-001	6.3276892e-003	5.9021542e-002
1.4644661e-001	1.6582953e-001	8.8002396e-003	5.6207663e-002
1.9561929e-001	1.8614406e-001	1.1500810e-002	5.4438397e-002
2.5000000e-001	2.0091800e-001	1.4432237e-002	5.2929691e-002
3.0865828e-001	2.0881617e-001	1.7475252e-002	4.9088698e-002
3.7059048e-001	2.0864034e-001	2.0333099e-002	4.0744363e-002
4.3473690e-001	1.9965937e-001	2.2587902e-002	3.2143847e-002
5.0000000e-001	1.8209038e-001	2.4486045e-002	2.7626625e-002
5.6526310e-001	1.5785266e-001	2.6193900e-002	2.4388393e-002
6.2940952e-001	1.2987365e-001	2.7646078e-002	1.7665399e-002
6.9134172e-001	1.0109065e-001	2.8442772e-002	3.0448671e-003
7.5000000e-001	7.4521340e-002	2.8075854e-002	-2.1747461e-002
8.0438071e-001	5.2223797e-002	2.6112167e-002	-5.5160982e-002
8.5355339e-001	3.5103389e-002	2.2552682e-002	-9.1633710e-002
8.9667667e-001	2.2960697e-002	1.7873279e-002	-1.2718206e-001
9.3301270e-001	1.4900952e-002	1.2680372e-002	-1.5848741e-001
9.6193977e-001	9.7346020e-003	7.7371466e-003	-1.8349345e-001
9.8296291e-001	6.4489801e-003	3.6869068e-003	-2.0492106e-001
9.9572243e-001	4.4655498e-003	9.7723269e-004	-2.2450760e-001
1.0000000e+000	3.7960897e-003	-5.2714042e-007	-1.0113921e-001
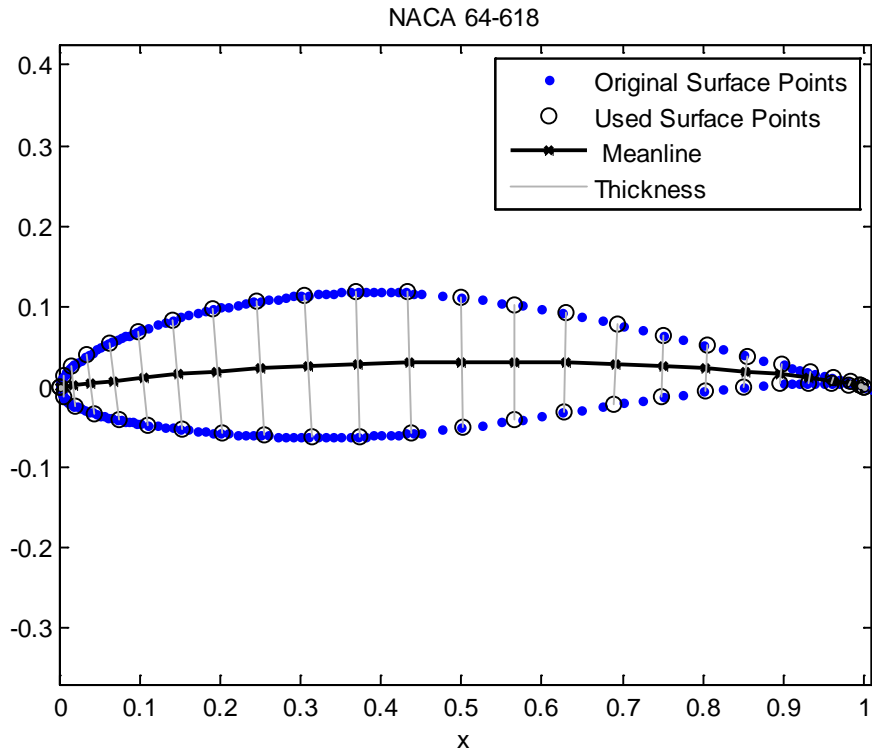
Figure C.1. 2D geometry of model blade airfoil sections.

```
NACA_ft.txt
  x/c                t(x)/c             f(x)/c             df/dx(x)
  0.0000000e+000    0.0000000e+000    0.0000000e+000    0.0000000e+000
  4.2775693e-003    2.6553072e-002   -2.3949415e-006    1.3829899e-002
  1.7037087e-002    5.0001579e-002    7.2174641e-004    7.7804219e-002
  3.8060234e-002    7.3096404e-002    3.0866209e-003    1.1770161e-001
  6.6987298e-002    9.5861079e-002    6.6988548e-003    1.2053392e-001
  1.0332333e-001    1.1741418e-001    1.0880493e-002    1.0730649e-001
  1.4644661e-001    1.3706976e-001    1.5109942e-002    9.0193195e-002
  1.9561929e-001    1.5403784e-001    1.9102871e-002    7.3725337e-002
  2.5000000e-001    1.6748167e-001    2.2662446e-002    5.8487166e-002
  3.0865828e-001    1.7649808e-001    2.5652233e-002    4.4374572e-002
  3.7059048e-001    1.7988768e-001    2.7969209e-002    3.1036321e-002
  4.3473690e-001    1.7503222e-001    2.9536512e-002    1.8181153e-002
  5.0000000e-001    1.6219929e-001    3.0307939e-002    5.5587147e-003
  5.6526310e-001    1.4422493e-001    3.0262070e-002   -7.0823963e-003
  6.2940952e-001    1.2295329e-001    2.9405536e-002   -1.9939289e-002
  6.9134172e-001    1.0017464e-001    2.7776817e-002   -3.3233133e-002
  7.5000000e-001    7.7618932e-002    2.5442143e-002   -4.7298814e-002
  8.0438071e-001    5.6692175e-002    2.2492010e-002   -6.2494055e-002
  8.5355339e-001    3.8606660e-002    1.9052435e-002   -7.9354625e-002
  8.9667667e-001    2.4135989e-002    1.5274697e-002   -9.8657381e-002
  9.3301270e-001    1.3509143e-002    1.1351433e-002   -1.2192152e-001
  9.6193977e-001    6.5303625e-003    7.5033541e-003   -1.5086316e-001
  9.8296291e-001    2.5523596e-003    4.0592187e-003   -2.0813133e-001
  9.9572243e-001    5.3710290e-004    1.0604577e-003   -2.4467500e-001
  1.0000000e+000    0.0000000e+000    0.0000000e+000   -1.7363690e-001
```

Blade Geometry Source Code

Tip_section_distribution.m

```
% --- Script to generate and interpolate blade tip information.---
% H. Martin
% 11/6/10

% Identify tip airfoil locations along blade length:
n       = 8;                               % Number of sections -1:
r       = zeros(1,n);
for i = 0:n-1
    r(i+1) = cosd(90*(i/(n-1)));           % Cosine spacing from 1 to 0
end
r       = fliplr(r);                       % Reverse spacing to 0 to 1.
r       = r*(63-61.6333);                  % Range r = [0:1.1.3667]

% ----------------- Tip chord distribution: ------------------------
c       = tip_c_dist(r);                   % Quadratic function see below
c(end)  = 0.200;
c_nd    = c./126;                          % Non-dimensional chord,c/D
                                           % where D = 126m full scale
% Full quatratic distribution:
dist = [0:1.3667/100:1.3667];
disty = tip_c_dist(dist);
dist_roR = (dist+61.6333)/63;

% Plot chord distribution of each section and full distribution:
figure(1)
plot(dist_roR, disty./126);
hold on
roR = (r+61.6333)/63;
plot(roR,c_nd, 'or');
legend('Quadratic Distribution','Selected chord lengths')
xlabel('r/R')
ylabel('c/D')

% ------------------ Tip pitch distribution: -----------------------
% Find pitch angle (theta_p) of each blade section based on NREL given
% distribution:
load NREL_5MWBlade.txt                 % Table 2-1 of (Jonkman, 2009)
roR         = NREL_5MWBlade(:,1);      % BlFract
theta       = NREL_5MWBlade(:,3);      % StrcTwst

roR_tip     = roR(45:end);
theta_tip   = theta(45:end);
roR_tip_cos = (r+61.6333)/63;          % Cosine spacing tip span
locations.

% Interpolate pitch angle based on established distribution:
theta_tip_ext = pchip(roR_tip, theta_tip, roR_tip_cos');

% Plot full distribution
figure(2)
NREL1 = plot(roR, theta, '.-');
hold on
```

```
Interp = plot(roR_tip_cos, theta_tip_ext, 'ro');
legend('NREL StrcTwst','Pchip interpolation')
xlabel('r/R'); ylabel('{\theta}_p, (°)');

% Zoom in on tip section distribution
figure(3)
NREL = plot(roR_tip, theta_tip, '.-');
hold on
Interp = plot(roR_tip_cos, theta_tip_ext, 'ro');
legend('NREL StrcTwst','Pchip interpolation')
axis tight
xlabel('r/R'); ylabel('{\theta}_p, (°)');
```

---

tip_c_dist.m

```
function c = tip_c_dist(y)
% Function to project a quadratic chord distribution
% H. Martin
% 11/6/10
%
% The quadratic form, y = a(c-0.200)^2 + 1.3667 was used where:
%       y   = location along blade span
%       c   = chord length
%
% and   y = 0,       c = 0.200 and
%       y = 1.3667, c = 1.419
%
% gives:

a    = (1.3667/(1.419-0.200)^2);
c    = sqrt((1.3667-y)/a) + 0.200;
```

SmoothThickness.m

```
% ---Script to calculate new airfoil thickness distribution and
%     generate a fair blade.
%
% A. Goupee and H. Martin
% 11/15/11

% Load original airfoil geometry:
R = 1.23;
o = load('rRto.txt');               % [r/R, t/c] - r/R from Table 3.1,
                                    %  t/c from NREL distribution.
c = load('c.txt');                  % Full scale chord length.
c = c/50;                           % [c] model scale.

% Create array to base spline:
n  = 100;
ta = linspace(0,1,n);
xa = linspace(0.1685,0.8696,n);

% Cubic Hermite spline:
p0 = 0.05078;                       % Starting point
m0 = -0.09;                         % Starting tangent
```

118

```
p1 = 0.01084;                          % Ending point
m1 = -0.021;                           % Ending tangent


for i = 1:n;
    t = ta(i);
    ra(i) = (2*t^3-3*t^2+1)*p0+(t^3-2*t^2+t)*m0+(-2*t^3+3*t^2)*p1+(t^3-
t^2)*m1;
end;


xi      = o(6:13,1).*R;        % Section to focus smoothing, model scale
xi_n    = o(6:13,1);           % " " " ", non-dimensional

% Extrapolated thickness along cubic spline
ri      = interp1(xa,ra,xi,'pchip');
ci      = c(6:13);                     % Chords along section
ri_n    = ri./ci;                      % Non-dimensional thickness

% Generate comparison plot of original thickness and spline thickness:
figure(1), clf
plot(o(:,1),o(:,2),'.-')               % non-dimensional NREL distribution
hold on
plot(xi./R,ri./ci,'r*')                % non-dimensional extrapolation
% plot(xa,ra,'r')
xs      = [o(5,1);xi_n;o(14,1)];
rs      = [o(5,2);ri_n;o(14,2)];
plot(xs,rs,'r')
legend('Original thickness','Cubic spline interpolation')
% title('Section thickness vs span location')
xlabel('r/R'); ylabel('t/c')
```

ProjectAirfoil.m
```
% Project airfoils along blade span with correct pitch, chord,
% thickness, and pitch axis origin.
% H. Martin
% 11/16/11
%
% Updates:
% 11/22/10 - Incorporate thickness, meanline values instead of x
% and y surface point values:
% 11/24/10 - Incorporated thickness smoothing along length

close all
% ---- Generate and load base information -------------------------
num_coord   = 49;                      % # surface points/airfoil
Np          = 25;                      % To make 49 points total.
lambda      = 50;                      % Scale factor

% Load full scale blade properties: (Table 3.1 w/ D = 126 m)
load BladeProps.txt
% Define properties in model scale
r           = BladeProps(:,1)/lambda;  % [m]   Span location
c           = BladeProps(:,2)/lambda;  % [m]   Chord length
theta       = BladeProps(:,3);         % [deg] Pitch angle
```

```matlab
xoc          = BladeProps(:,4);          % [%]   Pitch axis origin

% Cubic thickness interpolation:
% Updated: 11/24/10 - See SmoothThickness.m
tn           = [0.4772, 0.3834 0.3306 0.2897 0.2600 0.2381 0.2194
0.2015];
% New max thickness for: [DU40, DU35, DU35, DU30, DU25, DU25, DU21,
DU21]

% Trailing edge thickness: Determine wedge profile for each airfoil:
t_reqd       = 2e-3;                      % [m] required TE thickness
                                          % of each airfoil at model
                                          scale
lambda       = 50;                        % Desired scale factor
tnd_reqd     = (1./c)*t_reqd;%*lambda;    % Non-dimensional required
                                          % TE thickness.
% Determine number of sections:
s            = size(r);
num_sec      = s(1,1);

% ---------- Generate 2D section profiles -------------------------
% y2D_nd [m], y position in 2D space for foil with wedge prior to
% rotation.
% x2Dr [m], x position in 2D space after rotation for pitch angle &
% scale
% for chord
% y2Dr [m], y position in 2D space after rotation for pitch angle &
% scale for chord

y2D_nd  = zeros(num_coord,1);
x2Dr    = zeros(num_coord, num_sec);
y2Dr    = zeros(num_coord, num_sec);
x2D     = zeros(num_coord, num_sec);
y2D     = zeros(num_coord, num_sec);
str_prefix = {'r/R = '};
flag = 1;
count = 1;
taper = [2:(6-2)/6:6];

for i = 1:num_sec                      % for each section along the
span
    if (i == 1)||(i ==2)               % Use the DU 40 section
        props   = load('DU40_ft.txt');
    elseif (i == 3)%||(i == 3)         % Use the DU 35 section
        props   = load('DU35_ft.txt');
    elseif i == 4                      % Use the DU 30 section
        props   = load('DU30_ft.txt');
    elseif (i == 5)||(i == 6)          % Use the DU 25 section
        props   = load('DU25_ft.txt');
    elseif (i == 7)||(i == 8)          % Use the DU 21 section
         props   = load('DU21_ft.txt');
    else                               % Use the DU 21 section
         props   = load('NACA_ft.txt');
    end
```

```
Np        = max(size(props));
x1        = props(:,1);
t         = props(:,2);

% Incorporate thickness smoothing for DU foils:
if (i >= 1) && (i <= 8)
    t         = tn(i)/max(t).*t;
end
to(i)    = max(t);
f         = props(:,3);
dfdx      = props(:,4);
t_final(i) = max(t);
for j = 1:Np                        % for EA point along the chord
    x2D_u(j) = x1(j) - (t(j)/2)*sin(atan(dfdx(j))); % 2D upper
                                                    % surface x
     x2D_l(j) = x1(j) + (t(j)/2)*sin(atan(dfdx(j))); % 2D lower
                                                     % surface x
    y2D_u(j) =  f(j) + (t(j)/2)*cos(atan(dfdx(j)));  % 2D upper
                                                    % surface y
    y2D_l(j) =  f(j) - (t(j)/2)*cos(atan(dfdx(j))); % 2D lower
                                                    % surface y
end

 % Combine coordinates:
 x2D_nd                = zeros(Np*2-1,1);
 y2D_nd1               = zeros(Np*2-1,1);
 x2D_nd(1:Np)          = flipud(x2D_u');
 x2D_nd(Np+1:Np*2-1)   = x2D_l(2:end)';
 y2D_nd1(1:Np)         = flipud(y2D_u');
 y2D_nd1(Np+1:Np*2-1)  = y2D_l(2:end)';

% Implement wedge:
for j = 1:Np
    if i <=  15
        % Upper surface
        y2D_nd(j) = y2D_nd1(j) + x2D_nd(j)*(tnd_reqd(i)/2 -
                    y2D_nd1(1));
        % Lower surface
        y2D_nd(j+Np-1)  = y2D_nd1(j+Np-1) - x2D_nd(j+Np-
                    1)*(tnd_reqd(i)/2 + y2D_nd1(end));
    else
        % tip geometry:
        % Upper surface
        y2D_nd(j)        = y2D_nd1(j) +
                    x2D_nd(j)*(tnd_reqd(i)/(taper(count)) -
                    y2D_nd1(1));
        % Lower surface
        y2D_nd(j+Np-1)  = y2D_nd1(j+Np-1) - x2D_nd(j+Np-
                    1)*(tnd_reqd(i)/(taper(count)) +
                    y2D_nd1(end));
    end
end

if i > 15; count = count+1; end
```

121

```matlab
    % Implement chord length
    x2D(:,i)  = c(i).*(x2D_nd - xoc(i));
    y2D(:,i)  = c(i).*y2D_nd;

    % Implement pitch angle:
    % rotated 2D upper and lower surface x
    x2Dr(:,i) = x2D(:,i)*cosd(theta(i)) - y2D(:,i)*sind(theta(i));
    % rotated 2D upper and lower surface y
    y2Dr(:,i) = x2D(:,i)*sind(theta(i)) + y2D(:,i)*cosd(theta(i));

    % Build legend string for plots:
    str_legend(flag)=strcat(str_prefix,num2str(r(i)/(63/lambda)));
    flag = flag + 1;
    clear x2D_nd y2D_nd1 y2D_nd
end

% Plot pitched and unpitched sections:
figure(1)
plot(x2Dr,y2Dr, '.-')
title('Rotated 2D DU Sections')
legend(str_legend,'location','northwest');
axis equal

figure(3)
plot(x2D,y2D, '.-')
title('Unrotated 2D Sections')
legend(str_legend,'location','northwest');
axis equal

% ------------------ Project Airfoils 3D coordinates ---------------
--------
% X3D [m], X position in 3D space (corresponds to y position in 2D
% space)
% Y2D [m], Y position in 3D space
% Z3D [m], Z position in 3D space

X3D = zeros(num_coord, num_sec);
Y3D = zeros(num_coord, num_sec);
Z3D = zeros(num_coord, num_sec);

% for i = 1:num_sec        % for each section along the span
for j = 1:num_sec          % for each section along the span
   for i = 1:num_coord     % for each point along the upper and
                           % lower surfaces
            X3D(i,j) = r(j)*(pi/180)*tand(theta(j)) + y2Dr(i,j);
            Y3D(i,j) = r(j)*sind((180/pi)*x2Dr(i,j)/r(j));
            Z3D(i,j) = r(j)*cosd((180/pi)*x2Dr(i,j)/r(j));
    end
end

% Plot projected airfoils:
figure(2)
plot3(X3D, Y3D, Z3D, '.-')
```

122

```matlab
axis equal
legend(str_legend,'location','northwest');

% -------- Create SolidWorks File:--------------------------------
% This creates the SectionCurves for the DU40-NACA64 airfoil
% section, or Sections 6-26

filename    = 'NREL_Blade';
filename_SolidWorks = strcat(filename,'_SolidWorks.txt');
fid = fopen(filename_SolidWorks,'w');
fid2 = fopen('DeepCwind.txt','w');
% Prop Parameters at beginning of file
Z = 3;
fprintf(fid,'%g, ' ,num_coord);
fprintf(fid,'%g, ' ,num_sec);
fprintf(fid,'%g,\n',Z);

% Output curves defining each 2D section along the span
% for each section along the span
for j = 1:num_sec
    fprintf(fid,strcat('SectionCurve',num2str(j+5),',\n'));
    % for each point along the suction and pressure surfaces
    % (trailing edge -> leading edge -> trailing edge, close the
curve)
    for i = 1:num_coord %
        fprintf(fid,'%f,%f,%f,\n',X3D(i,j),Y3D(i,j),Z3D(i,j));
        fprintf(fid2,'%f,%f,%f,\n',X3D(i,j),Y3D(i,j),Z3D(i,j));
        %Reprint 1st and last sections
        if i == 1
            fprintf(fid,'%f,%f,%f,\n',X3D(i,j),Y3D(i,j),Z3D(i,j));
            fprintf(fid2,'%f,%f,%f,\n',X3D(i,j),Y3D(i,j),Z3D(i,j));
        elseif i == num_coord
            fprintf(fid,'%f,%f,%f,\n',X3D(i,j),Y3D(i,j),Z3D(i,j));
            fprintf(fid2,'%f,%f,%f,\n',X3D(i,j),Y3D(i,j),Z3D(i,j));
        else
        end

    end
end

%Tip Curves:
for j = num_sec
    fprintf(fid,strcat('TipSectionCurve',num2str(j+5),',\n'));
    for i = 1:num_coord
        fprintf(fid,'%f,%f,%f,\n',X3D(i,j),Y3D(i,j),Z3D(i,j))
    end
    for i = 1:Np-1
        fprintf(fid,'%f,%f,%f,\n',X3D(i+1,j),Y3D(i+1,j),Z3D(i+1,j));
        fprintf(fid,'%f,%f,%f,\n',tip(-i,1),tip(s(1,1)-i,2),...
            tip(s(1,1) - i,3));
    end
end
```

Solidworks Blade Input File

SWBladeInput.txt
```
26, 25, 3,
SectionCurve1,
0.000000,0.035000,0.030000,
0.004387,0.034724,0.030000,
0.008704,0.033900,0.030000,
0.012884,0.032542,0.030000,
0.016861,0.030671,0.030000,
0.020572,0.028316,0.030000,
0.023959,0.025514,0.030000,
0.026968,0.022310,0.030000,
0.029551,0.018754,0.030000,
0.031669,0.014902,0.030000,
0.033287,0.010816,0.030000,
0.034380,0.006558,0.030000,
0.034931,0.002198,0.030000,
0.034931,-0.002198,0.030000,
0.034380,-0.006558,0.030000,
0.033287,-0.010816,0.030000,
0.031669,-0.014902,0.030000,
0.029551,-0.018754,0.030000,
0.026968,-0.022310,0.030000,
0.023959,-0.025514,0.030000,
0.020572,-0.028316,0.030000,
0.016861,-0.030671,0.030000,
0.012884,-0.032542,0.030000,
0.008704,-0.033900,0.030000,
0.004387,-0.034724,0.030000,
0.000000,-0.035000,0.030000,
-0.004387,-0.034724,0.030000,
-0.008704,-0.033900,0.030000,
-0.012884,-0.032542,0.030000,
-0.016861,-0.030671,0.030000,
-0.020572,-0.028316,0.030000,
-0.023959,-0.025514,0.030000,
-0.026968,-0.022310,0.030000,
-0.029551,-0.018754,0.030000,
-0.031669,-0.014902,0.030000,
-0.033287,-0.010816,0.030000,
-0.034380,-0.006558,0.030000,
-0.034931,-0.002198,0.030000,
-0.034931,0.002198,0.030000,
-0.034380,0.006558,0.030000,
-0.033287,0.010816,0.030000,
-0.031669,0.014902,0.030000,
-0.029551,0.018754,0.030000,
-0.026968,0.022310,0.030000,
-0.023959,0.025514,0.030000,
-0.020572,0.028316,0.030000,
-0.016861,0.030671,0.030000,
-0.012884,0.032542,0.030000,
-0.008704,0.033900,0.030000,
-0.004387,0.034724,0.030000,
0.000000,0.035000,0.030000,
SectionCurve2,
0.000000,0.035000,0.039200,
0.004387,0.034724,0.039200,
0.008704,0.033900,0.039200,
0.012884,0.032542,0.039200,
0.016861,0.030671,0.039200,
```

```
0.020572,0.028316,0.039200,
0.023959,0.025514,0.039200,
0.026968,0.022310,0.039200,
0.029551,0.018754,0.039200,
0.031669,0.014902,0.039200,
0.033287,0.010816,0.039200,
0.034380,0.006558,0.039200,
0.034931,0.002198,0.039200,
0.034931,-0.002198,0.039200,
0.034380,-0.006558,0.039200,
0.033287,-0.010816,0.039200,
0.031669,-0.014902,0.039200,
0.029551,-0.018754,0.039200,
0.026968,-0.022310,0.039200,
0.023959,-0.025514,0.039200,
0.020572,-0.028316,0.039200,
0.016861,-0.030671,0.039200,
0.012884,-0.032542,0.039200,
0.008704,-0.033900,0.039200,
0.004387,-0.034724,0.039200,
0.000000,-0.035000,0.039200,
-0.004387,-0.034724,0.039200,
-0.008704,-0.033900,0.039200,
-0.012884,-0.032542,0.039200,
-0.016861,-0.030671,0.039200,
-0.020572,-0.028316,0.039200,
-0.023959,-0.025514,0.039200,
-0.026968,-0.022310,0.039200,
-0.029551,-0.018754,0.039200,
-0.031669,-0.014902,0.039200,
-0.033287,-0.010816,0.039200,
-0.034380,-0.006558,0.039200,
-0.034931,-0.002198,0.039200,
-0.034931,0.002198,0.039200,
-0.034380,0.006558,0.039200,
-0.033287,0.010816,0.039200,
-0.031669,0.014902,0.039200,
-0.029551,0.018754,0.039200,
-0.026968,0.022310,0.039200,
-0.023959,0.025514,0.039200,
-0.020572,0.028316,0.039200,
-0.016861,0.030671,0.039200,
-0.012884,0.032542,0.039200,
-0.008704,0.033900,0.039200,
-0.004387,0.034724,0.039200,
0.000000,0.035000,0.039200,
SectionCurve3,
0.008492,0.035901,0.067978,
0.008005,0.036013,0.067986,
0.007512,0.036100,0.067995,
0.005924,0.036303,0.068019,
0.005323,0.036356,0.068026,
0.002795,0.036453,0.068048,
-0.000627,0.036255,0.068061,
-0.004309,0.035627,0.068050,
-0.009796,0.033878,0.067984,
-0.014660,0.031459,0.067880,
-0.020261,0.027460,0.067714,
-0.026100,0.021313,0.067490,
-0.030193,0.014655,0.067293,
-0.033082,0.005978,0.067069,
-0.033745,-0.001970,0.066965,
-0.032366,-0.010689,0.067191,
```

```
-0.029581,-0.017444,0.067381,
-0.026355,-0.022330,0.067537,
-0.022006,-0.026869,0.067700,
-0.018732,-0.029366,0.067796,
-0.015449,-0.031295,0.067873,
-0.012883,-0.032474,0.067920,
-0.011015,-0.033170,0.067950,
-0.009208,-0.033727,0.067976,
-0.008620,-0.033883,0.067984,
-0.008041,-0.034028,0.067992,
-0.007457,-0.034158,0.067999,
-0.006860,-0.034282,0.068007,
-0.004986,-0.034594,0.068027,
-0.004335,-0.034678,0.068033,
-0.001597,-0.034886,0.068050,
0.002110,-0.034801,0.068053,
0.006092,-0.034239,0.068028,
0.011981,-0.032456,0.067944,
0.017101,-0.029841,0.067829,
0.022768,-0.025406,0.067659,
0.028230,-0.018579,0.067450,
0.031623,-0.011387,0.067272,
0.033521,-0.002401,0.067065,
0.033347,0.005495,0.066974,
0.031295,0.013855,0.067213,
0.028290,0.020203,0.067407,
0.025112,0.024765,0.067559,
0.021016,0.029018,0.067714,
0.017997,0.031384,0.067799,
0.014998,0.033241,0.067866,
0.012663,0.034403,0.067909,
0.010964,0.035106,0.067939,
0.009456,0.035635,0.067964,
0.008977,0.035780,0.067971,
0.008492,0.035901,0.067978,
SectionCurve4,
0.009688,0.040955,0.113521,
0.009270,0.041053,0.113524,
0.008848,0.041107,0.113529,
0.008423,0.041120,0.113538,
0.007995,0.041092,0.113546,
0.007469,0.041041,0.113554,
0.004670,0.040567,0.113600,
0.000980,0.039437,0.113659,
-0.004388,0.036873,0.113707,
-0.010103,0.033042,0.113686,
-0.015955,0.027956,0.113611,
-0.021580,0.021601,0.113529,
-0.025837,0.014999,0.113482,
-0.029229,0.006436,0.113452,
-0.030505,-0.001502,0.113454,
-0.029916,-0.010361,0.113527,
-0.027743,-0.017338,0.113581,
-0.024925,-0.022418,0.113618,
-0.020934,-0.027112,0.113653,
-0.017877,-0.029652,0.113673,
-0.014212,-0.031877,0.113692,
-0.011295,-0.033146,0.113704,
-0.009108,-0.033856,0.113712,
-0.008585,-0.033999,0.113714,
-0.008073,-0.034129,0.113716,
-0.008073,-0.034129,0.113716,
-0.007554,-0.034242,0.113718,
```

```
-0.007020,-0.034349,0.113719,
-0.006472,-0.034447,0.113721,
-0.005908,-0.034537,0.113722,
-0.004737,-0.034694,0.113725,
-0.001546,-0.034872,0.113729,
0.004273,-0.034236,0.113726,
0.010688,-0.032029,0.113709,
0.015544,-0.029084,0.113683,
0.020788,-0.024171,0.113636,
0.025600,-0.016806,0.113561,
0.028448,-0.009301,0.113494,
0.029943,-0.000151,0.113431,
0.029734,0.007813,0.113419,
0.028082,0.016329,0.113497,
0.024546,0.025523,0.113580,
0.020963,0.031431,0.113600,
0.017553,0.035465,0.113582,
0.014111,0.038474,0.113550,
0.011735,0.040054,0.113532,
0.011275,0.040319,0.113529,
0.010897,0.040526,0.113528,
0.010508,0.040707,0.113524,
0.010106,0.040855,0.113521,
0.009688,0.040955,0.113521,
SectionCurve5,
0.011074,0.046815,0.166769,
0.010662,0.046912,0.166770,
0.010241,0.046994,0.166771,
0.009867,0.046967,0.166782,
0.009479,0.046757,0.166798,
0.009027,0.046495,0.166811,
0.006681,0.044961,0.166881,
0.003663,0.042633,0.166958,
-0.000734,0.038733,0.167012,
-0.005595,0.033985,0.166993,
-0.010854,0.028419,0.166927,
-0.016230,0.021991,0.166862,
-0.020608,0.015586,0.166831,
-0.024516,0.007372,0.166817,
-0.026518,-0.000311,0.166825,
-0.026973,-0.009067,0.166874,
-0.025752,-0.016177,0.166908,
-0.023654,-0.021513,0.166926,
-0.020293,-0.026578,0.166938,
-0.017533,-0.029365,0.166943,
-0.014079,-0.031807,0.166946,
-0.011252,-0.033172,0.166949,
-0.009107,-0.033911,0.166952,
-0.008592,-0.034058,0.166953,
-0.008087,-0.034189,0.166953,
-0.008087,-0.034189,0.166953,
-0.007574,-0.034298,0.166954,
-0.007045,-0.034396,0.166955,
-0.006502,-0.034484,0.166956,
-0.005944,-0.034563,0.166957,
-0.004784,-0.034699,0.166959,
-0.001630,-0.034756,0.166963,
0.004053,-0.033709,0.166971,
0.010099,-0.030832,0.166977,
0.014455,-0.027298,0.166971,
0.018892,-0.021758,0.166946,
0.022686,-0.013934,0.166892,
0.024787,-0.006283,0.166841,
```

```
0.025771,0.002829,0.166798,
0.025508,0.010699,0.166794,
0.024267,0.019182,0.166853,
0.021835,0.028611,0.166917,
0.019432,0.035003,0.166922,
0.017110,0.039678,0.166885,
0.014664,0.043477,0.166828,
0.012876,0.045655,0.166792,
0.012518,0.046039,0.166787,
0.012218,0.046346,0.166784,
0.011879,0.046564,0.166775,
0.011485,0.046717,0.166769,
0.011074,0.046815,0.166769,
SectionCurve6,
0.015066,0.054739,0.228536,
0.015066,0.054739,0.228536,
0.015090,0.054397,0.228617,
0.015193,0.053219,0.228895,
0.015379,0.051278,0.229337,
0.015655,0.048596,0.229920,
0.016039,0.045188,0.230614,
0.016566,0.041065,0.231384,
0.017236,0.036251,0.232187,
0.018017,0.030819,0.232970,
0.018854,0.024881,0.233679,
0.019666,0.018567,0.234265,
0.020350,0.012024,0.234692,
0.020767,0.005446,0.234937,
0.020788,-0.000914,0.234998,
0.020382,-0.006754,0.234903,
0.019734,-0.011200,0.234733,
0.018795,-0.014829,0.234532,
0.016999,-0.019108,0.234222,
0.014414,-0.023427,0.233829,
0.011293,-0.027198,0.233421,
0.007732,-0.030176,0.233055,
0.004010,-0.032109,0.232796,
0.000301,-0.033211,0.232641,
-0.003366,-0.033560,0.232591,
-0.006897,-0.033149,0.232650,
-0.010252,-0.031985,0.232813,
-0.013397,-0.030088,0.233066,
-0.016249,-0.027486,0.233387,
-0.018781,-0.024318,0.233738,
-0.020967,-0.020854,0.234073,
-0.022676,-0.016917,0.234390,
-0.023755,-0.012407,0.234672,
-0.023998,-0.006884,0.234899,
-0.022714,-0.000058,0.235000,
-0.019979,0.006292,0.234916,
-0.016665,0.011582,0.234714,
-0.012834,0.016536,0.234417,
-0.008688,0.021280,0.234035,
-0.004476,0.025881,0.233571,
-0.000425,0.030342,0.233033,
0.003275,0.034630,0.232434,
0.006456,0.038709,0.231790,
0.009000,0.042537,0.231118,
0.010864,0.046040,0.230446,
0.012102,0.049101,0.229813,
0.012796,0.051616,0.229261,
0.013063,0.053495,0.228830,
0.013109,0.054656,0.228556,
```

```
0.013099,0.055102,0.228449,
0.013099,0.055102,0.228449,
SectionCurve7,
0.013685,0.056520,0.311921,
0.013685,0.056520,0.311921,
0.013719,0.056158,0.311986,
0.013846,0.054947,0.312202,
0.014051,0.052957,0.312545,
0.014319,0.050217,0.312997,
0.014654,0.046753,0.313533,
0.015079,0.042590,0.314126,
0.015588,0.037762,0.314743,
0.016152,0.032347,0.315345,
0.016730,0.026450,0.315895,
0.017262,0.020196,0.316356,
0.017665,0.013718,0.316703,
0.017830,0.007189,0.316918,
0.017657,0.000831,0.316999,
0.017127,-0.005094,0.316959,
0.016397,-0.009849,0.316847,
0.015520,-0.013904,0.316695,
0.014026,-0.018450,0.316463,
0.011889,-0.022953,0.316168,
0.009306,-0.026912,0.315856,
0.006343,-0.030105,0.315567,
0.003234,-0.032308,0.315349,
0.000146,-0.033686,0.315205,
-0.002899,-0.034296,0.315139,
-0.005820,-0.034126,0.315158,
-0.008587,-0.033179,0.315259,
-0.011172,-0.031472,0.315434,
-0.013509,-0.029030,0.315668,
-0.015570,-0.025975,0.315934,
-0.017343,-0.022534,0.316198,
-0.018738,-0.018566,0.316456,
-0.019628,-0.014002,0.316691,
-0.019856,-0.008488,0.316886,
-0.018801,-0.001802,0.316995,
-0.016431,0.004572,0.316967,
-0.013526,0.010128,0.316838,
-0.010181,0.015442,0.316624,
-0.006582,0.020595,0.316330,
-0.002943,0.025618,0.315963,
0.000539,0.030487,0.315531,
0.003702,0.035153,0.315045,
0.006402,0.039565,0.314521,
0.008537,0.043669,0.313978,
0.010073,0.047387,0.313438,
0.011064,0.050609,0.312934,
0.011586,0.053237,0.312498,
0.011746,0.055190,0.312159,
0.011737,0.056391,0.311944,
0.011710,0.056841,0.311862,
0.011710,0.056841,0.311862,
SectionCurve8,
0.012069,0.054531,0.395256,
0.012069,0.054531,0.395256,
0.012100,0.054174,0.395305,
0.012212,0.053009,0.395463,
0.012386,0.051100,0.395714,
0.012595,0.048479,0.396044,
0.012843,0.045171,0.396435,
0.013139,0.041207,0.396866,
```

```
0.013476,0.036631,0.397315,
0.013829,0.031523,0.397753,
0.014164,0.025982,0.398153,
0.014439,0.020107,0.398493,
0.014598,0.014004,0.398754,
0.014577,0.007810,0.398924,
0.014317,0.001705,0.398996,
0.013802,-0.004043,0.398980,
0.013168,-0.008632,0.398907,
0.012468,-0.012371,0.398808,
0.011251,-0.016620,0.398654,
0.009447,-0.021022,0.398446,
0.007258,-0.024905,0.398222,
0.004805,-0.028102,0.398009,
0.002249,-0.030503,0.397832,
-0.000234,-0.032082,0.397708,
-0.002548,-0.032863,0.397644,
-0.004651,-0.032873,0.397643,
-0.006618,-0.032135,0.397704,
-0.008541,-0.030682,0.397819,
-0.010425,-0.028570,0.397976,
-0.012255,-0.025874,0.398160,
-0.013945,-0.022638,0.398357,
-0.015408,-0.018850,0.398554,
-0.016516,-0.014477,0.398737,
-0.017028,-0.009007,0.398898,
-0.016129,-0.002407,0.398993,
-0.013854,0.003701,0.398983,
-0.011153,0.008997,0.398899,
-0.008180,0.014132,0.398750,
-0.005093,0.019198,0.398538,
-0.002039,0.024184,0.398266,
0.000864,0.029037,0.397942,
0.003507,0.033680,0.397576,
0.005783,0.038042,0.397182,
0.007591,0.042069,0.396776,
0.008888,0.045692,0.396375,
0.009713,0.048818,0.396002,
0.010120,0.051360,0.395681,
0.010196,0.053245,0.395431,
0.010135,0.054401,0.395274,
0.010091,0.054825,0.395215,
0.010091,0.054825,0.395215,
SectionCurve9,
0.010642,0.052220,0.478157,
0.010642,0.052220,0.478157,
0.010677,0.051876,0.478194,
0.010797,0.050767,0.478313,
0.010976,0.048949,0.478503,
0.011190,0.046455,0.478751,
0.011437,0.043315,0.479046,
0.011720,0.039559,0.479370,
0.012028,0.035231,0.479708,
0.012338,0.030395,0.480039,
0.012619,0.025147,0.480342,
0.012837,0.019592,0.480601,
0.012947,0.013841,0.480801,
0.012901,0.008015,0.480933,
0.012656,0.002260,0.480995,
0.012170,-0.003205,0.480989,
0.011484,-0.007871,0.480936,
0.010654,-0.011854,0.480854,
0.009410,-0.015908,0.480737,
```

```
0.007741,-0.019918,0.480587,
0.005811,-0.023487,0.480426,
0.003740,-0.026478,0.480271,
0.001647,-0.028805,0.480137,
-0.000336,-0.030422,0.480037,
-0.002092,-0.031326,0.479979,
-0.003660,-0.031452,0.479971,
-0.005113,-0.030862,0.480009,
-0.006578,-0.029620,0.480087,
-0.008136,-0.027694,0.480202,
-0.009710,-0.025132,0.480343,
-0.011206,-0.021970,0.480498,
-0.012520,-0.018223,0.480655,
-0.013503,-0.013884,0.480800,
-0.013893,-0.008719,0.480921,
-0.013126,-0.002862,0.480991,
-0.011283,0.002727,0.480992,
-0.008978,0.007858,0.480936,
-0.006408,0.012886,0.480827,
-0.003730,0.017855,0.480668,
-0.001070,0.022730,0.480463,
0.001448,0.027455,0.480216,
0.003707,0.031970,0.479936,
0.005593,0.036221,0.479634,
0.007025,0.040150,0.479321,
0.007992,0.043680,0.479013,
0.008548,0.046716,0.478726,
0.008776,0.049172,0.478480,
0.008779,0.050980,0.478291,
0.008703,0.052086,0.478172,
0.008659,0.052486,0.478128,
0.008659,0.052486,0.478128,
SectionCurve10,
0.009132,0.049443,0.560825,
0.009132,0.049443,0.560825,
0.009178,0.049118,0.560853,
0.009320,0.048081,0.560943,
0.009527,0.046372,0.561087,
0.009788,0.044021,0.561276,
0.010107,0.041065,0.561500,
0.010485,0.037537,0.561747,
0.010910,0.033468,0.562004,
0.011368,0.028905,0.562257,
0.011823,0.023938,0.562491,
0.012233,0.018698,0.562689,
0.012530,0.013334,0.562842,
0.012657,0.007987,0.562943,
0.012552,0.002767,0.562993,
0.012140,-0.002314,0.562995,
0.011316,-0.007194,0.562954,
0.010119,-0.011693,0.562879,
0.008674,-0.015748,0.562780,
0.007053,-0.019362,0.562667,
0.005330,-0.022492,0.562551,
0.003585,-0.025082,0.562441,
0.001880,-0.027134,0.562346,
0.000237,-0.028655,0.562270,
-0.001265,-0.029586,0.562222,
-0.002731,-0.029761,0.562213,
-0.004111,-0.029256,0.562239,
-0.005427,-0.028151,0.562296,
-0.006777,-0.026315,0.562385,
-0.008001,-0.023759,0.562498,
```

```
-0.009018,-0.020575,0.562624,
-0.009771,-0.016866,0.562747,
-0.010179,-0.012694,0.562857,
-0.010168,-0.008153,0.562941,
-0.009689,-0.003392,0.562990,
-0.008725,0.001501,0.562998,
-0.007260,0.006540,0.562962,
-0.005315,0.011597,0.562881,
-0.003048,0.016512,0.562758,
-0.000646,0.021233,0.562599,
0.001681,0.025741,0.562411,
0.003724,0.030036,0.562198,
0.005318,0.034101,0.561966,
0.006400,0.037881,0.561724,
0.007018,0.041280,0.561485,
0.007263,0.044195,0.561263,
0.007279,0.046542,0.561073,
0.007218,0.048259,0.560928,
0.007168,0.049304,0.560837,
0.007145,0.049678,0.560804,
0.007145,0.049678,0.560804,
SectionCurve11,
0.007626,0.046406,0.643328,
0.007626,0.046406,0.643328,
0.007675,0.046101,0.643350,
0.007823,0.045132,0.643419,
0.008043,0.043536,0.643529,
0.008320,0.041341,0.643674,
0.008652,0.038582,0.643845,
0.009032,0.035293,0.644034,
0.009446,0.031506,0.644230,
0.009878,0.027265,0.644423,
0.010298,0.022653,0.644602,
0.010671,0.017787,0.644755,
0.010943,0.012801,0.644873,
0.011067,0.007819,0.644953,
0.010993,0.002941,0.644993,
0.010662,-0.001817,0.644997,
0.009976,-0.006398,0.644968,
0.008968,-0.010637,0.644912,
0.007749,-0.014477,0.644838,
0.006381,-0.017909,0.644751,
0.004925,-0.020892,0.644662,
0.003450,-0.023371,0.644576,
0.002010,-0.025343,0.644502,
0.000619,-0.026808,0.644443,
-0.000657,-0.027714,0.644404,
-0.001912,-0.027918,0.644396,
-0.003101,-0.027485,0.644414,
-0.004246,-0.026482,0.644456,
-0.005430,-0.024801,0.644523,
-0.006515,-0.022452,0.644609,
-0.007427,-0.019515,0.644705,
-0.008115,-0.016081,0.644800,
-0.008509,-0.012207,0.644884,
-0.008542,-0.007977,0.644951,
-0.008171,-0.003524,0.644990,
-0.007384,0.001072,0.644999,
-0.006168,0.005816,0.644974,
-0.004534,0.010591,0.644913,
-0.002619,0.015250,0.644820,
-0.000585,0.019738,0.644698,
0.001382,0.024030,0.644552,
```

```
0.003097,0.028115,0.644387,
0.004416,0.031970,0.644207,
0.005284,0.035540,0.644020,
0.005746,0.038738,0.643836,
0.005889,0.041474,0.643665,
0.005840,0.043672,0.643520,
0.005739,0.045277,0.643409,
0.005666,0.046255,0.643339,
0.005636,0.046603,0.643314,
0.005636,0.046603,0.643314,
SectionCurve12,
0.006278,0.043478,0.725699,
0.006278,0.043478,0.725699,
0.006338,0.043194,0.725716,
0.006505,0.042294,0.725769,
0.006753,0.040811,0.725854,
0.007075,0.038771,0.725965,
0.007465,0.036202,0.726098,
0.007920,0.033141,0.726244,
0.008432,0.029624,0.726396,
0.008981,0.025704,0.726545,
0.009539,0.021456,0.726683,
0.010071,0.016977,0.726802,
0.010513,0.012367,0.726895,
0.010793,0.007706,0.726959,
0.010815,0.003062,0.726994,
0.010501,-0.001498,0.726998,
0.009841,-0.005857,0.726976,
0.008902,-0.009909,0.726932,
0.007756,-0.013608,0.726873,
0.006464,-0.016915,0.726803,
0.005080,-0.019782,0.726731,
0.003671,-0.022149,0.726663,
0.002304,-0.023995,0.726604,
0.001016,-0.025302,0.726560,
-0.000151,-0.026008,0.726535,
-0.001263,-0.026144,0.726530,
-0.002290,-0.025687,0.726546,
-0.003166,-0.024626,0.726583,
-0.004000,-0.023020,0.726635,
-0.004751,-0.020855,0.726701,
-0.005379,-0.018186,0.726773,
-0.005854,-0.015072,0.726844,
-0.006128,-0.011558,0.726908,
-0.006154,-0.007712,0.726959,
-0.005899,-0.003623,0.726991,
-0.005350,0.000617,0.727000,
-0.004507,0.004974,0.726983,
-0.003366,0.009407,0.726939,
-0.001992,0.013825,0.726869,
-0.000506,0.018139,0.726774,
0.000949,0.022284,0.726658,
0.002225,0.026218,0.726527,
0.003213,0.029901,0.726385,
0.003873,0.033283,0.726238,
0.004239,0.036291,0.726094,
0.004381,0.038851,0.725961,
0.004390,0.040903,0.725848,
0.004348,0.042401,0.725762,
0.004305,0.043312,0.725709,
0.004284,0.043637,0.725689,
0.004284,0.043637,0.725689,
SectionCurve13,
```

0.005005,0.040513,0.807985,
0.005005,0.040513,0.807985,
0.005064,0.040249,0.807998,
0.005230,0.039414,0.808039,
0.005478,0.038040,0.808105,
0.005799,0.036148,0.808192,
0.006185,0.033767,0.808295,
0.006629,0.030931,0.808409,
0.007121,0.027676,0.808526,
0.007639,0.024049,0.808642,
0.008160,0.020122,0.808750,
0.008655,0.015980,0.808842,
0.009071,0.011713,0.808915,
0.009348,0.007394,0.808966,
0.009403,0.003086,0.808994,
0.009169,-0.001151,0.808999,
0.008632,-0.005211,0.808983,
0.007855,-0.008996,0.808950,
0.006896,-0.012460,0.808904,
0.005810,-0.015565,0.808850,
0.004643,-0.018264,0.808794,
0.003450,-0.020501,0.808740,
0.002291,-0.022253,0.808694,
0.001196,-0.023503,0.808659,
0.000201,-0.024193,0.808638,
-0.000749,-0.024351,0.808633,
-0.001632,-0.023956,0.808645,
-0.002391,-0.022998,0.808673,
-0.003119,-0.021530,0.808713,
-0.003781,-0.019542,0.808764,
-0.004344,-0.017081,0.808820,
-0.004781,-0.014204,0.808875,
-0.005050,-0.010948,0.808926,
-0.005110,-0.007377,0.808966,
-0.004934,-0.003572,0.808992,
-0.004509,0.000386,0.809000,
-0.003838,0.004459,0.808988,
-0.002915,0.008609,0.808954,
-0.001795,0.012751,0.808900,
-0.000579,0.016801,0.808826,
0.000611,0.020694,0.808735,
0.001644,0.024386,0.808632,
0.002425,0.027838,0.808521,
0.002923,0.031000,0.808406,
0.003168,0.033805,0.808293,
0.003226,0.036189,0.808190,
0.003179,0.038097,0.808102,
0.003100,0.039489,0.808036,
0.003036,0.040336,0.807994,
0.003008,0.040635,0.807979,
0.003008,0.040635,0.807979,
SectionCurve14,
0.003899,0.037503,0.890210,
0.003899,0.037503,0.890210,
0.003960,0.037246,0.890221,
0.004146,0.036479,0.890253,
0.004383,0.035214,0.890304,
0.004701,0.033474,0.890371,
0.005102,0.031285,0.890451,
0.005580,0.028681,0.890538,
0.006121,0.025702,0.890629,
0.006696,0.022398,0.890718,
0.007263,0.018821,0.890801,

```
0.007780,0.015033,0.890873,
0.008194,0.011100,0.890931,
0.008453,0.007094,0.890972,
0.008508,0.003087,0.890995,
0.008278,-0.000840,0.891000,
0.007764,-0.004613,0.890988,
0.007055,-0.008170,0.890963,
0.006197,-0.011448,0.890926,
0.005230,-0.014389,0.890884,
0.004197,-0.016939,0.890839,
0.003144,-0.019040,0.890797,
0.002130,-0.020640,0.890761,
0.001225,-0.021717,0.890735,
0.000434,-0.022337,0.890720,
-0.000382,-0.022539,0.890715,
-0.001170,-0.022227,0.890723,
-0.001793,-0.021318,0.890745,
-0.002281,-0.019884,0.890778,
-0.002673,-0.018031,0.890818,
-0.002986,-0.015791,0.890860,
-0.003228,-0.013185,0.890902,
-0.003391,-0.010242,0.890941,
-0.003463,-0.007006,0.890972,
-0.003425,-0.003530,0.890993,
-0.003252,0.000126,0.891000,
-0.002870,0.003900,0.890991,
-0.002292,0.007735,0.890966,
-0.001608,0.011574,0.890925,
-0.000874,0.015358,0.890868,
-0.000146,0.019025,0.890797,
0.000526,0.022513,0.890716,
0.001102,0.025763,0.890627,
0.001552,0.028716,0.890537,
0.001859,0.031319,0.890449,
0.002026,0.033521,0.890369,
0.002071,0.035281,0.890301,
0.002031,0.036563,0.890249,
0.001940,0.037349,0.890217,
0.001902,0.037612,0.890206,
0.001902,0.037612,0.890206,
SectionCurve15,
0.003085,0.034474,0.972389,
0.003085,0.034474,0.972389,
0.003144,0.034239,0.972397,
0.003324,0.033537,0.972422,
0.003556,0.032377,0.972461,
0.003868,0.030784,0.972513,
0.004261,0.028779,0.972574,
0.004731,0.026394,0.972642,
0.005263,0.023666,0.972712,
0.005828,0.020639,0.972781,
0.006391,0.017362,0.972845,
0.006909,0.013891,0.972901,
0.007334,0.010285,0.972946,
0.007619,0.006610,0.972978,
0.007715,0.002932,0.972996,
0.007550,-0.000676,0.973000,
0.007122,-0.004147,0.972991,
0.006511,-0.007422,0.972972,
0.005761,-0.010443,0.972944,
0.004908,-0.013156,0.972911,
0.003988,-0.015510,0.972876,
0.003046,-0.017453,0.972843,
```

```
0.002134,-0.018935,0.972816,
0.001314,-0.019936,0.972796,
0.000595,-0.020515,0.972784,
-0.000151,-0.020711,0.972780,
-0.000879,-0.020435,0.972785,
-0.001464,-0.019609,0.972802,
-0.001933,-0.018298,0.972828,
-0.002319,-0.016601,0.972858,
-0.002639,-0.014549,0.972891,
-0.002898,-0.012159,0.972924,
-0.003089,-0.009458,0.972954,
-0.003201,-0.006488,0.972978,
-0.003217,-0.003296,0.972994,
-0.003110,0.000064,0.973000,
-0.002813,0.003535,0.972994,
-0.002337,0.007063,0.972974,
-0.001764,0.010597,0.972942,
-0.001144,0.014081,0.972898,
-0.000528,0.017458,0.972843,
0.000039,0.020670,0.972780,
0.000522,0.023662,0.972712,
0.000893,0.026380,0.972642,
0.001138,0.028774,0.972574,
0.001259,0.030799,0.972512,
0.001275,0.032416,0.972460,
0.001220,0.033593,0.972420,
0.001125,0.034313,0.972395,
0.001087,0.034555,0.972386,
0.001087,0.034555,0.972386,
SectionCurve16,
0.002328,0.031433,1.054532,
0.002328,0.031433,1.054532,
0.002385,0.031219,1.054538,
0.002556,0.030582,1.054557,
0.002781,0.029528,1.054587,
0.003082,0.028080,1.054626,
0.003463,0.026259,1.054673,
0.003917,0.024092,1.054725,
0.004431,0.021614,1.054779,
0.004980,0.018863,1.054831,
0.005528,0.015886,1.054880,
0.006038,0.012730,1.054923,
0.006466,0.009451,1.054958,
0.006765,0.006107,1.054982,
0.006893,0.002759,1.054996,
0.006782,-0.000530,1.055000,
0.006431,-0.003697,1.054994,
0.005911,-0.006688,1.054979,
0.005261,-0.009449,1.054958,
0.004513,-0.011931,1.054933,
0.003701,-0.014087,1.054906,
0.002864,-0.015869,1.054881,
0.002049,-0.017230,1.054859,
0.001314,-0.018152,1.054844,
0.000665,-0.018689,1.054834,
-0.000012,-0.018877,1.054831,
-0.000679,-0.018635,1.054835,
-0.001224,-0.017889,1.054848,
-0.001670,-0.016701,1.054868,
-0.002046,-0.015160,1.054891,
-0.002366,-0.013294,1.054916,
-0.002636,-0.011120,1.054941,
-0.002849,-0.008662,1.054964,
```

-0.002993,-0.005958,1.054983,
-0.003053,-0.003051,1.054996,
-0.003003,0.000011,1.055000,
-0.002781,0.003177,1.054995,
-0.002398,0.006397,1.054981,
-0.001926,0.009624,1.054956,
-0.001412,0.012805,1.054922,
-0.000899,0.015889,1.054880,
-0.000428,0.018823,1.054832,
-0.000030,0.021555,1.054780,
0.000269,0.024035,1.054726,
0.000458,0.026219,1.054674,
0.000540,0.028066,1.054627,
0.000531,0.029539,1.054586,
0.000465,0.030611,1.054556,
0.000368,0.031266,1.054537,
0.000329,0.031486,1.054530,
0.000329,0.031486,1.054530,
SectionCurve17,
0.001731,0.028891,1.122962,
0.001731,0.028891,1.122962,
0.001785,0.028695,1.122967,
0.001948,0.028112,1.122982,
0.002163,0.027147,1.123006,
0.002454,0.025820,1.123037,
0.002819,0.024150,1.123074,
0.003256,0.022165,1.123115,
0.003751,0.019894,1.123158,
0.004280,0.017374,1.123200,
0.004810,0.014644,1.123239,
0.005307,0.011751,1.123273,
0.005729,0.008744,1.123300,
0.006035,0.005676,1.123320,
0.006183,0.002601,1.123331,
0.006110,-0.000421,1.123334,
0.005816,-0.003333,1.123329,
0.005365,-0.006086,1.123318,
0.004793,-0.008629,1.123301,
0.004128,-0.010916,1.123281,
0.003402,-0.012905,1.123260,
0.002649,-0.014551,1.123240,
0.001913,-0.015810,1.123223,
0.001246,-0.016665,1.123210,
0.000655,-0.017165,1.123203,
0.000034,-0.017345,1.123200,
-0.000581,-0.017129,1.123203,
-0.001091,-0.016450,1.123214,
-0.001515,-0.015363,1.123229,
-0.001879,-0.013952,1.123247,
-0.002196,-0.012242,1.123267,
-0.002471,-0.010247,1.123287,
-0.002696,-0.007992,1.123306,
-0.002862,-0.005509,1.123320,
-0.002952,-0.002839,1.123330,
-0.002944,-0.000026,1.123334,
-0.002779,0.002884,1.123330,
-0.002467,0.005846,1.123319,
-0.002073,0.008815,1.123299,
-0.001639,0.011743,1.123273,
-0.001206,0.014581,1.123239,
-0.000809,0.017281,1.123201,
-0.000477,0.019794,1.123160,
-0.000233,0.022076,1.123117,

```
-0.000086,0.024085,1.123076,
-0.000034,0.025781,1.123038,
-0.000060,0.027135,1.123006,
-0.000134,0.028119,1.122982,
-0.000231,0.028720,1.122967,
-0.000269,0.028921,1.122962,
-0.000269,0.028921,1.122962,
SectionCurve18,
0.001301,0.026066,1.177712,
0.001301,0.026066,1.177712,
0.001351,0.025890,1.177715,
0.001501,0.025365,1.177727,
0.001701,0.024496,1.177745,
0.001970,0.023301,1.177770,
0.002310,0.021799,1.177798,
0.002715,0.020012,1.177830,
0.003174,0.017968,1.177863,
0.003665,0.015699,1.177895,
0.004159,0.013241,1.177926,
0.004623,0.010636,1.177952,
0.005021,0.007928,1.177973,
0.005314,0.005163,1.177989,
0.005464,0.002391,1.177998,
0.005416,-0.000334,1.178000,
0.005167,-0.002964,1.177996,
0.004776,-0.005449,1.177987,
0.004274,-0.007747,1.177975,
0.003688,-0.009815,1.177959,
0.003044,-0.011615,1.177943,
0.002374,-0.013104,1.177927,
0.001718,-0.014246,1.177914,
0.001121,-0.015021,1.177904,
0.000591,-0.015477,1.177898,
0.000032,-0.015644,1.177896,
-0.000525,-0.015455,1.177899,
-0.000992,-0.014846,1.177906,
-0.001385,-0.013869,1.177918,
-0.001727,-0.012599,1.177933,
-0.002030,-0.011059,1.177948,
-0.002297,-0.009263,1.177964,
-0.002523,-0.007230,1.177978,
-0.002697,-0.004993,1.177989,
-0.002804,-0.002586,1.177997,
-0.002825,-0.000048,1.178000,
-0.002705,0.002577,1.177997,
-0.002453,0.005251,1.177988,
-0.002127,0.007931,1.177973,
-0.001765,0.010575,1.177953,
-0.001402,0.013138,1.177927,
-0.001071,0.015576,1.177897,
-0.000797,0.017846,1.177865,
-0.000599,0.019906,1.177832,
-0.000486,0.021718,1.177800,
-0.000455,0.023249,1.177771,
-0.000492,0.024470,1.177746,
-0.000569,0.025356,1.177727,
-0.000662,0.025897,1.177715,
-0.000699,0.026079,1.177711,
-0.000699,0.026079,1.177711,
SectionCurve19,
0.001073,0.017735,1.232538,
0.001073,0.017735,1.232538,
0.001106,0.017615,1.232540,
```

```
0.001206,0.017259,1.232545,
0.001338,0.016668,1.232553,
0.001516,0.015856,1.232564,
0.001740,0.014835,1.232577,
0.002007,0.013621,1.232591,
0.002310,0.012232,1.232605,
0.002634,0.010690,1.232620,
0.002959,0.009020,1.232633,
0.003263,0.007249,1.232645,
0.003521,0.005408,1.232654,
0.003708,0.003528,1.232661,
0.003798,0.001643,1.232665,
0.003752,-0.000211,1.232666,
0.003571,-0.002000,1.232664,
0.003294,-0.003692,1.232660,
0.002942,-0.005257,1.232655,
0.002534,-0.006666,1.232648,
0.002088,-0.007892,1.232641,
0.001625,-0.008907,1.232634,
0.001173,-0.009686,1.232628,
0.000764,-0.010215,1.232624,
0.000401,-0.010527,1.232621,
0.000020,-0.010642,1.232620,
-0.000361,-0.010515,1.232621,
-0.000685,-0.010103,1.232625,
-0.000962,-0.009439,1.232630,
-0.001209,-0.008576,1.232636,
-0.001431,-0.007530,1.232643,
-0.001633,-0.006309,1.232650,
-0.001808,-0.004927,1.232656,
-0.001951,-0.003405,1.232661,
-0.002050,-0.001768,1.232665,
-0.002091,-0.000042,1.232666,
-0.002038,0.001744,1.232665,
-0.001895,0.003564,1.232661,
-0.001703,0.005388,1.232654,
-0.001485,0.007188,1.232645,
-0.001266,0.008933,1.232634,
-0.001067,0.010592,1.232620,
-0.000905,0.012137,1.232606,
-0.000792,0.013539,1.232592,
-0.000736,0.014773,1.232577,
-0.000731,0.015814,1.232565,
-0.000769,0.016645,1.232554,
-0.000831,0.017248,1.232545,
-0.000900,0.017615,1.232540,
-0.000927,0.017739,1.232538,
-0.000927,0.017739,1.232538,
SectionCurve20,
0.001054,0.015934,1.238646,
0.001054,0.015934,1.238646,
0.001083,0.015826,1.238647,
0.001172,0.015506,1.238651,
0.001289,0.014975,1.238657,
0.001446,0.014246,1.238666,
0.001644,0.013329,1.238676,
0.001880,0.012238,1.238688,
0.002148,0.010990,1.238699,
0.002434,0.009605,1.238711,
0.002720,0.008104,1.238721,
0.002988,0.006514,1.238731,
0.003214,0.004860,1.238738,
0.003376,0.003171,1.238744,
```

```
0.003451,0.001478,1.238747,
0.003404,-0.000188,1.238748,
0.003235,-0.001796,1.238747,
0.002981,-0.003316,1.238744,
0.002660,-0.004722,1.238739,
0.002288,-0.005988,1.238734,
0.001884,-0.007089,1.238728,
0.001465,-0.008002,1.238722,
0.001057,-0.008701,1.238717,
0.000687,-0.009177,1.238714,
0.000360,-0.009457,1.238712,
0.000017,-0.009561,1.238711,
-0.000325,-0.009447,1.238712,
-0.000618,-0.009077,1.238715,
-0.000870,-0.008481,1.238719,
-0.001095,-0.007705,1.238724,
-0.001299,-0.006765,1.238730,
-0.001485,-0.005668,1.238735,
-0.001648,-0.004427,1.238740,
-0.001782,-0.003060,1.238744,
-0.001878,-0.001589,1.238747,
-0.001921,-0.000038,1.238748,
-0.001881,0.001566,1.238747,
-0.001760,0.003201,1.238744,
-0.001594,0.004840,1.238739,
-0.001405,0.006457,1.238731,
-0.001215,0.008025,1.238722,
-0.001043,0.009516,1.238711,
-0.000904,0.010904,1.238700,
-0.000808,0.012164,1.238688,
-0.000762,0.013272,1.238677,
-0.000762,0.014208,1.238667,
-0.000800,0.014954,1.238658,
-0.000858,0.015495,1.238651,
-0.000921,0.015826,1.238647,
-0.000946,0.015937,1.238645,
-0.000946,0.015937,1.238645,
SectionCurve21,
0.001037,0.013963,1.244448,
0.001037,0.013963,1.244448,
0.001063,0.013869,1.244449,
0.001139,0.013589,1.244452,
0.001239,0.013124,1.244457,
0.001373,0.012485,1.244463,
0.001542,0.011681,1.244471,
0.001745,0.010725,1.244480,
0.001974,0.009631,1.244489,
0.002218,0.008417,1.244498,
0.002462,0.007103,1.244506,
0.002690,0.005709,1.244513,
0.002880,0.004260,1.244519,
0.003014,0.002780,1.244523,
0.003072,0.001296,1.244525,
0.003024,-0.000164,1.244526,
0.002869,-0.001573,1.244525,
0.002639,-0.002905,1.244523,
0.002351,-0.004137,1.244519,
0.002020,-0.005246,1.244515,
0.001661,-0.006212,1.244510,
0.001290,-0.007012,1.244506,
0.000929,-0.007625,1.244503,
0.000602,-0.008042,1.244500,
0.000315,-0.008288,1.244498,
```

```
0.000014,-0.008379,1.244498,
-0.000287,-0.008279,1.244498,
-0.000545,-0.007954,1.244501,
-0.000769,-0.007432,1.244504,
-0.000971,-0.006753,1.244508,
-0.001154,-0.005929,1.244512,
-0.001323,-0.004968,1.244516,
-0.001472,-0.003880,1.244520,
-0.001596,-0.002682,1.244523,
-0.001688,-0.001393,1.244525,
-0.001734,-0.000034,1.244526,
-0.001707,0.001372,1.244525,
-0.001610,0.002805,1.244523,
-0.001473,0.004241,1.244519,
-0.001316,0.005658,1.244513,
-0.001157,0.007032,1.244506,
-0.001014,0.008339,1.244498,
-0.000899,0.009555,1.244489,
-0.000822,0.010659,1.244480,
-0.000788,0.011630,1.244472,
-0.000793,0.012450,1.244464,
-0.000830,0.013104,1.244457,
-0.000883,0.013579,1.244452,
-0.000941,0.013869,1.244449,
-0.000963,0.013966,1.244448,
-0.000963,0.013966,1.244448,
SectionCurve22,
0.000773,0.011849,1.249652,
0.000773,0.011849,1.249652,
0.000795,0.011769,1.249653,
0.000861,0.011531,1.249655,
0.000948,0.011137,1.249658,
0.001065,0.010594,1.249663,
0.001213,0.009912,1.249669,
0.001389,0.009101,1.249675,
0.001588,0.008173,1.249681,
0.001801,0.007143,1.249688,
0.002015,0.006028,1.249693,
0.002214,0.004845,1.249699,
0.002383,0.003615,1.249703,
0.002504,0.002360,1.249706,
0.002560,0.001101,1.249708,
0.002526,-0.000138,1.249708,
0.002401,-0.001334,1.249707,
0.002212,-0.002464,1.249706,
0.001974,-0.003510,1.249703,
0.001698,-0.004451,1.249700,
0.001397,-0.005271,1.249697,
0.001086,-0.005949,1.249694,
0.000783,-0.006470,1.249691,
0.000508,-0.006824,1.249689,
0.000265,-0.007032,1.249688,
0.000010,-0.007110,1.249688,
-0.000245,-0.007025,1.249688,
-0.000463,-0.006750,1.249690,
-0.000651,-0.006307,1.249692,
-0.000819,-0.005730,1.249695,
-0.000971,-0.005031,1.249698,
-0.001110,-0.004216,1.249701,
-0.001232,-0.003293,1.249704,
-0.001333,-0.002276,1.249706,
-0.001405,-0.001183,1.249707,
-0.001439,-0.000030,1.249708,
```

```
-0.001410,0.001164,1.249707,
-0.001322,0.002379,1.249706,
-0.001199,0.003598,1.249703,
-0.001061,0.004801,1.249699,
-0.000920,0.005967,1.249694,
-0.000794,0.007076,1.249688,
-0.000691,0.008108,1.249682,
-0.000621,0.009045,1.249675,
-0.000588,0.009869,1.249669,
-0.000589,0.010565,1.249663,
-0.000617,0.011119,1.249659,
-0.000661,0.011522,1.249655,
-0.000708,0.011768,1.249653,
-0.000727,0.011850,1.249652,
-0.000727,0.011850,1.249652,
SectionCurve23,
0.000613,0.009617,1.253999,
0.000613,0.009617,1.253999,
0.000630,0.009552,1.254000,
0.000684,0.009359,1.254001,
0.000755,0.009039,1.254003,
0.000850,0.008599,1.254007,
0.000970,0.008045,1.254010,
0.001114,0.007387,1.254014,
0.001276,0.006634,1.254018,
0.001450,0.005798,1.254023,
0.001624,0.004893,1.254026,
0.001787,0.003933,1.254030,
0.001925,0.002935,1.254033,
0.002023,0.001916,1.254035,
0.002070,0.000894,1.254036,
0.002043,-0.000112,1.254036,
0.001942,-0.001082,1.254036,
0.001790,-0.001999,1.254034,
0.001597,-0.002848,1.254033,
0.001374,-0.003612,1.254031,
0.001131,-0.004277,1.254029,
0.000879,-0.004828,1.254027,
0.000633,-0.005251,1.254025,
0.000410,-0.005538,1.254024,
0.000213,-0.005707,1.254023,
0.000006,-0.005770,1.254023,
-0.000201,-0.005702,1.254023,
-0.000377,-0.005478,1.254024,
-0.000530,-0.005119,1.254026,
-0.000666,-0.004651,1.254027,
-0.000789,-0.004084,1.254029,
-0.000902,-0.003422,1.254031,
-0.001001,-0.002673,1.254033,
-0.001083,-0.001848,1.254035,
-0.001141,-0.000960,1.254036,
-0.001168,-0.000024,1.254036,
-0.001145,0.000944,1.254036,
-0.001072,0.001931,1.254035,
-0.000973,0.002920,1.254033,
-0.000860,0.003896,1.254030,
-0.000746,0.004842,1.254027,
-0.000643,0.005742,1.254023,
-0.000559,0.006580,1.254019,
-0.000502,0.007340,1.254015,
-0.000475,0.008009,1.254010,
-0.000476,0.008574,1.254007,
-0.000499,0.009024,1.254004,
```

```
-0.000534,0.009351,1.254001,
-0.000573,0.009551,1.254000,
-0.000587,0.009617,1.253999,
-0.000587,0.009617,1.253999,
SectionCurve24,
0.000505,0.007295,1.257273,
0.000505,0.007295,1.257273,
0.000519,0.007246,1.257273,
0.000559,0.007099,1.257274,
0.000612,0.006856,1.257275,
0.000683,0.006523,1.257277,
0.000772,0.006103,1.257279,
0.000879,0.005603,1.257282,
0.001001,0.005032,1.257284,
0.001130,0.004398,1.257286,
0.001260,0.003712,1.257289,
0.001380,0.002984,1.257290,
0.001482,0.002226,1.257292,
0.001554,0.001453,1.257293,
0.001587,0.000678,1.257294,
0.001564,-0.000084,1.257294,
0.001485,-0.000820,1.257294,
0.001367,-0.001516,1.257293,
0.001218,-0.002160,1.257292,
0.001047,-0.002740,1.257291,
0.000860,-0.003244,1.257290,
0.000668,-0.003662,1.257289,
0.000480,-0.003983,1.257288,
0.000310,-0.004201,1.257287,
0.000160,-0.004329,1.257287,
0.000003,-0.004377,1.257286,
-0.000154,-0.004325,1.257287,
-0.000289,-0.004156,1.257287,
-0.000406,-0.003883,1.257288,
-0.000510,-0.003528,1.257289,
-0.000606,-0.003098,1.257290,
-0.000693,-0.002596,1.257291,
-0.000771,-0.002028,1.257292,
-0.000835,-0.001402,1.257293,
-0.000882,-0.000729,1.257294,
-0.000906,-0.000019,1.257294,
-0.000891,0.000716,1.257294,
-0.000839,0.001464,1.257293,
-0.000766,0.002215,1.257292,
-0.000684,0.002955,1.257291,
-0.000600,0.003673,1.257289,
-0.000525,0.004356,1.257286,
-0.000464,0.004991,1.257284,
-0.000423,0.005568,1.257282,
-0.000405,0.006075,1.257279,
-0.000407,0.006504,1.257277,
-0.000426,0.006845,1.257275,
-0.000453,0.007093,1.257274,
-0.000483,0.007244,1.257273,
-0.000495,0.007295,1.257273,
-0.000495,0.007295,1.257273,
SectionCurve25,
0.000430,0.004913,1.259304,
0.000430,0.004913,1.259304,
0.000438,0.004880,1.259305,
0.000464,0.004781,1.259305,
0.000498,0.004617,1.259306,
0.000543,0.004393,1.259306,
```

```
0.000600,0.004110,1.259307,
0.000669,0.003774,1.259308,
0.000746,0.003389,1.259309,
0.000828,0.002962,1.259311,
0.000910,0.002500,1.259312,
0.000986,0.002009,1.259312,
0.001048,0.001500,1.259313,
0.001091,0.000979,1.259314,
0.001107,0.000457,1.259314,
0.001085,-0.000057,1.259314,
0.001026,-0.000552,1.259314,
0.000941,-0.001021,1.259314,
0.000836,-0.001455,1.259313,
0.000716,-0.001845,1.259313,
0.000587,-0.002185,1.259312,
0.000454,-0.002466,1.259312,
0.000325,-0.002682,1.259311,
0.000209,-0.002829,1.259311,
0.000107,-0.002915,1.259311,
0.000001,-0.002948,1.259311,
-0.000105,-0.002913,1.259311,
-0.000198,-0.002798,1.259311,
-0.000278,-0.002615,1.259311,
-0.000352,-0.002376,1.259312,
-0.000419,-0.002086,1.259312,
-0.000482,-0.001748,1.259313,
-0.000539,-0.001365,1.259313,
-0.000587,-0.000944,1.259314,
-0.000624,-0.000491,1.259314,
-0.000646,-0.000013,1.259314,
-0.000642,0.000482,1.259314,
-0.000613,0.000986,1.259314,
-0.000570,0.001492,1.259313,
-0.000520,0.001990,1.259312,
-0.000470,0.002474,1.259312,
-0.000424,0.002933,1.259311,
-0.000388,0.003361,1.259310,
-0.000365,0.003750,1.259308,
-0.000357,0.004091,1.259307,
-0.000362,0.004380,1.259306,
-0.000377,0.004610,1.259306,
-0.000398,0.004777,1.259305,
-0.000419,0.004879,1.259305,
-0.000427,0.004913,1.259304,
-0.000427,0.004913,1.259304,
SectionCurve26,
0.000375,0.002500,1.259998,
0.000375,0.002500,1.259998,
0.000379,0.002483,1.259998,
0.000390,0.002433,1.259998,
0.000404,0.002350,1.259998,
0.000422,0.002235,1.259998,
0.000446,0.002091,1.259998,
0.000474,0.001920,1.259999,
0.000505,0.001725,1.259999,
0.000539,0.001507,1.259999,
0.000571,0.001272,1.259999,
0.000600,0.001023,1.260000,
0.000622,0.000763,1.260000,
0.000633,0.000498,1.260000,
0.000631,0.000233,1.260000,
0.000609,-0.000029,1.260000,
0.000570,-0.000281,1.260000,
```

```
0.000517,-0.000520,1.260000,
0.000455,-0.000740,1.260000,
0.000386,-0.000939,1.260000,
0.000313,-0.001112,1.260000,
0.000240,-0.001255,1.259999,
0.000170,-0.001365,1.259999,
0.000108,-0.001440,1.259999,
0.000055,-0.001484,1.259999,
0.000000,-0.001500,1.259999,
-0.000055,-0.001482,1.259999,
-0.000104,-0.001424,1.259999,
-0.000149,-0.001331,1.259999,
-0.000191,-0.001209,1.259999,
-0.000231,-0.001062,1.260000,
-0.000270,-0.000890,1.260000,
-0.000306,-0.000695,1.260000,
-0.000339,-0.000480,1.260000,
-0.000367,-0.000250,1.260000,
-0.000388,-0.000006,1.260000,
-0.000395,0.000245,1.260000,
-0.000391,0.000502,1.260000,
-0.000379,0.000759,1.260000,
-0.000364,0.001013,1.260000,
-0.000348,0.001259,1.259999,
-0.000334,0.001493,1.259999,
-0.000324,0.001710,1.259999,
-0.000320,0.001908,1.259999,
-0.000323,0.002082,1.259998,
-0.000331,0.002229,1.259998,
-0.000343,0.002346,1.259998,
-0.000357,0.002431,1.259998,
-0.000370,0.002483,1.259998,
-0.000375,0.002500,1.259998,
-0.000375,0.002500,1.259998,
GuideCurve1,
0.000000,0.035000,0.030000,
0.000000,0.035000,0.039200,
0.008492,0.035901,0.067978,
0.009688,0.040955,0.113521,
0.011074,0.046815,0.166769,
0.015066,0.054739,0.228536,
0.013685,0.056520,0.311921,
0.012069,0.054531,0.395256,
0.010642,0.052220,0.478157,
0.009132,0.049443,0.560825,
0.007626,0.046406,0.643328,
0.006278,0.043478,0.725699,
0.005005,0.040513,0.807985,
0.003899,0.037503,0.890210,
0.003085,0.034474,0.972389,
0.002328,0.031433,1.054532,
0.001731,0.028891,1.122962,
0.001301,0.026066,1.177712,
0.001073,0.017735,1.232538,
0.001054,0.015934,1.238646,
0.001037,0.013963,1.244448,
0.000773,0.011849,1.249652,
0.000613,0.009617,1.253999,
0.000505,0.007295,1.257273,
0.000430,0.004913,1.259304,
0.000375,0.002500,1.259998,
GuideCurve2,
0.026968,0.022310,0.030000,
```

```
0.026968,0.022310,0.039200,
-0.004309,0.035627,0.068050,
0.000980,0.039437,0.113659,
0.003663,0.042633,0.166958,
0.016566,0.041065,0.231384,
0.015079,0.042590,0.314126,
0.013139,0.041207,0.396866,
0.011720,0.039559,0.479370,
0.010485,0.037537,0.561747,
0.009032,0.035293,0.644034,
0.007920,0.033141,0.726244,
0.006629,0.030931,0.808409,
0.005580,0.028681,0.890538,
0.004731,0.026394,0.972642,
0.003917,0.024092,1.054725,
0.003256,0.022165,1.123115,
0.002715,0.020012,1.177830,
0.002007,0.013621,1.232591,
0.001880,0.012238,1.238688,
0.001745,0.010725,1.244480,
0.001389,0.009101,1.249675,
0.001114,0.007387,1.254014,
0.000879,0.005603,1.257282,
0.000669,0.003774,1.259308,
0.000474,0.001920,1.259999,
GuideCurve3,
0.031669,-0.014902,0.030000,
0.031669,-0.014902,0.039200,
-0.029581,-0.017444,0.067381,
-0.027743,-0.017338,0.113581,
-0.025752,-0.016177,0.166908,
0.019734,-0.011200,0.234733,
0.016397,-0.009849,0.316847,
0.013168,-0.008632,0.398907,
0.011484,-0.007871,0.480936,
0.011316,-0.007194,0.562954,
0.009976,-0.006398,0.644968,
0.009841,-0.005857,0.726976,
0.008632,-0.005211,0.808983,
0.007764,-0.004613,0.890988,
0.007122,-0.004147,0.972991,
0.006431,-0.003697,1.054994,
0.005816,-0.003333,1.123329,
0.005167,-0.002964,1.177996,
0.003571,-0.002000,1.232664,
0.003235,-0.001796,1.238747,
0.002869,-0.001573,1.244525,
0.002401,-0.001334,1.249707,
0.001942,-0.001082,1.254036,
0.001485,-0.000820,1.257294,
0.001026,-0.000552,1.259314,
0.000570,-0.000281,1.260000,
GuideCurve4,
0.004387,-0.034724,0.030000,
0.004387,-0.034724,0.039200,
-0.008620,-0.033883,0.067984,
-0.008073,-0.034129,0.113716,
-0.008087,-0.034189,0.166953,
-0.003366,-0.033560,0.232591,
-0.002899,-0.034296,0.315139,
-0.002548,-0.032863,0.397644,
-0.002092,-0.031326,0.479979,
-0.001265,-0.029586,0.562222,
```

```
-0.000657,-0.027714,0.644404,
-0.000151,-0.026008,0.726535,
0.000201,-0.024193,0.808638,
0.000434,-0.022337,0.890720,
0.000595,-0.020515,0.972784,
0.000665,-0.018689,1.054834,
0.000655,-0.017165,1.123203,
0.000591,-0.015477,1.177898,
0.000401,-0.010527,1.232621,
0.000360,-0.009457,1.238712,
0.000315,-0.008288,1.244498,
0.000265,-0.007032,1.249688,
0.000213,-0.005707,1.254023,
0.000160,-0.004329,1.257287,
0.000107,-0.002915,1.259311,
0.000055,-0.001484,1.259999,
GuideCurve5,
-0.029551,-0.018754,0.030000,
-0.029551,-0.018754,0.039200,
0.011981,-0.032456,0.067944,
0.010688,-0.032029,0.113709,
0.010099,-0.030832,0.166977,
-0.023998,-0.006884,0.234899,
-0.019856,-0.008488,0.316886,
-0.017028,-0.009007,0.398898,
-0.013893,-0.008719,0.480921,
-0.010168,-0.008153,0.562941,
-0.008542,-0.007977,0.644951,
-0.006154,-0.007712,0.726959,
-0.005110,-0.007377,0.808966,
-0.003463,-0.007006,0.890972,
-0.003201,-0.006488,0.972978,
-0.002993,-0.005958,1.054983,
-0.002862,-0.005509,1.123320,
-0.002697,-0.004993,1.177989,
-0.001951,-0.003405,1.232661,
-0.001782,-0.003060,1.238744,
-0.001596,-0.002682,1.244523,
-0.001333,-0.002276,1.249706,
-0.001083,-0.001848,1.254035,
-0.000835,-0.001402,1.257293,
-0.000587,-0.000944,1.259314,
-0.000339,-0.000480,1.260000,
GuideCurve6,
-0.031669,0.014902,0.030000,
-0.031669,0.014902,0.039200,
0.028290,0.020203,0.067407,
0.024546,0.025523,0.113580,
0.021835,0.028611,0.166917,
0.003275,0.034630,0.232434,
0.003702,0.035153,0.315045,
0.003507,0.033680,0.397576,
0.003707,0.031970,0.479936,
0.003724,0.030036,0.562198,
0.003097,0.028115,0.644387,
0.002225,0.026218,0.726527,
0.001644,0.024386,0.808632,
0.000526,0.022513,0.890716,
0.000039,0.020670,0.972780,
-0.000428,0.018823,1.054832,
-0.000809,0.017281,1.123201,
-0.001071,0.015576,1.177897,
-0.001067,0.010592,1.232620,
```

```
-0.001043,0.009516,1.238711,
-0.001014,0.008339,1.244498,
-0.000794,0.007076,1.249688,
-0.000643,0.005742,1.254023,
-0.000525,0.004356,1.257286,
-0.000424,0.002933,1.259311,
-0.000334,0.001493,1.259999,
GuideCurve7,
-0.004387,0.034724,0.030000,
-0.004387,0.034724,0.039200,
0.008977,0.035780,0.067971,
0.010106,0.040855,0.113521,
0.011485,0.046717,0.166769,
0.013099,0.055102,0.228449,
0.011710,0.056841,0.311862,
0.010091,0.054825,0.395215,
0.008659,0.052486,0.478128,
0.007145,0.049678,0.560804,
0.005636,0.046603,0.643314,
0.004284,0.043637,0.725689,
0.003008,0.040635,0.807979,
0.001902,0.037612,0.890206,
0.001087,0.034555,0.972386,
0.000329,0.031486,1.054530,
-0.000269,0.028921,1.122962,
-0.000699,0.026079,1.177711,
-0.000927,0.017739,1.232538,
-0.000946,0.015937,1.238645,
-0.000963,0.013966,1.244448,
-0.000727,0.011850,1.249652,
-0.000587,0.009617,1.253999,
-0.000495,0.007295,1.257273,
-0.000427,0.004913,1.259304,
-0.000375,0.002500,1.259998,
TipSectionCurve26,
0.000375,0.002500,1.259998,
0.000375,0.002500,1.259998,
0.000379,0.002483,1.259998,
0.000390,0.002433,1.259998,
0.000404,0.002350,1.259998,
0.000422,0.002235,1.259998,
0.000446,0.002091,1.259998,
0.000474,0.001920,1.259999,
0.000505,0.001725,1.259999,
0.000539,0.001507,1.259999,
0.000571,0.001272,1.259999,
0.000600,0.001023,1.260000,
0.000622,0.000763,1.260000,
0.000633,0.000498,1.260000,
0.000631,0.000233,1.260000,
0.000609,-0.000029,1.260000,
0.000570,-0.000281,1.260000,
0.000517,-0.000520,1.260000,
0.000455,-0.000740,1.260000,
0.000386,-0.000939,1.260000,
0.000313,-0.001112,1.260000,
0.000240,-0.001255,1.259999,
0.000170,-0.001365,1.259999,
0.000108,-0.001440,1.259999,
0.000055,-0.001484,1.259999,
0.000000,-0.001500,1.259999,
-0.000055,-0.001482,1.259999,
-0.000104,-0.001424,1.259999,
```

```
-0.000149,-0.001331,1.259999,
-0.000191,-0.001209,1.259999,
-0.000231,-0.001062,1.260000,
-0.000270,-0.000890,1.260000,
-0.000306,-0.000695,1.260000,
-0.000339,-0.000480,1.260000,
-0.000367,-0.000250,1.260000,
-0.000388,-0.000006,1.260000,
-0.000395,0.000245,1.260000,
-0.000391,0.000502,1.260000,
-0.000379,0.000759,1.260000,
-0.000364,0.001013,1.260000,
-0.000348,0.001259,1.259999,
-0.000334,0.001493,1.259999,
-0.000324,0.001710,1.259999,
-0.000320,0.001908,1.259999,
-0.000323,0.002082,1.259998,
-0.000331,0.002229,1.259998,
-0.000343,0.002346,1.259998,
-0.000357,0.002431,1.259998,
-0.000370,0.002483,1.259998,
-0.000375,0.002500,1.259998,
-0.000375,0.002500,1.259998,
TipCurve1,
0.000375,0.002500,1.259998,
-0.000375,0.002500,1.259998,
TipCurve2,
0.000379,0.002483,1.259998,
-0.000370,0.002483,1.259998,
TipCurve3,
0.000390,0.002433,1.259998,
-0.000357,0.002431,1.259998,
TipCurve4,
0.000404,0.002350,1.259998,
-0.000343,0.002346,1.259998,
TipCurve5,
0.000422,0.002235,1.259998,
-0.000331,0.002229,1.259998,
TipCurve6,
0.000446,0.002091,1.259998,
-0.000323,0.002082,1.259998,
TipCurve7,
0.000474,0.001920,1.259999,
-0.000320,0.001908,1.259999,
TipCurve8,
0.000505,0.001725,1.259999,
-0.000324,0.001710,1.259999,
TipCurve9,
0.000539,0.001507,1.259999,
-0.000334,0.001493,1.259999,
TipCurve10,
0.000571,0.001272,1.259999,
-0.000348,0.001259,1.259999,
TipCurve11,
0.000600,0.001023,1.260000,
-0.000364,0.001013,1.260000,
TipCurve12,
0.000622,0.000763,1.260000,
-0.000379,0.000759,1.260000,
TipCurve13,
0.000633,0.000498,1.260000,
-0.000391,0.000502,1.260000,
TipCurve14,
```

```
0.000631,0.000233,1.260000,
-0.000395,0.000245,1.260000,
TipCurve15,
0.000609,-0.000029,1.260000,
-0.000388,-0.000006,1.260000,
TipCurve16,
0.000570,-0.000281,1.260000,
-0.000367,-0.000250,1.260000,
TipCurve17,
0.000517,-0.000520,1.260000,
-0.000339,-0.000480,1.260000,
TipCurve18,
0.000455,-0.000740,1.260000,
-0.000306,-0.000695,1.260000,
TipCurve19,
0.000386,-0.000939,1.260000,
-0.000270,-0.000890,1.260000,
TipCurve20,
0.000313,-0.001112,1.260000,
-0.000231,-0.001062,1.260000,
TipCurve21,
0.000240,-0.001255,1.259999,
-0.000191,-0.001209,1.259999,
TipCurve22,
0.000170,-0.001365,1.259999,
-0.000149,-0.001331,1.259999,
TipCurve23,
0.000108,-0.001440,1.259999,
-0.000104,-0.001424,1.259999,
TipCurve24,
0.000055,-0.001484,1.259999,
-0.000055,-0.001482,1.259999,
RootSectionCurve1,
0.000000,0.035000,0.030000,
0.004387,0.034724,0.030000,
0.008704,0.033900,0.030000,
0.012884,0.032542,0.030000,
0.016861,0.030671,0.030000,
0.020572,0.028316,0.030000,
0.023959,0.025514,0.030000,
0.026968,0.022310,0.030000,
0.029551,0.018754,0.030000,
0.031669,0.014902,0.030000,
0.033287,0.010816,0.030000,
0.034380,0.006558,0.030000,
0.034931,0.002198,0.030000,
0.034931,-0.002198,0.030000,
0.034380,-0.006558,0.030000,
0.033287,-0.010816,0.030000,
0.031669,-0.014902,0.030000,
0.029551,-0.018754,0.030000,
0.026968,-0.022310,0.030000,
0.023959,-0.025514,0.030000,
0.020572,-0.028316,0.030000,
0.016861,-0.030671,0.030000,
0.012884,-0.032542,0.030000,
0.008704,-0.033900,0.030000,
0.004387,-0.034724,0.030000,
0.000000,-0.035000,0.030000,
-0.004387,-0.034724,0.030000,
-0.008704,-0.033900,0.030000,
-0.012884,-0.032542,0.030000,
-0.016861,-0.030671,0.030000,
```

```
-0.020572,-0.028316,0.030000,
-0.023959,-0.025514,0.030000,
-0.026968,-0.022310,0.030000,
-0.029551,-0.018754,0.030000,
-0.031669,-0.014902,0.030000,
-0.033287,-0.010816,0.030000,
-0.034380,-0.006558,0.030000,
-0.034931,-0.002198,0.030000,
-0.034931,0.002198,0.030000,
-0.034380,0.006558,0.030000,
-0.033287,0.010816,0.030000,
-0.031669,0.014902,0.030000,
-0.029551,0.018754,0.030000,
-0.026968,0.022310,0.030000,
-0.023959,0.025514,0.030000,
-0.020572,0.028316,0.030000,
-0.016861,0.030671,0.030000,
-0.012884,0.032542,0.030000,
-0.008704,0.033900,0.030000,
-0.004387,0.034724,0.030000,
0.000000,0.035000,0.030000,
RootCurve1,
0.004387,0.034724,0.030000,
-0.004387,0.034724,0.030000,
RootCurve2,
0.008704,0.033900,0.030000,
-0.008704,0.033900,0.030000,
RootCurve3,
0.012884,0.032542,0.030000,
-0.012884,0.032542,0.030000,
RootCurve4,
0.016861,0.030671,0.030000,
-0.016861,0.030671,0.030000,
RootCurve5,
0.020572,0.028316,0.030000,
-0.020572,0.028316,0.030000,
RootCurve6,
0.023959,0.025514,0.030000,
-0.023959,0.025514,0.030000,
RootCurve7,
0.026968,0.022310,0.030000,
-0.026968,0.022310,0.030000,
RootCurve8,
0.029551,0.018754,0.030000,
-0.029551,0.018754,0.030000,
RootCurve9,
0.031669,0.014902,0.030000,
-0.031669,0.014902,0.030000,
RootCurve10,
0.033287,0.010816,0.030000,
-0.033287,0.010816,0.030000,
RootCurve11,
0.034380,0.006558,0.030000,
-0.034380,0.006558,0.030000,
RootCurve12,
0.034931,0.002198,0.030000,
-0.034931,0.002198,0.030000,
RootCurve13,
0.034931,-0.002198,0.030000,
-0.034931,-0.002198,0.030000,
RootCurve14,
0.034380,-0.006558,0.030000,
-0.034380,-0.006558,0.030000,
```

```
RootCurve15,
0.033287,-0.010816,0.030000,
-0.033287,-0.010816,0.030000,
RootCurve16,
0.031669,-0.014902,0.030000,
-0.031669,-0.014902,0.030000,
RootCurve17,
0.029551,-0.018754,0.030000,
-0.029551,-0.018754,0.030000,
RootCurve18,
0.026968,-0.022310,0.030000,
-0.026968,-0.022310,0.030000,
RootCurve19,
0.023959,-0.025514,0.030000,
-0.023959,-0.025514,0.030000,
RootCurve20,
0.020572,-0.028316,0.030000,
-0.020572,-0.028316,0.030000,
RootCurve21,
0.016861,-0.030671,0.030000,
-0.016861,-0.030671,0.030000,
RootCurve22,
0.012884,-0.032542,0.030000,
-0.012884,-0.032542,0.030000,
RootCurve23,
0.008704,-0.033900,0.030000,
-0.008704,-0.033900,0.030000,
RootCurve24,
0.004387,-0.034724,0.030000,
-0.004387,-0.034724,0.030000,
```

APPENDIX D. CHARACTERIZATION INFORMATION AND DATA

Cable Mass Excluded						
Elevation [m]	Height Fraction	Mass [kg/m]	Fore-Aft Stiffness [N·m^2]	Side-Side Stiffness [N·m^2]	Torsional Stiffness [N·m^2]	Extensional Stiffness [N]
10.00-10.31	0.000-0.004	53,897.6	1.12E+12	1.12E+12	8.55E+11	3.85E+12
10.31-18.54	0.004-0.110	2,825.2	1.12E+12	1.12E+12	8.55E+11	3.85E+12
18.54-21.56	0.110-0.149	4,034.2	1.37E+12	1.37E+12	1.04E+12	5.34E+12
21.56-22.26	0.149-0.158	14,270.4	1.37E+12	1.37E+12	1.04E+12	5.34E+12
22.26-81.63	0.158-0.923	1,209.0	2.49E+11	2.49E+11	1.89E+11	1.49E+12
81.63-82.87	0.923-0.939	3,354.7	2.49E+11	2.49E+11	1.89E+11	1.49E+12
82.87-83.49	0.939-0.947	10,047.6	2.49E+11	2.49E+11	1.89E+11	1.49E+12
83.49-84.42	0.947-0.959	8,659.9	2.49E+11	2.49E+11	1.89E+11	1.49E+12
84.42-87.6	0.959-1.000	3,937.0	1.10E+12	1.10E+12	8.40E+11	4.87E+12

Table D.1. Model tower distributed properties including cable mass.

Cable Mass Included						
Elevation [m]	Height Fraction	Mass [kg/m]	Fore-Aft Stiffness [N·m^2]	Side-Side Stiffness [N·m^2]	Torsional Stiffness [N·m^2]	Extensional Stiffness [N]
10.00-10.31	0.000-0.004	55,671.5	1.123E+12	1.123E+12	8.548E+11	3.853E+12
10.31-18.54	0.004-0.110	4599.0	1.123E+12	1.123E+12	8.548E+11	3.853E+12
18.54-21.56	0.110-0.149	5808.1	1.371E+12	1.371E+12	1.044E+12	5.342E+12
21.56-22.26	0.149-0.158	16,044.3	1.371E+12	1.371E+12	1.044E+12	5.342E+12
22.26-81.63	0.158-0.923	2982.9	2.485E+11	2.485E+11	1.892E+11	1.489E+12
81.63-82.87	0.923-0.939	5128.5	2.485E+11	2.485E+11	1.892E+11	1.489E+12
82.87-83.49	0.939-0.947	11,821.4	2.485E+11	2.485E+11	1.892E+11	1.489E+12
83.49-84.42	0.947-0.959	10,433.7	2.485E+11	2.485E+11	1.892E+11	1.489E+12
84.42-87.6	0.959-1.000	5710.8	1.104E+12	1.104E+12	8.404E+11	4.867E+12

Table D.2. Model tower distributed properties excluding cable mass.
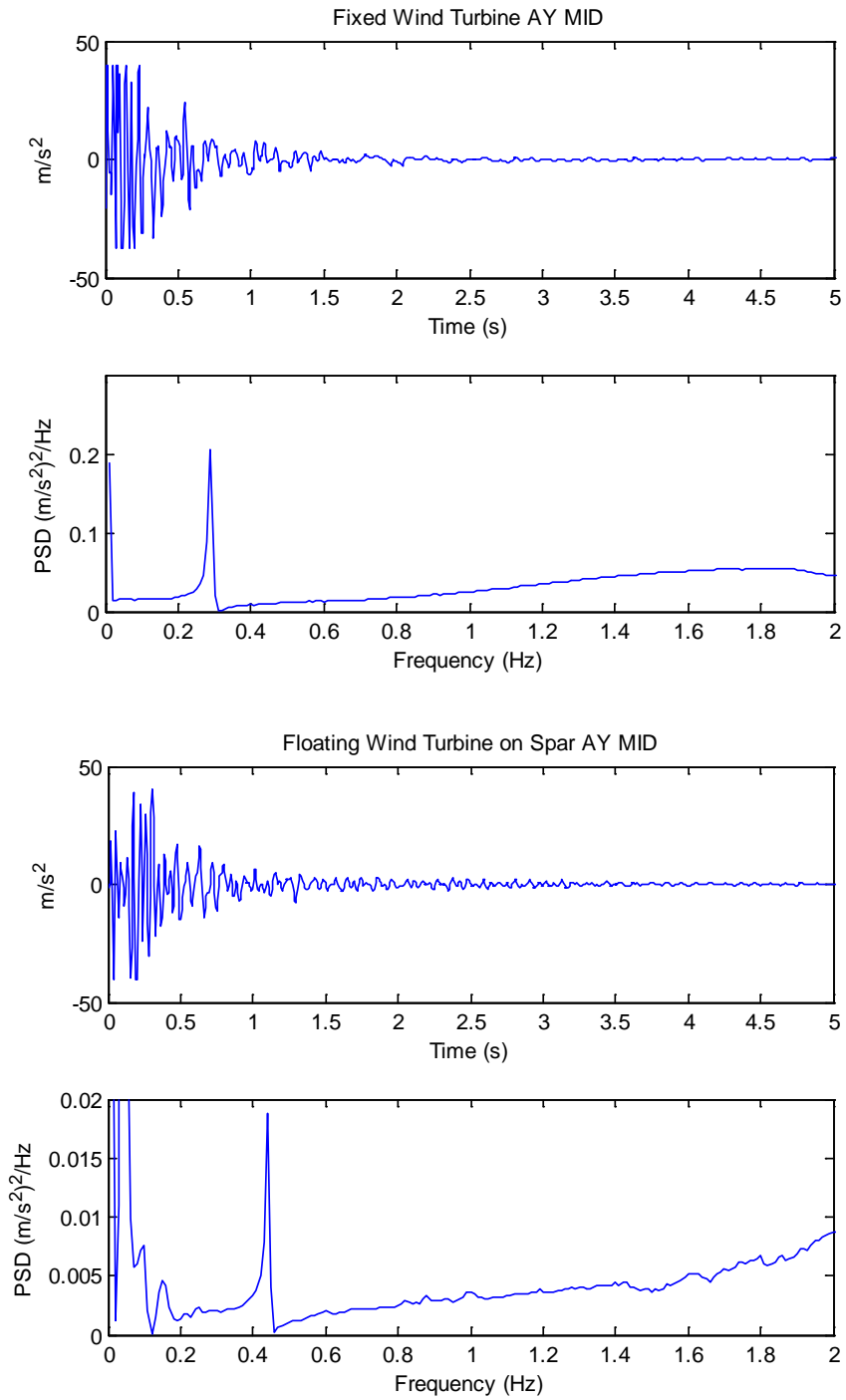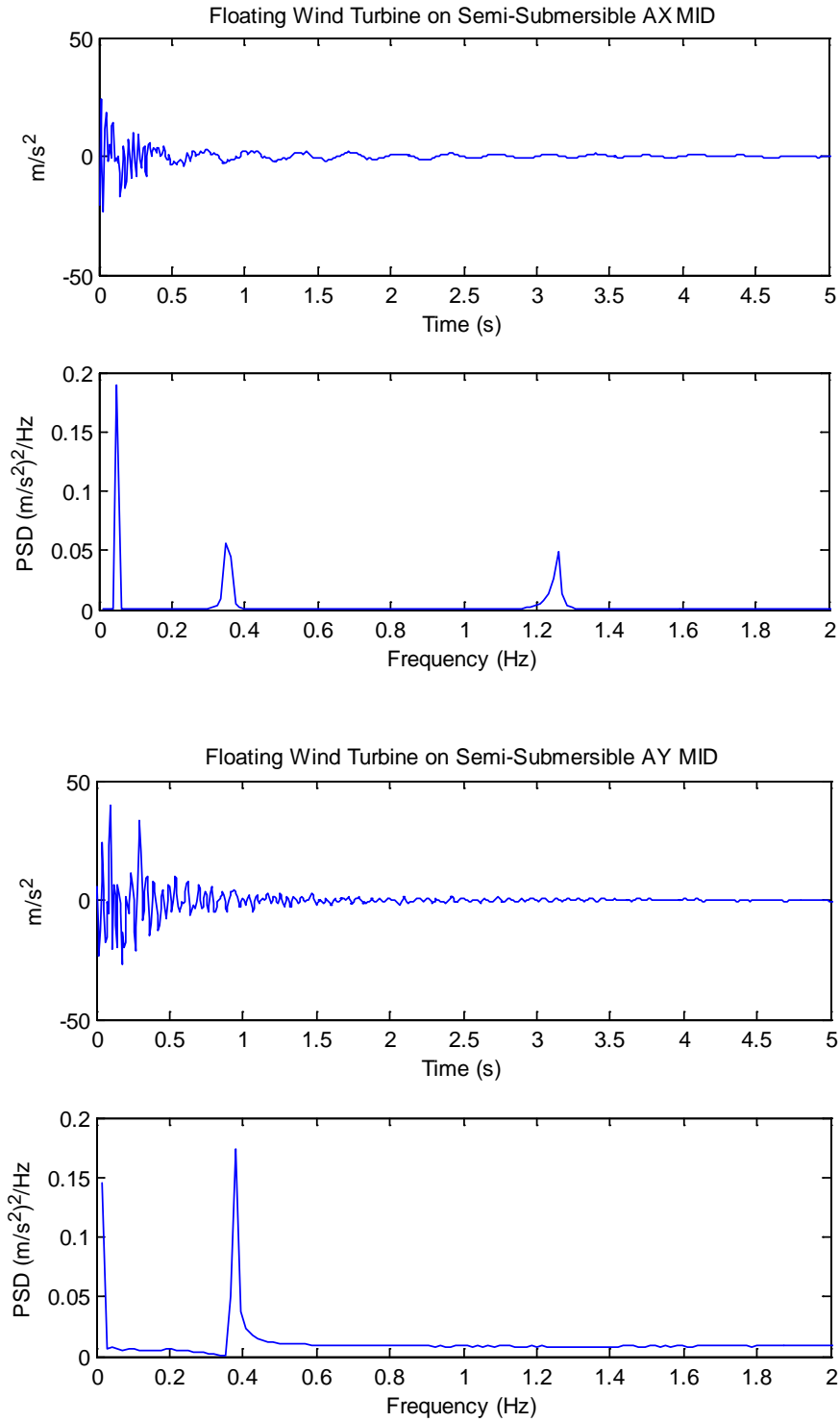
Hammer Test Data Results

Figure D.1. Acceleration and Power Spectral Density (PSD) plots from tower hammer tests.

Figure D.1. Acceleration and Power Spectral Density (PSD) plots from tower hammer tests.
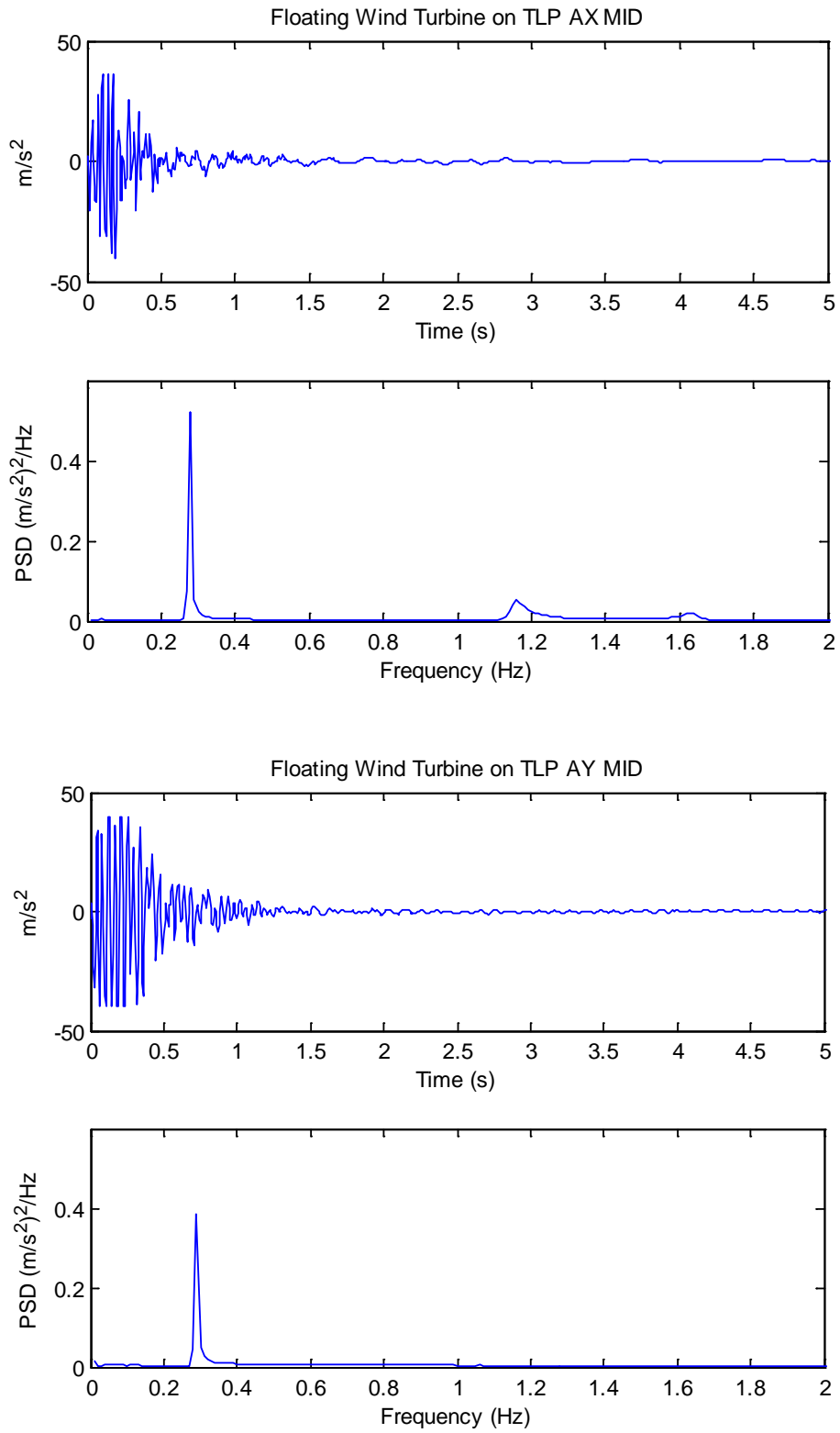
Figure D.1. Acceleration and Power Spectral Density (PSD) plots from tower hammer tests.

BIBLIOGRAPHY

Bae, Y. H., M. H. Kim, and Y. S. Shin. *Rotor-floater-mooring Coupled Analysis of Mini-TLP-Type Offshore Floating Wind Turbines.* Shanghai, China: OMAE 2010, 2010.

Bir, G. *BModes - Software for Computing Rotating Blade Coupled Modes.* NREL - National Wind Technology Center. Golden, 2008.

Çengel, Y.A., and J.M. Cimbala. *Fluid Mechanics: fundamentals and applications - 1st ed.* New York: McGraw-Hill, 2006.

Cermelli, C, A Aubault, D Roddier, and T McCoy. *Qualification of a Semi-Submersible Floating Foundation for Multi-Megawatt Wind Turbines.* Houston: Offshore Technology Conference, 2010.

Chakrabarti, S.K. *Offshore Structure Modeling.* Singapore: World Scientific Publishing Co. Pte. Ltd., 1994.

Daniel, I.M., and O. Ishai. *Engineering Mechanics of Composite Materials.* New York: Oxford University Press, 2006.

Department of Energy (DOE). "20% Wind Energy by 2030, Increasing WInd Energy's Contribution to U.S. Electricity Supply." 2008.

Department of Energy (DOE). *2009 Renewable Energy Data Book.* Washington, DC: DOE, 2010.

Drela, M. "UIUC Applied Aerodynamics Group." *UIUC Airfoil Data Site.* 1995. http://www.ae.illinois.edu/m-selig/ads/coord_database.html (accessed 11 01, 2011).

Drela, M.. *XFOIL: An Analysis and Design System for Low Reynolds Number Airfoils.* University of Notre Dam: Conference on Low Reynolds number Airfoil Aerodynamics, 1989.

Energy Information Association (EIA). "State Energy Profiles: Maine." *US Energy Information Association.* May 16, 2011. http://www.eia.gov/state/state-energy-profiles-data.cfm?sid=ME#Consumption (accessed June 8, 2011).

Energy Information Association (EIA). "Total Energy: US Energy Information Administration." *Primary Energy Production by Source, 1949-2009.* August 19, 2010. http://www.eia.gov/totalenergy/data/annual/pdf/aer.pdf (accessed July 5, 2011).

Epps, B. P., and R.W. Kimball. "OpenProp v2.4 propeller/turbine design code." *openprop.mit.edu.* MIT. 2010. http://openprop.mit.edu (accessed October 03, 201).

Firgelli Technologies Inc. "Products, Firgelli." *Firgelli Technologies inc. Web site.* 2011. http://firgelli.com/products.php?id=16 (accessed July 13, 2011).

Gere, J.M. *Mechanics of Materials.* Canada: Thomson Learning, 2006.

Gueydon, S., and W. Xu. *Floating Wind Turbine Motion Assessment.* Kona, Hawaii: Oceans11 Conference, 2011.

Gurit. "ST 94 Single SPRINT." *Gurit - SPRINT DATASHEETS - MARINE.* 2011. http://www.gurit.com/files/documents/ST_94_v4.pdf (accessed 10 05, 2011).

Henkel. "Frekot Mold Release Solutions Guide." *Henkel.* 2010. http://www.henkelna.com/us/content_data/165094_LT4831_Frekote_Guide_10_6_Lo258132.pdf (accessed 10 10, 2011).

Jonkman, J. *Definition of the Floating System for Phase IV of OC3.* Golden, CO: NREL, 2010.

Jonkman, J. *Dynamics Modeling and Loads Analysis of an Offshore Floating Wind Turbine.* Golden, CO: NREL, 2007.

Jonkman, J., and D. Matha. *Quantitative Comparison of the Responses of Three Floating Platforms.* Golden, CO, CO: NREL, 2009.

Jonkman, J., and M. Buhl Jr. *Development and Verification of a Fully Coupled Simulator for Offshore Wind Turbines.* Golden, CO: National Renewable Energy Lab, 2007.

Jonkman, J., S. Butterfield, W. Musial, and G. Scott. *Definition of a 5MW Reference Wind Turbine for Offshore System Development.* Golden: NREL, 2009.

Kooijman, H.J.T., C Lindenburg, D. Winkelaar, and E.L. van der Hooft. *DOWEC 6 MW Pre-Design.* Energy Research Center of the Netherlands (ECN), 2003.

Lancaster, P., and K. Šalkauskas. *Curve and Surface Fitting: An Introduction.* London: Academic Press, 1986.

Lokocz, T. "Solid Mechanics of Cross Flow of Tidal Turbine Blades ." *University of Maine.* 2010. http://www.umaine.edu/mecheng/Peterson/Classes/Design/2009_10/Projects/TidalEnergy-TomLokocz/reports.html (accessed 10 10, 2011).

Main, I. G. *Vibartions in Waves and Physics.* 3. Cambridge: Cambridge University Press, 1999.

Manwell, J. F., J. G. McGowan, and A. L. Rogers. *Wind Energy Explained: Theory, Design, and Application.* West Sussex: John Wiley & Sons Ltd., 2002.

MARIN. *DeepCwind Floating WInd Turbine Model Tests.* Marin, 2011.

MARIN. "Marin: Offshore Basin." *MARIN: Marine Research Institute Netherlands.* July 19, 2010. http://www.marin.nl/web/Facilities-Tools/Basins/Offshore-Basin.htm (accessed August 10, 2011).

Moriarty, P.J., and A.C. Hansen. *AeroDyn Theory Manual.* Golden: NREL, 2005.

Musial, W. *Status of Wave and Tidal Power Technologies for the United States.* Technical Report, Golden, CO: NREL, 2008.

Musial, W., and B. Ram. *Large-Scale Offshore Wind Power in the United States.* Golden, CO: NREL, 2010.

Musial, W., S. Butterfield, and B. Ram. *Energy from Offshore Wind.* National Renewable Energy Lab, Houston, Texas: Offshore Technology Conference, 2006.

Neilsen, F G, T D Hanson, and B Skaar. *Integrated Dynamic Analysis of Floating Offshore Wind Turbines.* Hamburg: Hydro Oil & Energy, 2006.

Ocean Energy Task Force. "Final Report of the Ocean Energy Task Force to Governor John E. Baldacci." Maine State Planning Office, Augusta, 2009.

O'Neil, P.V. *Advanced Engineering Mathematics.* 5th Edition. Pacific Grove, CA: Brooks/Cole-Thomson Learning, Inc., 2003.

Piercan USA, Inc. "Composite bladder molding." *Piercan USA, Inc.* 2010. http://www.piercanusa.com/composite.html (accessed 11 05, 2011).

Principle Power Inc. "First WindFloat Sucessfully Deployed Offshore." November 30, 2011. http://www.principlepowerinc.com/news/press_PPI_WF_deployment.html (accessed December 2, 2011).

Rao, S. S. *Mechanical Vibrations.* 4. Upper Saddle River: Pearson Prentice Hall, 2004.

Robinson, M., and W. Musial. *Offshore Wind Technology Overview.* Presentation, NWTC, NREL, DOE, 2006.

Schwartz, M., D. Heimiller, S. Haymes, and W. Musial. *Assessment of Offshore Wind Energy Resources for the Unites States.* Technical Report, Golden, CO: NREL, 2010.

Serchuk, A. "The Environmental Imperative for Renewable Energy: An Update." Renewable Energy Policy Project (REPP), Washington, DC, 2000.

SolidWorks. *SolidWorks Education Edition.* Software. Dessault Systems. 2010.

Statoil Hydro. "Hywind Fact Sheet." *Statoil.com.* 2010.
  http://www.statoil.com/en/TechnologyInnovation/NewEnergy/RenewablePowerP
  roduction/Offshore/Hywind/Downloads/Hywind%20Fact%20sheet.pdf (accessed
  September 15, 2011).

Timmer, N. "DOWEC blade airfoil data, (excel document)." Delft University of
  Technology, 2009.

University of Maine and James W. Sewall Company. "Maine Deepwater Offshore Wind
  Report." *DeepCwind Consortium.* Febuary 2011.
  http://deepcwind.org/docs/OfficialOffshoreWindReport-22311.pdf (accessed
  September 14, 2011).

van Dam, C.P., Chow, R. *NREL 5MW [Blade] Description.* University of California
  Davis, 2010.

White, F.M. *Fluid Mechanics.* 4. WCB McGraw-Hill, 1999.

WindSea. *WindSea: Wave Basin.* 2 2, 2011. http://www.windsea.com/movie/wave-basin/
  (accessed June 8, 2011).

BIOGRAPHY OF THE AUTHOR

Heather Rae Martin was born in Presque Isle, Maine and raised in Caribou, Maine up until sixth grade. She attended middle school and high school in Richmond, Maine where she lived with her mother and stepfather, Deborah and Guy Cousins. Much of her upbringing was also spent with her father and stepmother, Andy and Gina Martin, in Frenchville and Madawaska, Maine.

After graduating from Richmond High School in 2005 as class valedictorian, Heather attended the University of Maine where she was accepted into the Top-Scholar Award program. During her sophomore year, she discovered an affinity for engineering and decided to pursue a Bachelor of Science degree in Civil and Environmental Engineering. In December 2009, Heather completed her Bachelor's degree with summa-cum laude honors and was selected as the Class of 2009 Outstanding Graduate of the College of Engineering.

Heather has interned at the Stantec Inc. office in Scarborough, Maine as well as with Kiewit Construction on the Willis Avenue Bridge Replacement in New York City. In addition to her professional life, she also enjoys sports, outdoor activities, spending time with her family and friends, traveling, cooking and of course laughing. In the future, she hopes to continue to work and live in her home state, Maine.